

UNIVERSITÄTSKLINIKUM HAMBURG-EPPENDORF

Transplantation und Stammzell Immunbiologie Labor (TSI)

Klinik und Poliklinik für Herz- und Gefäßchirurgie

Universitäres Herzzentrum Hamburg (UHZ)

Prof. Dr. med. Sonja Schrepfer

Individualized Cardiovascular Medicine: Identifying New Mechanisms to Inhibit the
Development of Myointimal Hyperplasia

Dissertation

zur Erlangung des Grades eines Doktors der Medizin an der Medizinischen Fakultät
der Universität Hamburg

vorgelegt von: Dong Wang aus Beijing, China

Hamburg 2015

Angenommen von der
Medizinischen Fakultät der Universität Hamburg am: 20.11.2015

Veröffentlicht mit Genehmigung der
Medizinischen Fakultät der Universität Hamburg.

Prüfungsausschuss, der/die Vorsitzende: Prof. Dr. Sonja Schrepfer

Prüfungsausschuss, zweite/r Gutachter/in: Prof. Dr. Friederike Cuello

Prüfungsausschuss, dritte/r Gutachter/in:

Inhaltsangabe

1. Hintergrund.....	4
2. Zielsetzung	6
3. Myointimale Hyperplasie	7
3.1. microRNA basierte Therapiestrategie zur Verhinderung der myointimalen Hyperplasie und In-Stent- Restenose	7
3.2. Identifizierung des PDK2-Pathways als neues therapeutisches Ziel zur Verhinderung der Entwicklung einer myointimalen Hyperplasie.....	11
4. Stammzell-Immunbiologie.....	14
5. Zusammenfassung	17
6. Literaturangabe	19
7. Appendix.....	27
7.1. Abkürzungen	27
7.2. Publikationen.....	28
7.3. Lebenslauf	29
8. Danksagung.....	32
9. Eidesstattliche Erklärung	33

1. Hintergrund

Jährlich versterben ca. 17 Millionen Menschen an kardiovaskulären Erkrankungen, der führenden Todesursache weltweit ^{1,2}.

Ein großer Teil dieser Patienten erliegt den Folgen von vaskuloproliferierenden Erkrankungen, wie der Atherosklerose oder der Myointimalen Hyperplasie. Neben den koronaren Herzerkrankungen (KHK) und Myokardinfarkten gelten Schlaganfälle als die bedrohlichste Folge von vaskuloproliferierenden Erkrankungen. Nach Schätzung der WHO wird im Jahr 2030 die Zahl der durch KHK bedingten Todesfälle auf 25 Millionen steigen¹. Wenn Patienten einen Myokardinfarkt überleben, führt die durch Ischämie bedingte Infarktnarbe oft zu einer Herzinsuffizienz verbunden mit einer verkürzten Lebenserwartung ³⁻⁵.

Die pathophysiologische Ursache vaskuloproliferativer Erkrankungen ist eine De-Differenzierung der glatten Gefäßmuskelzellen (VSMC), einhergehend mit gesteigerter Proliferation und Migration der Zellen, die zu einer Einengung des Gefäßlumens führt⁶.

Aktuelle Therapiestrategien fokussieren auf eine Wiederherstellung des Blutflusses durch Wiedereröffnen des Gefäßes oder der Anlage eines Bypasses. Bei der interventionellen Angioplastie wird ein Draht über das Gefäßsystem in die verengte Gefäßstelle vorgeschoben und die Verengung durch einen Ballon aufgedehnt. Die erste perkutane koronare Angioplastie (PTCA) wurde im Jahr 1977 von Andreas Grüntzig durchgeführt ⁷. Trotz der initial hohen Erfolgsraten zeigte sich bei vielen Patienten eine Gefäßrestenose. Unterschiedliche Studien beziffern die Restenoseraten zwischen 20-48% nach PTCA ⁸⁻¹¹. Eine deutliche Reduktion der Komplikationsrate wurde durch den Einsatz von Stents durch Ulrich Sigward im Jahr 1987 erzielt¹²⁻¹⁴. Nach erfolgreicher Ballondilatation wird im dilatierten Gefäßabschnitt ein expandierbares Metallgitter (Stent) implantiert und schützt das Gefäß vor einem akuten elastischen Rückzug¹⁵. Dennoch zeigte sich in Langzeitstudien, dass insgesamt die Restenoserate nicht unter 30% fiel ^{16,17}. Die Hauptursache hierfür war eine andauernde Irritation des Gefäßes durch den Stent, was einen Proliferations- und De-Differenzierungsreiz für die VSMCs darstellt ¹⁸⁻²¹. Mit der erhöhten Proliferation und Matrixsynthese der VSMCs verkleinert sich das Gefäßvolumen kontinuierlich bis zur Entwicklung der In-Stent-Restenose.

Um die erhöhte Proliferation der VSMCs zu verhindern, wurden um die Jahrtausendwende neuartige Stents eingeführt, die mit antiproliferativen Medikamenten beschichtet sind. Diese sogenannten Drug-Eluting-Stents (DES) hemmten die Proliferation von Zellen und konnten die Restenoserate auf unter 10%

deutlich senken²²⁻²⁵. Die antiproliferative Wirkung der Medikamente ist jedoch unspezifisch und beeinflusst deshalb auch die Proliferation von Endothelzellen. Endothelzellen kleiden als innerste Schicht die Gefäße aus und sind für die Gefäßbiologie und -physiologie von großer Bedeutung^{26,27}. Während einer Ballondilatation oder Stentimplantation wird diese Schicht iatrogen verletzt, und es kommt zu einer lokalen De-Endothelialisierung des Gefäßes. Das damit verbundene Ungleichgewicht zwischen relaxierenden und kontraktiven Faktoren, zwischen wachstumshemmenden und -fördernden Faktoren sowie zwischen anti- und prokoagulierenden Faktoren verursacht eine Reihe von schwerwiegenden Konsequenzen wie Gefäßspasmus, myointimale Hyperplasie oder Thrombusformation²⁸. Besonders die Komplikation der In-Stent-Thrombose tritt vermehrt bei DES auf und limitiert dessen klinischen Einsatz²⁹. Deshalb ist die Erforschung von neuen spezifischeren Medikamenten zur Verhinderung der Entwicklung einer myointimalen Hyperplasie und In-Stent-Restenose von großer Bedeutung.

2. Zielsetzung

Trotz großer Fortschritte in der Behandlung der myointimalen Hyperplasie in den letzten Jahrzehnten erzeugen die aktuellen Therapieoptionen Nebenwirkungen, wie Restenose, Gefäßthrombose oder lokale Überempfindlichkeitsreaktion. Die Erforschung von neueren, spezifischen und nebenwirkungsärmeren Behandlungsmöglichkeiten stellt eine wichtige Herausforderung in der Herz-Kreislaufforschung dar. Vielversprechende neue Zielgruppen für die Entwicklung neuer pharmakologischer Medikamente sind die sogenannten microRNAs, die als Genregulatoren eine Vielzahl von zellulären Prozessen steuern. Einen weiteren neuen therapeutischen Ansatz bieten niedermolekulare Moleküle, die aufgrund ihres geringen Molekulargewichtes die Zellmembran passieren und oral absorbiert werden.

Ziel dieser Arbeit ist es neue molekulare Ziele und Therapiestrategien zu untersuchen, um die Entwicklung der myointimalen Hyperplasie und In-Stent-Restenose zu verhindern. Dieses Ziel ist umso bedeutender, da andere aktuelle Therapieoptionen wie z.B. die Stammzelltransplantation zur Myokardregeneration, eine myointimale Hyperplasie nicht verhindern sondern das bereits abgestorbene Gewebe regenerieren sollen. Zur Myokardregeneration stellen die pluripotenten Stammzellen eine vielversprechende Zellpopulation dar. Ziel meiner Arbeit in diesem Gebiet war es ihre klinische Einsetzbarkeit aus immunbiologischer Sicht zu untersuchen.

3. Myointimale Hyperplasie

3.1. microRNA basierte Therapiestrategie zur Verhinderung der myointimalen Hyperplasie und In-Stent- Restenose

Am Anfang des Jahrhunderts führte die Entdeckung von microRNAs (miRs) als entscheidende Genexpressionsregulatoren, zu zuvor unvorstellbaren Möglichkeiten, den Zustand von diversen „Krankheits-Phänotypen“ zu verändern. MiRs sind kleine, endogene, antisense RNA Moleküle, die die Genexpression post-transkriptional durch mRNA-Degradation oder Translationsrepression regulieren³⁰⁻³². Das Besondere hierbei ist, dass eine miR mehrere unterschiedliche mRNAs bindet und somit Regulationspathways auf unterschiedlichen Ebenen gleichzeitig koordinieren kann³³. Die biologische Funktion von einer miR ist zell- und gewebs-spezifisch^{34,35}. So besitzt miR-21 einen pro-apoptotischen Effekt in Hela-Zellen, hemmt aber die Apoptose in Glioblastom Zellen^{36,37}. Ferner stehen abnormale miR- Level mit unterschiedlichen Erkrankungen in Verbindung, wie Tumorerkrankungen, viralen Infektionen oder kardiovaskuläre Erkrankungen³⁸⁻⁴⁰. Diese Eigenschaften machen miRs zu vielsprechenden diagnostischen und therapeutischen Zielstrukturen⁴¹⁻⁴³. So hat Miravirsen (ein miR-122 Inhibitor gegen Hepatitis C) bereits die Phase 2a Studie erfolgreich bestanden⁴⁴.

Vorausgegangene Studien deuten darauf hin, dass miRs maßgeblich verantwortlich sind für die Entwicklung der myointimalen Hyperplasie und Restenose⁴⁵. Durch die Hemmung oder Wiederherstellung spezifischer miRs kann die myointimale Formation inhibiert werden^{39,46,47}. Damit stellt sie ein erfolgsverheißendes Therapieziel dar. Trotz des zunehmenden Wissens über die biologische Funktion der miRs, besteht die Limitation, dass dieses Wissen überwiegend aus Versuchen mit Nagetieren stammt. Ferner wurde in vielen Studien eine systemische Gabe von einem miR-Modulator verwendet, was potenzielle Nebenwirkungen mit sich bringt⁴⁸. Diese Nebenwirkungen sind im Gegensatz zu anderen Medikamenten multidimensional, da miRs nicht nur ein Target, sondern ganze Genfamilien regulieren⁴³.

In der folgende Studie untersuchten wir die miR Expression in Patientenproben und in einem neuen humanisierten Tiermodell. Dieses Modell besitzt zum einen ein besseres translationales Potenzial als die bisher gängigen Tiermodelle, zum anderen erlaubt es die lokale Applikation eines miR-Modulators.

Zusammenfassend wird ein Stück humane *Arteria mammaria interna* (IMA) mit einem Ballon dilatiert um eine Gefäßverletzung zu induzieren. Die IMA wird in die abdominelle Aortenposition einer immundefizienten RNU-Ratte durch End-zu-End-Anastomosen transplantiert (hMa)⁴⁹. Für eine lokale Applikation wurde vor Implantation zusätzlich ein Stent in die IMA gesetzt⁵⁰. Innerhalb von 28 Tagen entwickelt sich eine myointimale Hyperplasie deren VSMC menschlichen Ursprungs sind.

Wang D, Deuse T, Stubbendorff M, Chernogubova E, Erben RG, Eken SM, Jin H, Behnisch B, Reichenspurner H, Robbins RC, Tsao PS, Maegdefessel L, Schrepfer S. Local microRNA modulation is feasible: A novel anti-miR-21-eluting stent prevents in-stent restenosis. *Arteriosclerosis, Thrombosis, and Vascular Biology* 2015 (in Revision).

Von sieben miRs, die eine potenziell bedeutende Rolle bei der myointimalen Hyperplasie besitzen, stellten wir in qRT-PCR Versuchen bei 6 miRs signifikante Veränderungen in unserem humanisierten Tiermodell fest, wobei nur die miR-21 erhöht war, während die Expression der anderen miRs durch Gefäßverletzung signifikant vermindert war. Interessanterweise gab es keine Unterschiede zwischen den ballondilatierten Gefäßen und denen mit einem zusätzlichen Stent. Ein Vergleich zwischen gesunden humanen Koronararterien und kranken gestenteten Koronargefäßen zeigte ähnliche Relationen der miR-21 Level. Das Vorhandensein von miR-21 in den myointimalen Läsionen der transplantierten Gefäße konnte mit Hilfe von In-situ Hybridisierungen dargestellt werden.

Um die funktionelle Bedeutung von miR-21 bei der myointimalen Hyperplasie zu untersuchen, verabreichten wir den Tieren einen Tag nach der Transplantation systemisch fluoreszenz-markierte anti-miR-21-LNA-Inhibitoren (anti-21) und werteten die Gefäße nach 28 Tagen aus. Nicht behandelte Tiere wurden mit einer Low-Dose Gruppe (1mg/kg Tiergewicht)(LD-Gruppe) und einer High-Dose Gruppe (5mg/kg Tiergewicht) (HD-Gruppe) verglichen. Es zeigten sich deutliche myointimale Läsionen in der unbehandelten und der LD-Gruppe. In der HD-Gruppe war die Läsion signifikant niedriger.

VSMCs besitzen die Fähigkeit, ihren Phänotyp zu regulieren als Reaktion auf eine Veränderung ihrer Umgebung⁵¹. Wachstumsfaktoren, Zytokine, Zell-Zell-Kontakte, Lipide und extrazelluläre Matrixproteine sind alles Einflussmöglichkeiten, die zu einer Phänotyp-Veränderung führen. Die Expression von Proteinen des Kontraktionssystems wie SM α -actin, SM myosin heavy chain, SM22 α , Calponin und

Smoothelin findet nur in differenzierten kontraktilen VSMCs statt, während in de-differenzierten synthetisierenden VSMCs die embryonale Form des SM myosin heavy chain (SMemb) primär exprimiert wird. Diese Alternation der Proteinexpression und deren Regulierung stellt einen wichtigen Teil des Phänotyp-Switches dar und macht sie zu einem vielversprechenden Angriffspunkt für die Therapie gegen Myointimale Hyperplasie^{6,52,53}. Immunfluoreszenz-Färbungen an hMa-Gefäßen demonstrieren, dass in myointimalen Läsion vermehrt SMemb positive Zellen lumennah zu finden sind, während VSMCs mit SM myosin heavy chain in der Nähe der Media lokalisiert sind.

Da das verwendete anti-21 mit einem Farbstoff markiert war, konnte die Verteilung in unterschiedlichen Organen von anti-21 mittels dem Xenogen IVIS Imaging System verfolgt werden. Hierbei beobachteten wir ein deutlich höheres Fluoreszenzsignal in den Nieren der HD-Gruppe als in den anderen beiden Gruppen und erniedrigte miR-21 Expression. Gleichzeitig zeigten sich bei den Tieren, die mit der hohen anti-21-Dosis behandelt wurden, signifikant höhere Serumkreatinin- Werte. Diese Ergebnisse deuten darauf hin, dass die nierenschädliche Wirkung von hochdosierten anti-21 bei systemischer Gabe für klinische Studien berücksichtigt werden sollte.

Um die unspezifischen Nebenwirkungen einer systemischen miR-21 Inhibition zu vermeiden, wurde in einer weiteren Studie die lokale Anwendung eines mit anti-21-beschichteten Stents untersucht. Die Menge des anti-21 auf dem Stent, entsprach dem der systemisch hoch dosierten Gruppe (5mg/kg Tiergewicht). Als Vergleichsgruppe dienten Tiere, die eine IMA mit einem unbeschichteten Stent (BMS-Gruppe) erhielten. Nach 28 Tagen zeigte sich in der anti-21-Stent Gruppe sowohl in den optischen Kohärenztomografie- Aufnahmen (OCT) als auch in den histopathologischen Schnitten eine deutlich geringer ausgeprägte myointimale Hyperplasie als in der BMS-Gruppe. Die lokale Applikation von anti-21 zeigte keine Nebenwirkungen. Die Serum-Kreatinin- Level waren bei lokaler Gabe nicht erhöht und es gab keine Akkumulation von anti-21 in den Organen.

Ein wesentlicher Nachteil von gegenwärtigen DES ist die verzögerte Re-Endothelialisierung aufgrund der unspezifischen Proliferationshemmung des beschichteten Medikaments. Um den Einfluss von anti-21 auf die Re-Endothelialisierung zu untersuchen, wurde in einer weiteren Studie anti-21 systemisch in Lewis Ratten appliziert, deren Aorta zuvor mit einem Ballonkatheter de-endothelialisiert wurde. Sowohl in immunhistologischen Färbungen als auch im Organbadversuch, welches die physiologische Funktion der Endothelzellen in der Gefäßwand untersucht, zeigten sich keine negativen Einflüsse durch die anti-21-

Gabe. Proliferationsversuche mit humanen Koronarendothelzellen bestätigten das Ergebnis, dass anti-21 die Endothelproliferation nicht beeinflusst.

Zusammenfassend haben diese experimentellen Studien gezeigt, dass miR-21 eine wichtige Rolle bei der Entstehung der myointimalen Hyperplasie spielt. Systemische miR-21 Hemmung reduziert zwar die Hyperplasie, geht aber mit Nebenwirkungen einher. Eine translationale Lösung bietet eine lokale anti-21 Applikation mittels eines beschichteten Stents ohne nachweisbare Nebenwirkungen.

3.2. Identifizierung des PDK2-Pathways als neues therapeutisches Ziel zur Verhinderung der Entwicklung einer myointimalen Hyperplasie

Als weiteres Therapietarget gegen die myointimale Hyperplasie haben wir erstmals ein Protein aus der Gruppe der Zellatmungsregulatoren identifiziert. Pyruvat-Dehydrogenase- Kinase (PDK) ist ein Kinase- Enzym und reguliert über die Inaktivierung von Pyruvat-Dehydrogenase (PDH) die oxidative Decarboxylierung in Zellen⁵⁴. Es nimmt eine zentrale Rolle in der Zellatmung ein, da die oxidative Decarboxylierung die Voraussetzung für aerobe Energiegewinnung im Mitochondrium ist. Durch Regulation dieser mitochondrialen Vorgänge nimmt es auch Einfluss auf die mitochondrialen Apoptosepathways⁵⁵. In unserer Studie stellten wir fest, dass PDK-Isotyp 2 (PDK2) eine essentielle Rolle bei der myointimalen Formation spielt und deren pharmakologische oder genetische Hemmung die myointimale Hyperplasie vermindert.

Deuse T, Hua XQ, Wang D, Maegdefessel L, Heeren J, Scheja L, Bolanos JP, Rakovic, SpinJM, Stubbendorff M, Ikeno F, Länger F, Zeller T, Schulte-Uentrop L, Stöhr A, Itagaki R, Haddad F, Eschenhagen T, Blankenberg S, Kiefmann R, Reichenspurner H, Velden J, Klein C, Yeung A, Robbins RC, Tsao PS, Schrepfer S.

Dichloroacetate prevents restenosis in preclinical animal models of vessel injury. *Nature*. 2014 May 29;509(7502):641-4.

Um ein genaues pathophysiologisches Verständnis der myointimalen Entstehung zu erlangen, wurde die myointimale Entwicklung über 28 Tagen hinweg histopathologisch und molekularbiologisch sowohl in einem Rattenmodel als auch in dem oben beschriebenen, humanen hMa Model verfolgt. Während der Entstehung der myointimalen Hyperplasie weisen VSMCs temporär eine Hyperpolarisation des mitochondrialen Membranpotentials ($\Delta\psi$) auf. Damit einhergehend ist eine erhöhte Proliferationsrate mit gleichzeitiger Resistenz gegen mitochondriale Apoptoseinduktion. Als wichtigen Auslöser der myointimalen Hyperplasie wurde der Wachstumsfaktor PDGF identifiziert, da dieser vermehrt in den ersten Tagen nach Gefäßverletzung freigesetzt wird und eine Blockade vom PDGF-Rezeptor die Krankheitsentstehung verhindert. Diese Ergebnisse konnten auch auf zellulärer Ebene reproduziert werden. PDGF-stimulierte VSMC-Kulturen zeigen eine Hyperpolarisation von $\Delta\psi$ und eine De-Differenzierung der Zellen mit verminderter

Apoptose. Hierbei kommt der Hyperpolarisation von $\Delta\psi$ eine besondere Bedeutung zu, da $\Delta\psi$ eng mit der Freisetzung von mitochondrialen Apoptosemolekülen verbunden ist⁵⁶⁻⁵⁸.

Eine Möglichkeit, $\Delta\psi$ zu reduzieren ist das niedermolekulare Molekül Dichloracetat (DCA). Die Gabe von DCA führte bei PDGF-stimulierten VSMC Zellen zur Wiederherstellung von $\Delta\psi$ und Apoptoserate. Auch *in vivo* zeigte sich eine signifikante Reduktion von $\Delta\psi$ in den mit DCA behandelten Tieren. Gleichzeitig zeigten sich erhöhte Apoptoseraten und signifikant weniger myointimale Läsionen.

Um die gefäßprotektive Wirkung von DCA genauer zu untersuchen, wurde der Effekt in fünf unterschiedlichen Tiermodellen studiert: dem Rattenaortenmodell, dem Kaninchenilicamodell, dem humanisierten IMA Model, dem humanisierten Koronararterienmodell und dem Schweineangioplastiemodell. Dabei war die Entwicklung der myointimalen Hyperplasie in allen Modellen in den DCA-behandelten Gruppen signifikant geringer ausgeprägt als in den unbehandelten Kontrollgruppen. Besonders vielversprechend für einen zukünftigen klinischen Einsatz von DCA ist die Beobachtung, dass DCA keine hemmende Wirkung auf die Re- Endothelialisierung oder Endothelzellenmigration hat.

Die molekulare Wirkung von DCA basiert auf einer Hemmung von PDK, da dieser die einzig bekannte Zielstruktur von DCA ist⁵⁹. Dabei besitzt PDK2 die höchste Affinität zu DCA⁶⁰. Lentiviraler Knockdown von PDK 2 führte in VSMCs zu PDGF-resistenten $\Delta\psi$ -Werten. Gleichzeitig beobachteten wir konstant hohe Apoptoseraten, die durch PDGF nicht beeinflussbar waren. Um die Bedeutung von PDK2 *in vivo* zu untersuchen, führten wir einen Knockdown von PDK2 in humanen IMA Gefäßen *ex vivo* durch und implantierten diese wie im hMA Modell in die Rattenaorta. Histologische Untersuchungen zeigten in PDK2-Knockdown Gefäßen einen ähnlichen Verlauf wie bei hMA-Tieren die mit DCA behandelt wurden: Niedrige $\Delta\psi$ Werte, konstant hohe Apoptoseraten und verminderte myointimale Läsionen sind dabei charakteristisch für eine PDK2 Hemmung, sowohl medikamentös mit DCA als auch Lentiviral mit short hairpin RNA (shRNA).

Zusammenfassend haben diese Untersuchungen gezeigt, dass eine Hyperpolarisation von $\Delta\psi$ eine wichtige Rolle bei der Entstehung der myointimalen Hyperplasie spielt. Die medikamentöse oder lentivirale Hemmung von PDK 2 senkt $\Delta\psi$ und inhibiert die Ausbildung von myointimalen Läsionen. Aufgrund der guten Bioverfügbarkeit und Verträglichkeit stellt die Hemmung des PDK2-Pathways durch

DCA eine vielversprechende klinische Option dar die Entwicklung einer myointimalen Hyperplasie nach Gefäßverletzung zu verhindern.

4. Stammzell-Immunbiologie

Werden koronarkranke Patienten nicht oder zu spät behandelt, können durch die Minderversorgung des Myokards irreversible Schäden am Herzen entstehen⁶¹. Verminderte Kontraktilität und Dilatation des Ventrikels sind Charakteristika der ischämischen Kardiomyopathie und führen zur Herzinsuffizienz⁶². Durch den Fortschritt in der Behandlung von KHK und Myokardinfarkten konnte zwar die Mortalität gesenkt werden, aber die Inzidenz der ischämischen Kardiomyopathien und die damit verbundene Herzinsuffizienz nahmen deutlich zu^{63,64}. Die Therapie solcher Patienten mit terminaler Herzinsuffizienz ist limitiert und basiert auf dem Prinzip, das geschädigte Herz durch eine mechanische Pumpe (Assist-Device) oder ein fremdes Herz zu ersetzen⁶⁵. Der Einsatz von Assist-Devices ist jedoch mit Nebenwirkungen und Einschränkungen verbunden⁶⁶⁻⁶⁹, und die Herztransplantation ist durch den deutlichen Mangel an Organspenden limitiert^{70,71}. Umso wichtiger ist es, neue Therapiestrategien für Patienten mit terminaler Herzinsuffizienz zu finden. Eine große Hoffnung wird in die regenerative Medizin gesetzt mit dem Wunsch, das geschädigte Gewebe durch Stammzellen zu regenerieren. Es konnte gezeigt werden, dass die Injektion von Knochenmark-Stammzellen die Herzfunktion verbessert^{72,73}, heute wird jedoch davon ausgegangen, dass dieser Effekt auf die parakrine Wirkung der transplantierten Zellen zurückzuführen ist^{74,75}. Eine Transdifferenzierung von hämatopoetischen Stammzellen zu Kardiomyozyten scheint nicht möglich zu sein⁷⁶. Stattdessen müssen pluripotente Stammzellen für eine effektive Regeneration von Kardiomyozyten verwendet werden. Humane embryonale pluripotente Stammzellen scheidet aufgrund ethischer Bedenken aus. Induzierte pluripotente Stammzellen (iPS) können zwar zu Kardiomyozyten differenziert werden⁷⁷, neigen aber zu Genomabberationen⁷⁸. Eine neue vielversprechende Möglichkeit ist der Einsatz von Zellkerntransferierten embryonalen Stammzellen (Nuclear Transfer Embryonic Stem Cell (NT-ESC)). Dabei entnimmt man einer Eizelle den Zellkern, und ersetzt ihn durch einen fremden somatischen Zellkern (Somatic Cell Nucleus Transfer (SCNT)). Anschließend wird die Zelle durch eine elektrische Stimulation zum Teilen angeregt und entwickelt sich zu einer Blastozyste, aus der pluripotente Stammzellen gewonnen werden können. Zwar wurde diese Methode bereits in den 50er Jahren beschrieben⁷⁹, es gelang jedoch erst in 2013, menschliche pluripotente Zellen durch SCNT zu gewinnen⁸⁰. Ein Merkmal dieser Methode ist, dass NT-ESCs Hybridzellen sind. Der Zellkern (Zellkernspender) und die Mitochondrien (Eizellspender) sind dabei unterschiedlichen Ursprungs.

Aus diesem Grund stellten wir uns die Frage, in wie weit diese Inkongruenz von Zellkern und Mitochondrien zu immunologischen Problemen führt und den klinischen Einsatz dieser neuen Technologie eingrenzt.

Deuse T, Wang D, Stubbendorff M, Itagaki R, Grabosch A, Greaves LC, Alawi M, Grünewald A, Hu X, Hua X, Velden J, Reichenspurner H, Robbins RC, Jaenisch R, Weissman IL, Schrepfer S.

SCNT-Derived ESCs with Mismatched Mitochondria Trigger an Immune Response in Allogeneic Hosts. *Cell Stem Cell*. 2015 Jan 8;16(1):33-8.

NT-ESCs wurden aus einer BDF1 Eizelle (Mausstamm) und dem Fibroblastenzellkern einer BALB/c (Mausstamm) generiert⁸¹. Um die mitochondrien-spezifische Antigenität zu untersuchen, wurden unterschiedliche Transplantationsversuche mit NT-ESCs im Mausmodell durchgeführt und die Immunantwort untersucht.

Die folgenden fünf Mausstämme dienten als Empfänger:

- BALB/c (Unterschied in Mitochondrien)
- BDF1 (Unterschied in minor histocompatibility antigen (MiHA))
- C57BL/6 (Unterschied in major histocompatibility antigen (MHC))
- NOD SCID (Immundefizient)
- CBA (Unterschied in MHC und Mitochondrien)

Die größte Immunantwort (gemessen anhand der TH1 Aktivität mittels ELISPOT) entwickelte sich wie erwartet in den CBA Mäusen gefolgt von C57BL/6 Mäusen. Etwas niedrigere Aktivitäten fanden wir zwischen BDF1 und BALB/c vor, die jeweils Unterschiede in MiHA oder Mitochondrien aufweisen. Die immundefizienten NOD-SCID Mäusen zeigten keine Reaktivität.

Ähnliche Relationen zwischen den Mäusestämmen wurden auch im Interleukin-4 (IL-4) ELISPOT Versuch beobachtet, durch den die TH2 Aktivität gemessen wird. Die IgM Produktion war in BALB/c und BDF1 Empfänger vorhanden, aber signifikant niedriger als im C57BL/6 Maus. Diese Ergebnisse demonstrieren, dass ein Mismatch von Mitochondrien ausreichend für eine Th1 und 2 Immunantwort und Immunglobulinproduktion ist. Die Intensität dieser Immunreaktion entspricht ungefähr dem des MiHA-Mismatches und ist schwächer als beim MHC Mismatch.

Das Überleben eines Transplantats bildet einen wichtigen Wegweiser für die Intensität der Abstoßungsreaktion. Während in den immundefizienten NOD SCID

Mäusen alle NT-ESC Transplantate überlebten und Teratome formten, wurden alle Transplantate in den CBAs abgestoßen. Auch in den C57BL/6 Empfängern, die sich im MHC vom NT-ESC unterscheidet, wurden viele Transplantate abgestoßen. Kongruent mit unseren ELISPOT Ergebnissen fanden wir in BDF1 und BALB/c Tieren eine schwache Abstoßung vor. Von den mitochondrien-inkongruenten BALB/c Tieren formten 60% ein Teratom. Das Tumorwachstum war jedoch stark verlangsamt.

Um den Fehler auszuschließen, dass die Immunantwort durch die Pluripotenz der Zellen bedingt ist, wiederholten wir die Versuche mit isogenen BALB/c ESCs (isoESCs). Die Transplantation in isogene BALB/c Mäuse zeigte im ELISPOT vernachlässigbare TH1 und TH2 Reaktionen. Wurden isoESCs in BDF1 Mäuse injiziert, die sich in Mitochondrien und MiHA unterscheiden, wurde eine schwache Immunreaktion induziert. Die stärkste Immunantwort zeigte sich in den C57BL/6 Tieren, die sich in Mitochondrien und MHC von den isoESC unterscheiden. Die angeborene Immunabwehr schien eine untergeordnete Rolle bei den Immunreaktionen gegen Mitochondrien zu spielen.

Die besondere Bedeutung der adaptiven Immunantwort wurde in einem modifizierten Medawar Experiment bestätigt⁸². Neonatale BALB/c Mäuse wurden mit NT-ESCs immunisiert und im ausgewachsenen Zustand ein zweites Mal mit NT-ESCs injiziert. Im Vergleich zu BALB/c Tieren, die nicht immunisiert wurden, zeigten immunisierte Tiere keine Immunreaktion in ELISPOT Versuchen und stießen das Transplantat nicht ab. Somit hatte das adaptive Immunsystem im neonatalen Alter gelernt die allogenen Zellen zu akzeptieren.

Zusammenfassend haben diese Versuche gezeigt, dass inkongruente Mitochondrien nicht zu vernachlässigende Antigene darstellen, die eine Abstoßungsreaktion trotz Zellkern-Kongruenz auslösen. Da die mitochondriale DNA beim Menschen eine deutlich höhere Variabilität als bei Mäusen hat^{83,84}, sind beim Menschen auch Immunreaktionen zu erwarten. Dabei erfolgt die Immunreaktion vor allem auf der adaptiven Immunzellebene mit Aktivierung von Lymphozyten. Diese Immunogenität von Mitochondrien sollte bei der Entwicklung von SCNT-basierten Therapiestrategien beachtet werden.

5. Zusammenfassung

Ziel meiner Doktorarbeit war die Identifizierung neuer therapeutischer Zielstrukturen zur Hemmung der myointimalen Hyperplasie nach Gefäßverletzung. Die myointimale Hyperplasie ist charakterisiert durch eine verminderte Apoptose, vermehrte Proliferation und Migration von VSMCs und die dadurch resultierende Zunahme der Gefäßwand und Verengung des Gefäßlumens. Vielversprechende therapeutische Targets sind miRs, die die Genexpression auf post-transkriptionaler Ebene beeinflussen. Die miR 21 ist ein wichtiger Akteur bei der Entstehung der myointimalen Hyperplasie. Die systemische Hemmung durch anti-21 verhindert zwar dosisabhängig die Hyperplasie, führt aber zu Nebenwirkungen in anderen Organen. In meiner Arbeit zeige ich, dass ein vielversprechender therapeutischer Ansatz der Einsatz eines mit anti-21 beschichteten Stents wäre. Hierdurch wird miR 21 lokal gehemmt ohne systemische Nebenwirkungen zu verursachen.

Neben der vermehrten Proliferation und verminderten Apoptose ist die Erhöhung des mitochondrialen Membranpotentials ($\Delta\psi$) ein pathophysiologisches Merkmal der myointimalen Hyperplasie. Hyperpolarisation von $\Delta\psi$ hemmt die Freisetzung von mitochondrialen Apoptosemolekülen und verleiht der Zelle eine Apoptoseresistenz. Dichloracetat (DCA) inhibiert PDK-2 und verhindert eine vermehrte Hyperpolarisation von $\Delta\psi$ in VSMCs. Die Wiederherstellung von $\Delta\psi$ durch DCA beseitigt die Apoptoseresistenz und hemmt eine Entwicklung der myointimalen Hyperplasie. In fünf unterschiedlichen Tiermodellen (unter anderem dem translationalen Schweineangioplastie-Modell) und in der Zellkultur zeigte sich der Einsatz von DCA als nebenwirkungsfrei und vaskuloprotektiv und stellt damit eine aussichtsreiche zukünftige Therapieoption dar.

Neben der Identifikation von neuen Behandlungsmöglichkeiten gegen die myointimale Hyperplasie, sollte die Therapie von Patienten, die durch die Gefäßverengung eine ischämische Kardiomyopathie und Herzinsuffizienz erleiden, nicht außer Acht gelassen werden. Den meisten Patienten mit terminaler Herzinsuffizienz kann nur durch eine Herztransplantation geholfen werden, jedoch ist diese Behandlungsoption stark durch den Organspendermangel eingeschränkt. Die regenerative Zelltherapie stellt eine vielversprechende neue Therapieoption dar. Embryonale Stammzellen, die durch den Transfer eines somatischen Zellkerns in eine fremde zellkernlose Eizelle (NT-ESC) entstehen, können zu Kardiomyozyten differenziert werden und sind damit für eine Zelltransplantationstherapie geeignet. In meiner Arbeit untersuchte ich die Immunogenität von NT-ESCs und stellte fest, dass

die allogenen Mitochondrien eine Immunreaktion auslösen, die zu einer Abstoßung des Zelltransplantates führt. Die Immunreaktion ist adaptiv, gegen mitochondriale Proteine gerichtet und empfänglich für Toleranzinduktion. Durch Verwendung von eigenen Eizellen oder die von nahen Verwandten (z.B. Mutter oder Schwester) kann die Abstoßungsreaktion umgangen und ein therapeutischer Einsatz ermöglicht werden.

Zusammenfassend eröffnen meine dargestellten Arbeiten neue konzeptionelle und methodische Ansätze zur Pharmakotherapie von Arterienverengung und zu zellbasierten Therapien.

6. Literaturangabe

- 1 MacKay J, M. G. *The Atlas of Heart Disease and Stroke*. (World Health Organization (WHO), 2004).
- 2 Pagidipati, N. J. & Gaziano, T. A. Estimating deaths from cardiovascular disease: a review of global methodologies of mortality measurement. *Circulation* **127**, 749-756, doi:10.1161/CIRCULATIONAHA.112.128413 (2013).
- 3 Vilahur, G. *et al.* Molecular and cellular mechanisms involved in cardiac remodeling after acute myocardial infarction. *Journal of molecular and cellular cardiology* **50**, 522-533, doi:10.1016/j.yjmcc.2010.12.021 (2011).
- 4 Pfeffer, M. A. & Braunwald, E. Ventricular remodeling after myocardial infarction. Experimental observations and clinical implications. *Circulation* **81**, 1161-1172 (1990).
- 5 Lewis, E. F. *et al.* Predictors of late development of heart failure in stable survivors of myocardial infarction: the CARE study. *Journal of the American College of Cardiology* **42**, 1446-1453 (2003).
- 6 Owens, G. K., Kumar, M. S. & Wamhoff, B. R. Molecular regulation of vascular smooth muscle cell differentiation in development and disease. *Physiological reviews* **84**, 767-801, doi:10.1152/physrev.00041.2003 (2004).
- 7 Gruntzig, A. Transluminal dilatation of coronary-artery stenosis. *Lancet* **1**, 263 (1978).
- 8 Serruys, P. W. *et al.* Incidence of restenosis after successful coronary angioplasty: a time-related phenomenon. A quantitative angiographic study in 342 consecutive patients at 1, 2, 3, and 4 months. *Circulation* **77**, 361-371 (1988).
- 9 Poon, M., Badimon, J. J. & Fuster, V. Overcoming restenosis with sirolimus: from alphabet soup to clinical reality. *Lancet* **359**, 619-622 (2002).
- 10 Nobuyoshi, M. *et al.* Restenosis after successful percutaneous transluminal coronary angioplasty: serial angiographic follow-up of 229 patients. *Journal of the American College of Cardiology* **12**, 616-623 (1988).
- 11 Sriram, V. & Patterson, C. Cell cycle in vasculoproliferative diseases: potential interventions and routes of delivery. *Circulation* **103**, 2414-2419 (2001).
- 12 Roubin, G. S. *et al.* Intracoronary stenting for acute and threatened closure complicating percutaneous transluminal coronary angioplasty. *Circulation* **85**, 916-927 (1992).

- 13 Serruys, P. W. *et al.* A comparison of balloon-expandable-stent implantation with balloon angioplasty in patients with coronary artery disease. Benestent Study Group. *The New England journal of medicine* **331**, 489-495, doi:10.1056/NEJM199408253310801 (1994).
- 14 Serruys, P. W. *et al.* Randomized comparison of primary stenting and provisional balloon angioplasty guided by flow velocity measurement. Doppler Endpoints Balloon Angioplasty Trial Europe (DEBATE) II Study Group. *Circulation* **102**, 2930-2937 (2000).
- 15 Sigwart, U., Puel, J., Mirkovitch, V., Joffre, F. & Kappenberger, L. Intravascular stents to prevent occlusion and restenosis after transluminal angioplasty. *The New England journal of medicine* **316**, 701-706, doi:10.1056/NEJM198703193161201 (1987).
- 16 Fischman, D. L. *et al.* A randomized comparison of coronary-stent placement and balloon angioplasty in the treatment of coronary artery disease. Stent Restenosis Study Investigators. *The New England journal of medicine* **331**, 496-501, doi:10.1056/NEJM199408253310802 (1994).
- 17 Elezi, S. *et al.* Vessel size and long-term outcome after coronary stent placement. *Circulation* **98**, 1875-1880 (1998).
- 18 Hoffmann, R. *et al.* Patterns and mechanisms of in-stent restenosis. A serial intravascular ultrasound study. *Circulation* **94**, 1247-1254 (1996).
- 19 Dzau, V. J., Braun-Dullaeus, R. C. & Sedding, D. G. Vascular proliferation and atherosclerosis: new perspectives and therapeutic strategies. *Nature medicine* **8**, 1249-1256, doi:10.1038/nm1102-1249 (2002).
- 20 Bennett, M. R. In-stent stenosis: pathology and implications for the development of drug eluting stents. *Heart* **89**, 218-224 (2003).
- 21 Aikawa, M. *et al.* Redifferentiation of smooth muscle cells after coronary angioplasty determined via myosin heavy chain expression. *Circulation* **96**, 82-90 (1997).
- 22 Morice, M. C. *et al.* A randomized comparison of a sirolimus-eluting stent with a standard stent for coronary revascularization. *The New England journal of medicine* **346**, 1773-1780, doi:10.1056/NEJMoa012843 (2002).
- 23 Coolong, A. & Kuntz, R. E. Understanding the drug-eluting stent trials. *The American journal of cardiology* **100**, 17K-24K, doi:10.1016/j.amjcard.2007.06.004 (2007).
- 24 Yoshida, T. *et al.* Short- and long-term benefits of drug-eluting stents compared to bare metal stents even in treatment for large coronary arteries. *Heart and vessels*, doi:10.1007/s00380-015-0655-3 (2015).

- 25 Alfonso, F., Byrne, R. A., Rivero, F. & Kastrati, A. Current treatment of in-stent restenosis. *Journal of the American College of Cardiology* **63**, 2659-2673, doi:10.1016/j.jacc.2014.02.545 (2014).
- 26 Mayr, U. *et al.* Accelerated arteriosclerosis of vein grafts in inducible NO synthase(-/-) mice is related to decreased endothelial progenitor cell repair. *Circulation research* **98**, 412-420, doi:10.1161/01.RES.0000201957.09227.6d (2006).
- 27 Bai, X. *et al.* Protein kinase C{delta} deficiency accelerates neointimal lesions of mouse injured artery involving delayed reendothelialization and vasohibin-1 accumulation. *Arteriosclerosis, thrombosis, and vascular biology* **30**, 2467-2474, doi:10.1161/ATVBAHA.110.215723 (2010).
- 28 Van Belle, E., Bauters, C., Asahara, T. & Isner, J. M. Endothelial regrowth after arterial injury: from vascular repair to therapeutics. *Cardiovascular research* **38**, 54-68 (1998).
- 29 Pfisterer, M. *et al.* Late clinical events after clopidogrel discontinuation may limit the benefit of drug-eluting stents: an observational study of drug-eluting versus bare-metal stents. *Journal of the American College of Cardiology* **48**, 2584-2591, doi:10.1016/j.jacc.2006.10.026 (2006).
- 30 Bartel, D. P. MicroRNAs: genomics, biogenesis, mechanism, and function. *Cell* **116**, 281-297 (2004).
- 31 Guo, H., Ingolia, N. T., Weissman, J. S. & Bartel, D. P. Mammalian microRNAs predominantly act to decrease target mRNA levels. *Nature* **466**, 835-840, doi:10.1038/nature09267 (2010).
- 32 Huntzinger, E. & Izaurralde, E. Gene silencing by microRNAs: contributions of translational repression and mRNA decay. *Nature reviews. Genetics* **12**, 99-110, doi:10.1038/nrg2936 (2011).
- 33 Bartel, D. P. MicroRNAs: target recognition and regulatory functions. *Cell* **136**, 215-233, doi:10.1016/j.cell.2009.01.002 (2009).
- 34 Torella, D. *et al.* MicroRNA-133 controls vascular smooth muscle cell phenotypic switch in vitro and vascular remodeling in vivo. *Circulation research* **109**, 880-893, doi:10.1161/CIRCRESAHA.111.240150 (2011).
- 35 Liu, X., Cheng, Y., Yang, J., Xu, L. & Zhang, C. Cell-specific effects of miR-221/222 in vessels: molecular mechanism and therapeutic application. *Journal of molecular and cellular cardiology* **52**, 245-255, doi:10.1016/j.yjmcc.2011.11.008 (2012).

- 36 Chan, J. A., Krichevsky, A. M. & Kosik, K. S. MicroRNA-21 is an antiapoptotic factor in human glioblastoma cells. *Cancer research* **65**, 6029-6033, doi:10.1158/0008-5472.CAN-05-0137 (2005).
- 37 Cheng, A. M., Byrom, M. W., Shelton, J. & Ford, L. P. Antisense inhibition of human miRNAs and indications for an involvement of miRNA in cell growth and apoptosis. *Nucleic acids research* **33**, 1290-1297, doi:10.1093/nar/gki200 (2005).
- 38 Calin, G. A. & Croce, C. M. MicroRNA signatures in human cancers. *Nature reviews. Cancer* **6**, 857-866, doi:10.1038/nrc1997 (2006).
- 39 Small, E. M., Frost, R. J. & Olson, E. N. MicroRNAs add a new dimension to cardiovascular disease. *Circulation* **121**, 1022-1032, doi:10.1161/CIRCULATIONAHA.109.889048 (2010).
- 40 van Rooij, E. & Olson, E. N. MicroRNA therapeutics for cardiovascular disease: opportunities and obstacles. *Nature reviews. Drug discovery* **11**, 860-872, doi:10.1038/nrd3864 (2012).
- 41 Mishra, P. K., Tyagi, N., Kumar, M. & Tyagi, S. C. MicroRNAs as a therapeutic target for cardiovascular diseases. *Journal of cellular and molecular medicine* **13**, 778-789, doi:10.1111/j.1582-4934.2009.00744.x (2009).
- 42 Li, Z. & Rana, T. M. Therapeutic targeting of microRNAs: current status and future challenges. *Nature reviews. Drug discovery* **13**, 622-638, doi:10.1038/nrd4359 (2014).
- 43 van Rooij, E., Purcell, A. L. & Levin, A. A. Developing microRNA therapeutics. *Circulation research* **110**, 496-507, doi:10.1161/CIRCRESAHA.111.247916 (2012).
- 44 Janssen, H. L. *et al.* Treatment of HCV infection by targeting microRNA. *The New England journal of medicine* **368**, 1685-1694, doi:10.1056/NEJMoa1209026 (2013).
- 45 Ji, R. *et al.* MicroRNA expression signature and antisense-mediated depletion reveal an essential role of MicroRNA in vascular neointimal lesion formation. *Circulation research* **100**, 1579-1588, doi:10.1161/CIRCRESAHA.106.141986 (2007).
- 46 Wei, Y., Schober, A. & Weber, C. Pathogenic arterial remodeling: the good and bad of microRNAs. *American journal of physiology. Heart and circulatory physiology* **304**, H1050-1059, doi:10.1152/ajpheart.00267.2012 (2013).
- 47 McDonald, R. A., Hata, A., MacLean, M. R., Morrell, N. W. & Baker, A. H. MicroRNA and vascular remodelling in acute vascular injury and pulmonary

- vascular remodelling. *Cardiovascular research* **93**, 594-604, doi:10.1093/cvr/cvr299 (2012).
- 48 Maegdefessel, L. *et al.* Micromanaging abdominal aortic aneurysms. *International journal of molecular sciences* **14**, 14374-14394, doi:10.3390/ijms140714374 (2013).
- 49 Deuse, T. *et al.* Dichloroacetate prevents restenosis in preclinical animal models of vessel injury. *Nature* **509**, 641-644, doi:10.1038/nature13232 (2014).
- 50 Hua, X. *et al.* Human internal mammary artery (IMA) transplantation and stenting: a human model to study the development of in-stent restenosis. *Journal of visualized experiments : JoVE*, e3663, doi:10.3791/3663 (2012).
- 51 Owens, G. K. Regulation of differentiation of vascular smooth muscle cells. *Physiological reviews* **75**, 487-517 (1995).
- 52 Rzucidlo, E. M., Martin, K. A. & Powell, R. J. Regulation of vascular smooth muscle cell differentiation. *Journal of vascular surgery* **45 Suppl A**, A25-32, doi:10.1016/j.jvs.2007.03.001 (2007).
- 53 Gomez, D. & Owens, G. K. Smooth muscle cell phenotypic switching in atherosclerosis. *Cardiovascular research* **95**, 156-164, doi:10.1093/cvr/cvs115 (2012).
- 54 Linn, T. C., Pettit, F. H. & Reed, L. J. Alpha-keto acid dehydrogenase complexes. X. Regulation of the activity of the pyruvate dehydrogenase complex from beef kidney mitochondria by phosphorylation and dephosphorylation. *Proceedings of the National Academy of Sciences of the United States of America* **62**, 234-241 (1969).
- 55 Sutendra, G. & Michelakis, E. D. Pyruvate dehydrogenase kinase as a novel therapeutic target in oncology. *Frontiers in oncology* **3**, 38, doi:10.3389/fonc.2013.00038 (2013).
- 56 Zamzami, N. & Kroemer, G. The mitochondrion in apoptosis: how Pandora's box opens. *Nature reviews. Molecular cell biology* **2**, 67-71, doi:10.1038/35048073 (2001).
- 57 Halestrap, A. P. What is the mitochondrial permeability transition pore? *Journal of molecular and cellular cardiology* **46**, 821-831, doi:10.1016/j.yjmcc.2009.02.021 (2009).
- 58 Bernardi, P. Modulation of the mitochondrial cyclosporin A-sensitive permeability transition pore by the proton electrochemical gradient. Evidence that the pore can be opened by membrane depolarization. *The Journal of biological chemistry* **267**, 8834-8839 (1992).

- 59 Whitehouse, S., Cooper, R. H. & Randle, P. J. Mechanism of activation of pyruvate dehydrogenase by dichloroacetate and other halogenated carboxylic acids. *The Biochemical journal* **141**, 761-774 (1974).
- 60 Roche, T. E. & Hiromasa, Y. Pyruvate dehydrogenase kinase regulatory mechanisms and inhibition in treating diabetes, heart ischemia, and cancer. *Cellular and molecular life sciences : CMLS* **64**, 830-849, doi:10.1007/s00018-007-6380-z (2007).
- 61 Elsasser, A. *et al.* Hibernating myocardium: an incomplete adaptation to ischemia. *Circulation* **96**, 2920-2931 (1997).
- 62 Anversa, P., Li, P., Zhang, X., Olivetti, G. & Capasso, J. M. Ischaemic myocardial injury and ventricular remodelling. *Cardiovascular research* **27**, 145-157 (1993).
- 63 Velagaleti, R. S. *et al.* Long-term trends in the incidence of heart failure after myocardial infarction. *Circulation* **118**, 2057-2062, doi:10.1161/CIRCULATIONAHA.108.784215 (2008).
- 64 Bourassa, M. G. *et al.* Natural history and patterns of current practice in heart failure. The Studies of Left Ventricular Dysfunction (SOLVD) Investigators. *Journal of the American College of Cardiology* **22**, 14A-19A (1993).
- 65 Friedrich, E. B. & Bohm, M. Management of end stage heart failure. *Heart* **93**, 626-631, doi:10.1136/hrt.2006.098814 (2007).
- 66 Rose, E. A. *et al.* Long-term use of a left ventricular assist device for end-stage heart failure. *The New England journal of medicine* **345**, 1435-1443, doi:10.1056/NEJMoa012175 (2001).
- 67 Marcuccilli, L. & Casida, J. J. Overcoming alterations in body image imposed by the left ventricular assist device: a case report. *Progress in transplantation* **22**, 212-216, doi:10.7182/pit2012579 (2012).
- 68 Schaffer, J. M. *et al.* Bleeding complications and blood product utilization with left ventricular assist device implantation. *The Annals of thoracic surgery* **91**, 740-747; discussion 747-749, doi:10.1016/j.athoracsur.2010.11.007 (2011).
- 69 Goldstein, D. J. & Beauford, R. B. Left ventricular assist devices and bleeding: adding insult to injury. *The Annals of thoracic surgery* **75**, S42-47 (2003).
- 70 Livi, U. *et al.* Donor shortage in heart transplantation. Is extension of donor age limits justified? *The Journal of thoracic and cardiovascular surgery* **107**, 1346-1354; discussion 1354-1345 (1994).

- 71 Struck, E., Hagl, S., Meisner, H. & Sebening, F. Heart transplantation: limitations and perspectives. *Zeitschrift fur Kardiologie* **74 Suppl 6**, 59-63 (1985).
- 72 Orlic, D. *et al.* Bone marrow cells regenerate infarcted myocardium. *Nature* **410**, 701-705, doi:10.1038/35070587 (2001).
- 73 Jackson, K. A. *et al.* Regeneration of ischemic cardiac muscle and vascular endothelium by adult stem cells. *The Journal of clinical investigation* **107**, 1395-1402, doi:10.1172/JCI12150 (2001).
- 74 Gneocchi, M. *et al.* Paracrine action accounts for marked protection of ischemic heart by Akt-modified mesenchymal stem cells. *Nature medicine* **11**, 367-368, doi:10.1038/nm0405-367 (2005).
- 75 Perez-Illarbe, M. *et al.* Characterization of the paracrine effects of human skeletal myoblasts transplanted in infarcted myocardium. *European journal of heart failure* **10**, 1065-1072, doi:10.1016/j.ejheart.2008.08.002 (2008).
- 76 Murry, C. E. *et al.* Haematopoietic stem cells do not transdifferentiate into cardiac myocytes in myocardial infarcts. *Nature* **428**, 664-668, doi:10.1038/nature02446 (2004).
- 77 Zhang, J. *et al.* Functional cardiomyocytes derived from human induced pluripotent stem cells. *Circulation research* **104**, e30-41, doi:10.1161/CIRCRESAHA.108.192237 (2009).
- 78 Laurent, L. C. *et al.* Dynamic changes in the copy number of pluripotency and cell proliferation genes in human ESCs and iPSCs during reprogramming and time in culture. *Cell stem cell* **8**, 106-118, doi:10.1016/j.stem.2010.12.003 (2011).
- 79 Gurdon, J. Nuclear reprogramming in eggs. *Nature medicine* **15**, 1141-1144, doi:10.1038/nm1009-1141 (2009).
- 80 Tachibana, M. *et al.* Human embryonic stem cells derived by somatic cell nuclear transfer. *Cell* **153**, 1228-1238, doi:10.1016/j.cell.2013.05.006 (2013).
- 81 Kirak, O. *et al.* Transnuclear mice with predefined T cell receptor specificities against *Toxoplasma gondii* obtained via SCNT. *Science* **328**, 243-248, doi:10.1126/science.1178590 (2010).
- 82 Billingham, R. E., Brent, L. & Medawar, P. B. Actively acquired tolerance of foreign cells. *Nature* **172**, 603-606 (1953).
- 83 Goios, A., Pereira, L., Bogue, M., Macaulay, V. & Amorim, A. mtDNA phylogeny and evolution of laboratory mouse strains. *Genome research* **17**, 293-298, doi:10.1101/gr.5941007 (2007).

- 84 Ridge, P. G. *et al.* Mitochondrial genomic variation associated with higher mitochondrial copy number: the Cache County Study on Memory Health and Aging. *BMC bioinformatics* **15 Suppl 7**, S6, doi:10.1186/1471-2105-15-S7-S6 (2014).

7. Appendix

7.1. Abkürzungen

Anti-21	anti-microRNA-21-Locked-Nucleic-Acid
BMS	Bare Metal Stent
DCA	Dichloracetat
DES	Drug Eluting Stent
ELISPOT	Enzyme Linked Immuno Spot Assay
hMa	Ballondilatierte humane Arterie mammaria interna
IMA	Arteria mammaria interna
iPS	induzierte pluripotente Stammzelle
IFN- γ	Interferon Gamma
IL-4	Interleukin 4
KHK	koronare Herzerkrankung
MHC	Major Histocompatibility Complex
MiHA	Minor Histocompatibility Antigen
miR	microRNA
NT-ESC	Zellkerntransferierte embryonale Stammzelle
OCT	Optische Kohärenztomografie
PDGF	Platelet Derived Growth Factor
PDK	Pyruvat-Dehydrogenase-Kinase
PDH	Pyruvat-Dehydrogenase
PTCA	perkutane transluminale Koronarangioplastie
qRT-PCR	quantitative real-time PCR
SCNT	Somatischer Zellkerntransfer
RNU	T-cell-defiziente Rowett nude Ratten
shRNA	short hairpin RNA
SMemb	Embryonic smooth muscle myosin heavy chain
VSMC	Gefäßmuskelzellen (Vascular Smooth Muscle Cell)
WHO	Weltgesundheitsorganisation
$\Delta\psi$	Mitochondriale Membranpotential

7.2. Publikationen

1. **Wang D**, Deuse T, Stubbendorff M, Chernogubova E, Erben RG, Eken SM, Jin H, Behnisch B, Reichenspurner H, Robbins RC, Tsao PS, Maegdefessel L, Schrepfer S. Local microRNA modulation is feasible: A novel anti-miR- 21-eluting stent prevents in-stent restenosis. **Arteriosclerosis, Thrombosis, and Vascular Biology** 2015 (in Revision).
2. Schmidt-Lucke C, Zobel T, Kühl U, Schrepfer S, **Wang D**, Klingel K, Becher PM, Fechner H, Pozzuto T, Van Linthout S, Lassner D, Spillmann F, Escher F, Holinski S, Volk HD, Schultheiss HP, Tschöpe C. Impaired endothelial regeneration through human parvovirus B19-infected circulating angiogenic cells in cardiomyopathy. **Journal of Infectious Diseases** 2015. Mar 24. pii: jiv178.
3. Deuse T, **Wang D**, Stubbendorff M, Itagaki R, Grabosch A, Greaves LC, Alawi M, Grünewald A, Hu X, Hua X, Velden J, Reichenspurner H, Robbins RC, Jaenisch R, Weissman IL, Schrepfer S. SCNT-Derived ESCs with Mismatched Mitochondria Trigger an Immune Response in Allogeneic Hosts. **Cell Stem Cell**. 2015 Jan 8;16(1):33-8.
4. Deuse T, Hua XQ, **Wang D**, Maegdefessel L, Heeren J, Scheja L, Bolanos JP, Rakovic, SpinJM, Stubbendorff M, Ikeno F, Länger F, Zeller T, Schulte-Uentrop L, Stöhr A, Itagaki R, Haddad F, Eschenhagen T, Blankenberg S, Kiefmann R, Reichenspurner H, Velden J, Klein C, Yeung A, Robbins RC, Tsao PS, Schrepfer S. Dichloroacetate prevents restenosis in preclinical animal models of vessel injury. **Nature**. 2014 May 29; 509(7502): 641-4.

8. Danksagung

Mein herzlichster Dank gilt Frau Prof. Dr. Sonja Schrepfer für die Überlassung des spannenden Themas, der herausragenden kontinuierlichen und immer wieder motivierenden Betreuung und der persönlichen Förderung.

Gleichzeitig möchte ich Herrn Prof. Dr. Tobias Deuse meinen Dank für seine Unterstützung während meiner Arbeit, seiner Diskussionsbereitschaft und seinen wissenschaftlichen Rat aussprechen.

Mein Dank gilt ebenso Frau Christiane Pahrman, Dr. Xiaoqin Hua und Dr. Mandy Stubbendorff und allen Mitarbeitern des Transplantation und Stammzell Immunbiologie Labors für die freundliche Anleitung, Unterstützung und Hilfeleistung bei meiner Arbeit.

Des Weiteren möchte ich mich für die Unterstützung durch den Cardiovascular Research Center (CVRC) Hamburg und dem Deutschen Zentrum für Herz-Kreislauf-Forschung (DZHK) bedanken.

Meinen Eltern danke ich von ganzem Herzen für all ihre Liebe, Unterstützung und Förderung, ohne die ich nicht derjenige wäre, der ich heute bin. Auch möchte ich mich bei meinem Bruder bedanken für seine Anregungen, Kritik und Geduld.

9. Eidesstattliche Erklärung

Hiermit versichere ich, dass ich die Arbeit selbständig und ohne fremde Hilfe verfasst, andere als die von mir angegebenen Quellen und Hilfsmittel nicht benutzt und die aus den benutzten Werken wörtlich oder inhaltlich entnommenen Stellen einzeln nach Ausgabe (Auflage und Jahr des Erscheinens), Band und Seite des benutzten Werkes kenntlich gemacht habe.

Ferner versichere ich, dass ich die Dissertation bisher nicht einem Fachvertreter an einer anderen Hochschule zur Überprüfung vorgelegt oder mich anderweitig um Zulassung zur Promotion beworben habe.

Ich erkläre mich einverstanden, dass meine Dissertation vom Dekanat der Medizinischen Fakultät mit einer gängigen Software zur Erkennung von Plagiaten überprüft werden kann.

Hamburg, den 01.04.2015



Dong Wang

Local microRNA modulation using a novel anti-miR-21-eluting stent effectively prevents in-stent restenosis

Dong Wang^{1,2}, Tobias Deuse^{1,2,3}, Mandy Stubbendorff^{1,2}, Ekaterina Chernogubova⁴, Reinhold G. Erben⁵, Suzanne M. Eken⁴, Hong Jin⁴, Yuhuang Li⁴, Christian H. Heeger⁶, Boris Behnisch⁷, Hermann Reichenspurner³, Robert C. Robbins⁸, Joshua M. Spin⁹, Philip S. Tsao⁹, Sonja Schrepfer^{1,2,8*} and Lars Maegdefessel^{4*}

¹TSI-laboratory, University Heart Center Hamburg, Martinistraße 52, 20246 Hamburg, Germany. ²Cardiovascular Research Center Hamburg (CVRC) and DZHK (German Center for Cardiovascular Research), partner site Hamburg/Kiel/Luebeck, University Medical Center Hamburg-Eppendorf, Martinistraße 52, 20246 Hamburg, Germany. ³Cardiovascular Surgery, University Heart Center Hamburg, Martinistraße 52, 20246 Hamburg, Germany. ⁴Department of Medicine, Atherosclerosis Research Unit, Karolinska Institute, CMM L8:03, 17176 Stockholm, Sweden. ⁵University of Veterinary Medicine, Vienna, Austria. ⁶Department of Cardiology Asklepios Clinic St. Georg, Hamburg, Germany. ⁷Translumina GmbH, Hechingen, Germany. ⁸Department of Cardiothoracic Surgery and Stanford Cardiovascular Institute, Stanford University, 300 Pasteur Drive, 94305 Stanford, California, USA. ⁹Veterans Affairs Palo Alto Health Care System, 3801 Miranda Avenue, 94304 Palo Alto, California, USA and Stanford Cardiovascular Institute, Stanford University, 300 Pasteur Drive, 94305 Stanford, California, USA.

* authors share senior authorship

Running title: Local mir-21 inhibition prevents restenosis

Corresponding author:

Prof. Dr. med. Sonja Schrepfer
University Heart Center Hamburg
Transplant and Stem Cell Immunobiology Lab (TSI)
Campus Forschung (N27), Martinistr. 52
20246 Hamburg
Germany
phone: +49-40-7410-59982
fax: +49-40-7410-59663
e-mail: schrepfer@stanford.edu

Key words: Myointimal hyperplasia, restenosis, microRNA, local drug delivery, rat, humanized model

Subject Codes:

[116] Restenosis
[130] Animal models of human disease
[162] Vascular Biology: Smooth muscle proliferation and differentiation

Word count: 3958 words; 4 figures in main manuscript

TOC category: Basic studies

TOC subcategory: Vascular Biology

Abstract

Despite advances in stent technology for vascular interventions, in-stent restenosis (ISR) due to myointimal hyperplasia (MH) remains a major complication. We investigated the regulatory role of microRNAs (miRNAs) in MH/ISR utilizing a humanized animal model, in which balloon-injured human internal mammary arteries (IMAs) with or without stenting were transplanted into RNU rats, followed by miRNA profiling. miR-21 was the only significantly up-regulated candidate known to be associated with vascular pathology. We systemically repressed miR-21 via intravenous FAM-tagged-LNA-anti-miR-21 (anti-21) in our humanized MH-model. Suppression of vascular miR-21 correlated dose-dependently with reduced luminal obliteration. Further, anti-21 did not impede re-endothelialization. However, systemic anti-miR-21 had substantial off-target effects, lowering miR-21 levels in liver, heart, lung, and kidney while increasing serum creatinine. We therefore assessed the feasibility of local miR-21 suppression using anti-21-coated stents. When compared to bare metal stents, anti-21-coated stents effectively reduced ISR, and we observed no significant off-target effects. This is the first study to demonstrate efficacy of an anti-miR-coated stent for the reduction of ISR.

Abbreviations

BMS: bare metal stent
DES: drug eluting stent
ECM: extracellular matrix
FAM: fluorescein
hCA: human coronary artery
HD: high dose
HLA I: human leukocyte antigen I
hMA: humanized mammary artery model
IMA: internal mammary artery
ISH: in situ hybridization
ISR: in-stent-restenosis
LD: low dose
LNA: locked nucleic acid
MH: myointimal hyperplasia
MHC I: major histocompatibility complex I
miR: microRNA
miRNA: microRNA
mRNA: messenger RNA
OCT: optical coherence tomography
PDGF: platelet derived growth factor
qRT-PCR: quantitative real time polymerase chain reaction
RNU: Rowett nude (rats)
SMA: smooth muscle cell α -actin
VSMC: vascular smooth muscle cell

Materials and Methods

Materials and Methods are available in the online-only Supplement.

Introduction

Cardiovascular disease is often characterized by myointimal hyperplasia (MH), with vascular smooth muscle cell (VSMC) de-differentiation, augmented proliferation and migration, and increased synthesis of extracellular matrix (ECM), with progressively decreasing vessel lumen¹. VSMC phenotypic switching occurs in response to various stimuli, including growth factors, cytokines, oxidized lipids, and changes in local environment, and is accompanied by gene expression changes, hyperpolarized mitochondria, and an imbalanced replication-apoptosis ratio^{2,3}. Mitigation of VSMC phenotypic switching may alleviate myointimal hyperplasia, and resultant obliterative vascular processes, like in-stent restenosis (ISR).

MicroRNAs (miRNAs) are small, endogenous antisense RNAs that regulate gene expression typically via mRNA degradation or translational repression⁴. miRNA manipulation can lead to broad alterations in regulatory pathways at multiple levels, as a single miRNA is capable of binding multiple mRNAs. These effects can be cell type- or tissue-specific. Previous studies suggest that miRNAs are critically involved in MH and ISR⁵. Modulation of various miRNAs can inhibit myointimal growth, suggesting a therapeutic approach for vascular disease^{5,6}.

Most *in vivo* studies examining MH have utilized rodent models, and systemic miRNA modulation which carries risks of off-target effects⁷. In order to increase translational potential, we decided to utilize our previously described orthotopic transplant model^{3,8}, and now report a novel strategy for local anti-miRNA (-21) delivery engaging coatable drug eluting stents (DES).

Results

miR-21 is up-regulated during myointima formation

Balloon-injured human IMAs were implanted into the abdominal aortic position of athymic RNU rats (hMA model) to study MH. In a second cohort, each IMA had a single bare metal stent (BM-stent model) deployed prior to implantation. Ten days post-implantation we retrieved the IMAs from both groups (denoted hMA₁₀ and BM-stent₁₀, respectively) and measured tissue expression of eight miRNAs previously shown to be associated with vascular (patho-)physiology and VSMC plasticity (miR-1, -21, -29b, -133a, -143, -145, -221, and -222)^{6,9}. Non-denuded native hMAs served as controls ("native"). Significant changes in miRNA expression were detected for all except one (miR-221) (Fig. 1A and Fig. S1). All other miRNAs were down-regulated except for miR-21 (significantly up-regulated). miRNA expression levels were similar in the hMA₁₀ and BM-stent₁₀ groups for all miRNAs measured. miR-21 expression was low in native hMA, and healthy human coronary arteries (hCA_{healthy}), while previously-stented, diseased human coronary arteries (hCA_{stent}) had similar miR-21 levels to the hMA₁₀/BM-stent₁₀ groups (Fig. 1A), suggesting that our humanized *in vivo* models closely mimic human ISR. As miR-21 was up-regulated, it appeared distinctly suitable for anti-miR-based therapeutic modulation.

SMA-positive myointimal cells in the hMA model co-localized with HLA I and did not express rat MHC I (Fig. 1B), confirming human myointimal origin. SMemb (VSMC de-differentiation marker), and SM heavy chain (VSMC-specific marker) were found in the myointima of hMA₂₈ vessels (immunofluorescence; Fig. 1C), as was miR-21 in

comparison to untreated control human coronary arteries when analyzed by *in situ* hybridization (ISH; Fig. 1D). miR-21 was approximately 4-fold up-regulated in injured human arteries, and abundantly expressed in the VSMC-rich human myointima.

Systemic miR-21 repression

We sought to inhibit miR-21 in the hMA model through systemic administration. RNU rats received one intravenous dose of either 1mg/kg anti-21 in the low-dose (LD) or 5mg/kg anti-21 in the high-dose (HD) group one day after hMA implantation. Vessels were retrieved after 28 days for histologic evaluation (Fig. 2A). Untreated hMA₂₈ arteries showed a circular, cell-rich myointima with increased extracellular matrix deposition. Myointimal area was reduced in both anti-21 treatment groups, an effect that was markedly more pronounced with HD treatment.

Confocal immunofluorescence staining revealed similar composition of the myointimas in all of the above groups (Fig. 2B). Double immunofluorescence staining against SMA and FAP showed high myointimal SMC content with fibroblastic cells indicating an area of active tissue remodeling. Quantification of luminal obliteration confirmed significantly more luminal preservation in the anti-21 HD group compared to both untreated controls and the anti-21 LD group (Fig. 2C). Effective knockdown of miR-21 in the hMA vessels with anti-21 HD treatment was confirmed by qRT-PCR (Fig. 2D).

We next evaluated miR-21 off-target knockdown in other organs. As expected, we observed significant reduction of miR-21 expression in the kidneys (Fig. 2E), as well as liver, heart, and lungs (Fig. S2A). While other measured serum markers did not change significantly, creatinine elevation coincided with kidney miR-21 repression, indicating that systemic anti-21 HD administration can negatively affect kidney function (Fig. 2F). As the LNA-antisense was FAM-tagged, we were able to demonstrate (by fluorescence imaging) heavy renal accumulation of systemically-delivered anti-21 (Fig. 2G). This potentially kidney-specific toxic side effect of anti-21 should be taken into account when considering translational systemic miR-21 inhibition.

Local miR-21 repression using anti-21-eluting stents

To minimize the above-noted off-target effects, we coated stents with anti-21 to permit local delivery to the injured hMA vessels. Successful stent coating with anti-21 was confirmed by FAM fluorescence and scanning electron microscopy (Fig. S3). The total anti-21 amount coated onto each stent was similar to the systemic HD dosage (5mg/kg). Anti-21-stents were compared with otherwise-identical BM-stents in the humanized model, and ISR was assessed after 28 days. Trichrome staining revealed marked myointima formation within the BM-stent lumen, and much reduced myointima in anti-21-stented hMA (Fig. 3A). Fixation and cutting protocols for stented vessels necessitated stent strut removal, leaving gaps adjacent to the internal elastic lamina. Despite this, ISR was clearly decreased in the anti-21-stent group by histological quantification (Fig. 3B). Optical coherence tomography (OCT) images obtained immediately after vessel retrieval and prior to fixation also showed markedly smaller myointimal growth within the anti-21-stent₂₈ lumen (Movie S1, Fig. 3C). Quantification of miR-21 expression in stented vessels was not technically feasible. Screening for off-target regulation did not reveal miR-21 expression changes in kidney (Fig. 3D), liver, heart, or lung (Fig. S2B). Further, serum creatinine was unaffected by anti-21-stent placement (Fig. 3E) and fluorescence confirmed no accumulation of anti-21 in the kidneys (Fig. 3F).

Anti-21 does not affect re-endothelialization

We investigated whether anti-21 affects re-endothelialization of balloon-injured arteries. Lewis rats underwent balloon injury of their abdominal aortas and received a single dose of anti-21 HD intravenously or remained untreated. After 28 days, endothelial cell (EC)-specific RECA-1 staining revealed near complete re-endothelialization in both groups (Fig. 4A-B). We also performed organ chamber experiments to assess the functional capacity of the regenerated endothelium to regulate vasodilatation (Fig. 4C). Both control and anti-21-treated aortas showed similar endothelial-dependent and -independent relaxation characteristics. Together, these results indicate that re-growth of functionally intact endothelium in denuded arteries occurs despite anti-21 treatment.

Of importance, *in vitro* proliferation of human coronary artery ECs (hCAECs) remained unaffected by anti-21 after applying either serum starvation or PDGF treatment (Fig. 4D-E). Interestingly, forced overexpression of miR-21 (pre-21 treatment) significantly increased MTT assay-detected EC proliferation (in comparison to scr-miR and anti-21; Fig. 4D-E), indicating a less prominent regulatory effect of miR-21 inhibition in vascular ECs, an effect that was previously reported by others as well^{5, 10}.

Anti-21 inhibits proliferation of smooth muscle cells ex vivo and in vitro

To confirm the observed anti-proliferative effect of miR-21 repression on SMCs *in vivo*, we stimulated fresh pieces of JMA with platelet derived growth factor (PDGF), an important driving factor for MH¹¹ and miR-21 up-regulation in SMCs¹² and fibroblasts¹³. PDGF not only increased miR-21 expression (Fig. 4F), but also decreased PTEN (Fig. 4G), a well-established target gene of miR-21 in vascular remodeling⁵. Simultaneous anti-21 treatment diminished PDGF-mediated PTEN suppression, confirming the intermediary role of miR-21 (Fig. 4G). Inhibition of miR-21 abolished the pro-proliferative effect of PDGF and serum starvation on human coronary artery SMCs, whereas miR-21 overexpression substantially induced the pro-proliferative response (Fig. 4H-I).

Discussion

Despite advances in device technology, the prevention of ISR remains challenging. BM stents are still widely used during percutaneous coronary interventions, particularly if extended-duration dual anti-platelet therapy is high-risk. This despite the increased rate of ISR, especially when utilized for complex pathologic lesions¹⁴. Anti-proliferative drug-eluting stents (DES) substantially decrease ISR. However, ISR occurring late after DES placement remains a significant problem. Further, DES are associated with delayed re-endothelialization and prolonged stent thrombogenicity. New agents that permit local delivery but avoid the above drawbacks would be appealing¹⁴.

Numerous miRNAs play a role in the proliferative mechanism of vascular disease. Of the miRNA candidates assessed in this study, all except for one miRNA (miR-221) were substantially altered in both injured (hMA group) and stented hMAs (BM-stent group). Of importance for treatment consideration, miR-21 was the only miRNA that was significantly up-regulated in response to injury. Such miRNAs are often amenable to antisense oligonucleotide (anti-miR) inhibition. While LNA-based miRNA-mimics are becoming available, traditional delivery has involved lenti- or adenoviral approaches, presenting risks common to gene therapy¹⁵. Some studies

from the cancer field have explored packaging synthetic miRNA duplexes within lipid nanoparticles in murine models¹⁶.

A major difference between the classical pharmacologic approach, and the novel field of miRNA-modulation is that the latter may regulate entire gene or protein networks⁶. Recent animal and human efficacy data are promising, suggesting that anti-miRs have the potential to become a new class of drugs^{17,18}. Anti-miRs have several advantages for drug development, including their small molecular size and the frequent conservation of their target miRNAs across species⁴. Using lessons learned from siRNA technologies, potent oligonucleotide anti-miR agents are currently being developed¹⁹. Regarding the use of anti-miRs in humans, there have been no immunogenic or toxicological safety issues reported to date²⁰.

miR-21 is considered to be among the most readily inducible vascular miRNAs, associated with increased cell proliferation and decreased apoptosis in the vessel wall^{21,10}. In a previous study, antisense-mediated inhibition of miR-21 using pluronic gel reduced myointima in balloon-injured rat carotid arteries⁵. The authors showed that PTEN and Bcl-2 up-regulation were involved in anti-miR-21-mediated cellular effects⁵. Similarly, in vein graft failure studies, miR-21 was significantly up-regulated following engraftment in mouse, pig, and human models. Genetic deletion of miR-21 in mice and grafted veins limited the proliferative response and reduced myointima formation²².

Our anti-21-eluting stent was highly effective in reducing VSMC proliferation and alleviating myointimal hyperplasia and ISR. Importantly, we did not observe miR-21 suppression in other organs, nor did we observe off-target side effects with this approach. Anti-21, in contrast to the currently employed DES medications such as rapamycin²³, did not delay vessel re-endothelization, a side effect believed to be a major cause of stent thrombosis and late ISR¹⁴. In our study, systemic anti-21 allowed re-coverage of balloon-injured rat aortas with functionally intact endothelium. Further, anti-21 did not inhibit EC proliferation *in vitro*. This was most likely due to the very low expression of miR-21 in the endothelium compared to the VSMC-enriched myointima and vessel media¹⁰.

We believe this proof-of-concept study for the efficacy and safety of anti-21-eluting stents demonstrates the feasibility of this approach. The method could potentially be optimized by modulating the release kinetics and dosing of the anti-miR, or potentially by combining multiple anti-miRs on a single stent. Future trials should address these issues, as well as its long-term efficacy in preventing the occurrence of late ISR.

Acknowledgements

We thank Christiane Pahrman, Claudia Bergow and Hartwig Wieboldt for their technical assistance. We also thank Martin W. Bergmann for his support with the OCT videos. Special thanks to Ethicon for providing the suture material. The confocal images were taken at the umif, University Medical Center Hamburg-Eppendorf (Bernd Zobiak).

Sources of funding

D.W. received a graduate student stipend "Individualized Cardiovascular Medicine" from the Cardiovascular Research Center (CVRC) at the University Medical Center Hamburg-Eppendorf and a student stipend from the German Center for Cardiovascular Research (DZHK), partner site Hamburg/Kiel/Luebeck. T.D. received the Else Kröner Excellence Stipend from the Else-Kröner-Fresenius-Stiftung (2012_EKES.04). S.S. received research grants from the Fondation Leducq (CDA 2013-2015; S.S.) and the Deutsche Forschungsgemeinschaft (DFG) (SCHR992/3-1, SCHR992/4-1). L.M. is a Ragnar Söderberg fellow in Medicine (M-14/55), and received funding from the Karolinska Institute Cardiovascular Program Career Development Grant and the Swedish Heart-Lung-Foundation (20120615, 20130664, 20140186).

Disclosures

None.

in revision ATVB

References

1. Powell JS, Rouge M, Muller RK, Baumgartner HR. Cilazapril suppresses myointimal proliferation after vascular injury: Effects on growth factor induction in vascular smooth muscle cells. *Basic research in cardiology*. 1991;86 Suppl 1:65-74
2. Aikawa M, Sakomura Y, Ueda M, Kimura K, Manabe I, Ishiwata S, et al. Redifferentiation of smooth muscle cells after coronary angioplasty determined via myosin heavy chain expression. *Circulation*. 1997;96:82-90
3. Deuse T, Hua X, Wang D, Maegdefessel L, Heeren J, Scheja L, et al. Dichloroacetate prevents restenosis in preclinical animal models of vessel injury. *Nature*. 2014;509:641-644
4. Bartel DP. Micrnas: Genomics, biogenesis, mechanism, and function. *Cell*. 2004;116:281-297
5. Ji R, Cheng Y, Yue J, Yang J, Liu X, Chen H, et al. Microrna expression signature and antisense-mediated depletion reveal an essential role of microrna in vascular neointimal lesion formation. *Circulation research*. 2007;100:1579-1588
6. Small EM, Frost RJ, Olson EN. Micrnas add a new dimension to cardiovascular disease. *Circulation*. 2010;121:1022-1032
7. Maegdefessel L, Spin JM, Adam M, Raaz U, Toh R, Nakagami F, et al. Micromanaging abdominal aortic aneurysms. *International journal of molecular sciences*. 2013;14:14374-14394
8. Hua X, Deuse T, Michelakis ED, Haromy A, Tsao PS, Maegdefessel L, et al. Human internal mammary artery (ima) transplantation and stenting: A human model to study the development of in-stent restenosis. *Journal of visualized experiments : JoVE*. 2012:e3663
9. Wei Y, Schober A, Weber C. Pathogenic arterial remodeling: The good and bad of micrnas. *American journal of physiology. Heart and circulatory physiology*. 2013;304:H1050-1059
10. Maegdefessel L, Azuma J, Toh R, Deng A, Merk DR, Raiesdana A, et al. Microrna-21 blocks abdominal aortic aneurysm development and nicotine-augmented expansion. *Science translational medicine*. 2012;4:122ra122
11. Sirois MG, Simons M, Edelman ER. Antisense oligonucleotide inhibition of pdgfr-beta receptor subunit expression directs suppression of intimal thickening. *Circulation*. 1997;95:669-676
12. Alshanwani A, Riches K, Wood I, Turner N, Porter K. 168 exploring the role of microrna-21 on human saphenous vein smooth muscle cell function. *Heart*. 2014;100 Suppl 3:A96
13. Polajeva J, Swartling FJ, Jiang Y, Singh U, Pietras K, Uhrbom L, et al. Mirna-21 is developmentally regulated in mouse brain and is co-expressed with sox2 in glioma. *BMC cancer*. 2012;12:378
14. Alfonso F, Byrne RA, Rivero F, Kastrati A. Current treatment of in-stent restenosis. *Journal of the American College of Cardiology*. 2014
15. Mishra PK, Tyagi N, Kumar M, Tyagi SC. Micrnas as a therapeutic target for cardiovascular diseases. *Journal of cellular and molecular medicine*. 2009;13:778-789
16. Trang P, Wiggins JF, Daige CL, Cho C, Omotola M, Brown D, et al. Systemic delivery of tumor suppressor microrna mimics using a neutral lipid emulsion inhibits lung tumors in mice. *Molecular therapy : the journal of the American Society of Gene Therapy*. 2011;19:1116-1122

17. van Rooij E, Olson EN. MicroRNA therapeutics for cardiovascular disease: Opportunities and obstacles. *Nature reviews. Drug discovery*. 2012;11:860-872
18. Janssen HL, Reesink HW, Lawitz EJ, Zeuzem S, Rodriguez-Torres M, Patel K, et al. Treatment of hcv infection by targeting microRNA. *The New England journal of medicine*. 2013;368:1685-1694
19. van Rooij E, Purcell AL, Levin AA. Developing microRNA therapeutics. *Circulation research*. 2012;110:496-507
20. Li Z, Rana TM. Therapeutic targeting of microRNAs: Current status and future challenges. *Nature reviews. Drug discovery*. 2014
21. Wang M, Li W, Chang GQ, Ye CS, Ou JS, Li XX, et al. MicroRNA-21 regulates vascular smooth muscle cell function via targeting tropomyosin 1 in arteriosclerosis obliterans of lower extremities. *Arteriosclerosis, thrombosis, and vascular biology*. 2011;31:2044-2053
22. McDonald RA, White KM, Wu J, Cooley BC, Robertson KE, Halliday CA, et al. Mirna-21 is dysregulated in response to vein grafting in multiple models and genetic ablation in mice attenuates neointima formation. *European heart journal*. 2013;34:1636-1643
23. Chen BX, Ma FY, Luo W, Ruan JH, Xie WL, Zhao XZ, et al. Neointimal coverage of bare-metal and sirolimus-eluting stents evaluated with optical coherence tomography. *Heart*. 2008;94:566-570

Significance

microRNA-based therapeutics have the potential of becoming a whole new class of drugs. However, the systemic form of their administration carries a substantial risk for off-target effects on organ systems, in which these modulators assimilate to a much higher extent than the targeted tissue, such as the vasculature in our case. The utilization of local forms of delivery, such as drug eluting stents could significantly elevate the therapeutic potential of microRNA modulation in cardiovascular pathologies.

Figure legends

Figure 1. MiR-21 is involved in human myointima hyperplasia. (A) Human IMAs underwent either balloon denudation (hMA), or denudation and stenting (BM-stent) and were implanted into the abdominal aortic position of RNU rats to await myointima development. After 10 days, qRT-PCR measurement of miR-21 revealed significant overexpression in both hMA and BM-stent groups as compared to native IMA (n=10 (native), n=6 (hMA), n=6 (BM-stent), ANOVA with Bonferroni's post-hoc test). Likewise, miR-21 levels in diseased, stented human coronary artery (hCA_{stent} n=5;) were similarly altered vs. normal vessels (hCA_{healthy} n=4; unpaired t-test). (B) Human origin of myointimal cells in the hMA model was confirmed by double-positive immunofluorescence staining for SMA and human leukocyte antigen class I (HLA I) and the lack of rat major histocompatibility complex class I (rat MHC I). (C) Smooth muscle cells (SMC) within the myointima of hMA₂₈ showed expression of SMemb and/or SM heavy chain. Synthetic, SMemb positive cells were distributed more in neo-myointimal regions and SM-heavy chain positive, contractile SMCs were found near the elastic laminae. (D) Presence of miR-21 in myointimal lesions of hMA₁₀ confirmed by *in situ hybridization* in comparison to uninjured healthy human coronary arteries (hCA_{healthy}; purple chromagen). † p<0.01.

Figure 2. Systemic modulation of miR-21 inhibits myointima development, but causes off-target effects. (A) To assess the effect of miR-21 modulation on myointimal hyperplasia, 1mg/kg (LD), 5mg/kg (HD) anti-miR-21 (anti-21) or vehicle were injected intravenously one day post-IMA-implantation. After 28 days, hMA-vessels were excised and stained with Masson's Trichrome. (B) Double immunofluorescence staining against SMA and FAP-alpha demonstrates similar myointimal composition in all groups. (C) Analysis of hMA vessels revealed marked luminal obliteration in the non-treated group, while anti-21-treated vessels showed less obliteration in a dose dependent manner (mean ± s.d., n=7 animals per group, ANOVA with Bonferroni's post-hoc test). (D) Sufficient inhibition of miR-21 in hMA vessel through anti-21 was confirmed by qRT-PCR. (mean ± s.d., n=7 (hMA), n=6 (anti-21 LD), n=6 (anti-21 HD), ANOVA with Bonferroni's post-hoc test). (E) Systemic miR-21 inhibition caused marked reduction of miR-21 expression in kidneys (mean ± s.d., n=6 (hMA), n=7 (anti-21 LD), n=7 (anti-21 HD), ANOVA with Bonferroni's post-hoc test). (F) This correlated with an increase in creatinine (mean ± s.d., n=7 animals per group, ANOVA with Bonferroni's post-hoc test). (G) Injected anti-21 was tracked via fluorescence imaging. High fluorescence signal was detected in HD-treated rat kidneys, indicating an accumulation of anti-21 (left: photo picture; right: overlay picture with fluorescence signal). * p<0.05, † p<0.01.

Figure 3. Local inhibition of miR-21 prevents myointima development without exerting off-target effects. (A) For local miR-21 inhibition, anti-21-coated stents were expanded into denuded IMAs, which were then implanted into RNU rats. Histological sections of stented vessel stained with Masson's Trichrome are shown 28 days after implantation. (B) Anti-21-stent coating resulted in significantly less luminal obliteration compared to the BM-stent group (mean± s.d., n=8 (BM-stent), n=6 (anti-21-stent), unpaired t-test). (C) OCT images revealed considerably less myointima formation in the anti-21-stent group (white arrow marks a stent strut, luminal side is to the right). (D) miR-21 levels in kidneys were not affected by anti-21-coated stent delivery (mean± s.d., n=6 per group, unpaired t-test) and (E) serum

creatinine showed no significant difference between the BM-stent and anti-21-stent groups (mean± s.d., n=8 (BM-stent), n=6 (anti-21-stent), unpaired t-test). (F) In fluorescence imaging, similar signals were detected in both groups (left: photo picture; right: overlay picture with fluorescence signal). † p<0.01.

Figure 4. Anti-21 treatment does not impair re-endothelialization and abolishes stimulatory proliferative effects on SMCs in vitro. (A) To assess the effect of anti-21 on vessel re-endothelialization, rat aortas underwent endothelial denudation via balloon injury. Animals in the treatment group received 5mg/kg anti-21 intravenously one day post-denudation. After 28 days, vessels were recovered and stained for endothelial cells. (B) There were no relevant differences in endothelial coverage between control₂₈ and anti-21₂₈ (mean± s.d., n=5 per group, unpaired t-test). (C) Endothelial function was assessed in organ chamber experiments (mean± SEM, n=6 (control₂₈), n=6 (anti-21 HD₂₈), n=3 (control₃)). All three groups showed similar endothelial-independent relaxation characteristics, when stimulated with nitroglycerine. In contrast, stimulation with acetylcholine had no effect 3 days after vessel injury, while both control₂₈ and anti-21 HD₂₈ groups showed similar physiologic endothelial-dependent relaxation. (D) Proliferation assays with hCAECs after PDGF or 48h serum starvation (E) treatment revealed a negligible effect of miR-21 inhibition on EC proliferation (mean± s.d., quadruplicates of 3 independent experiments, unpaired t-test). (F) To determine the effect of PDGF on miR-21 expression in vessels, fresh pieces of IMA were stimulated with PDGF. 24h post-stimulation, miR-21 expression was significantly elevated (mean± s.d., n=6 (control), n=10 (PDGF), unpaired t-test) (G), while PTEN expression was suppressed. Concurrent transfection with anti-21 abolished this effect (mean± s.d., n=5 (control), n= 5 (PDGF), n=4 (PDGF+anti-21), ANOVA with LSD post-hoc test). (H) Inhibition of miR-21 with anti-21 caused diminished proliferation in PDGF-stimulated hCASCs and (I) after 48h of serum starvation (mean± s.d., quadruplicates of 3 independent experiments, unpaired t-test). * p<0.05, † p<0.01.

Figures

Figure 1.

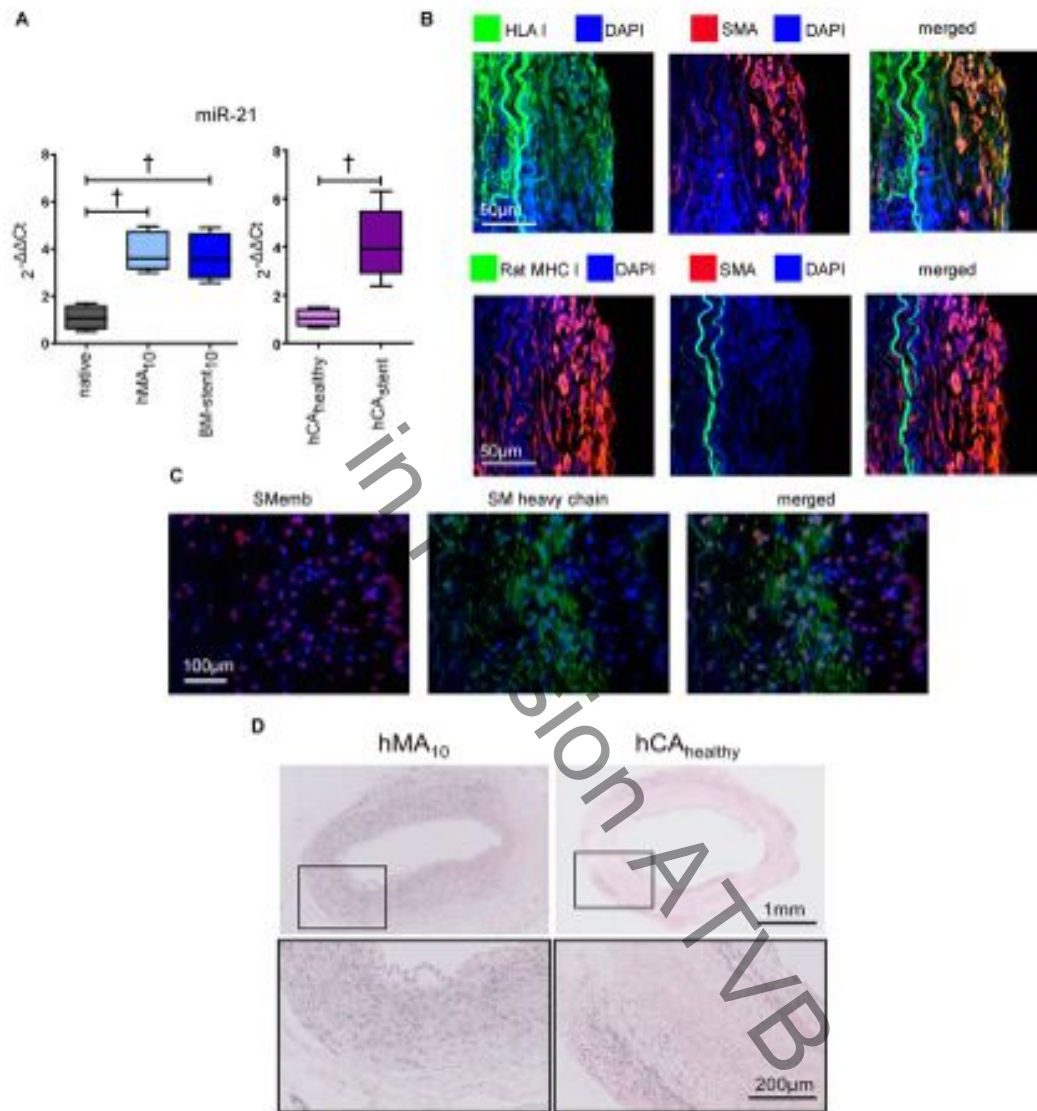


Figure 2.

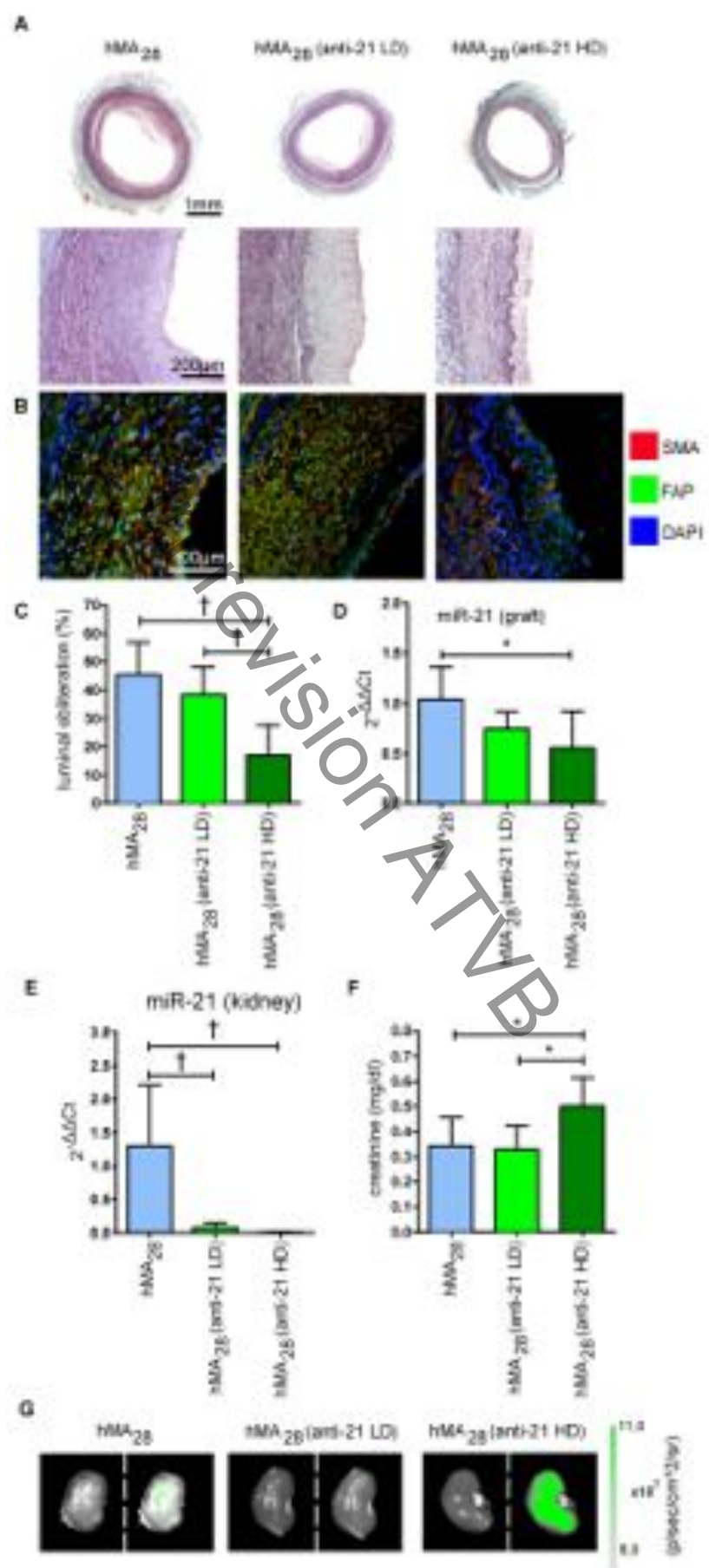


Figure 3.

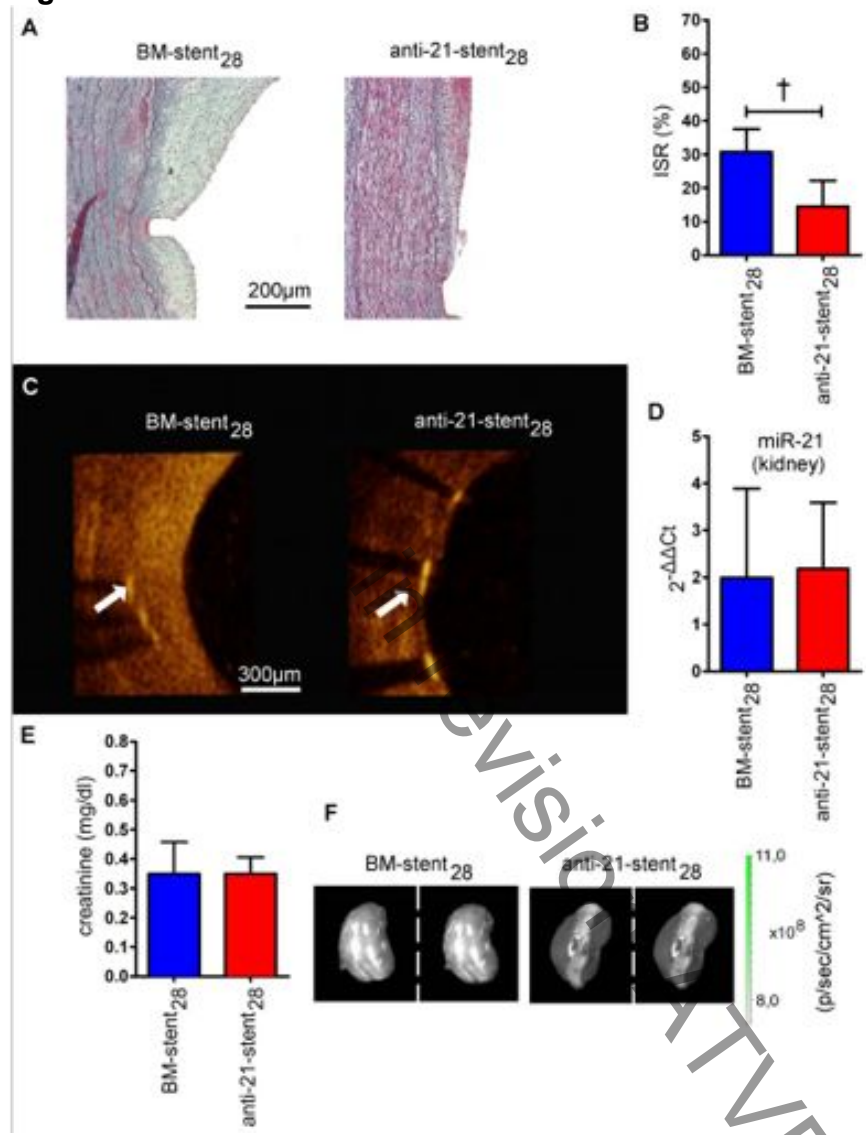
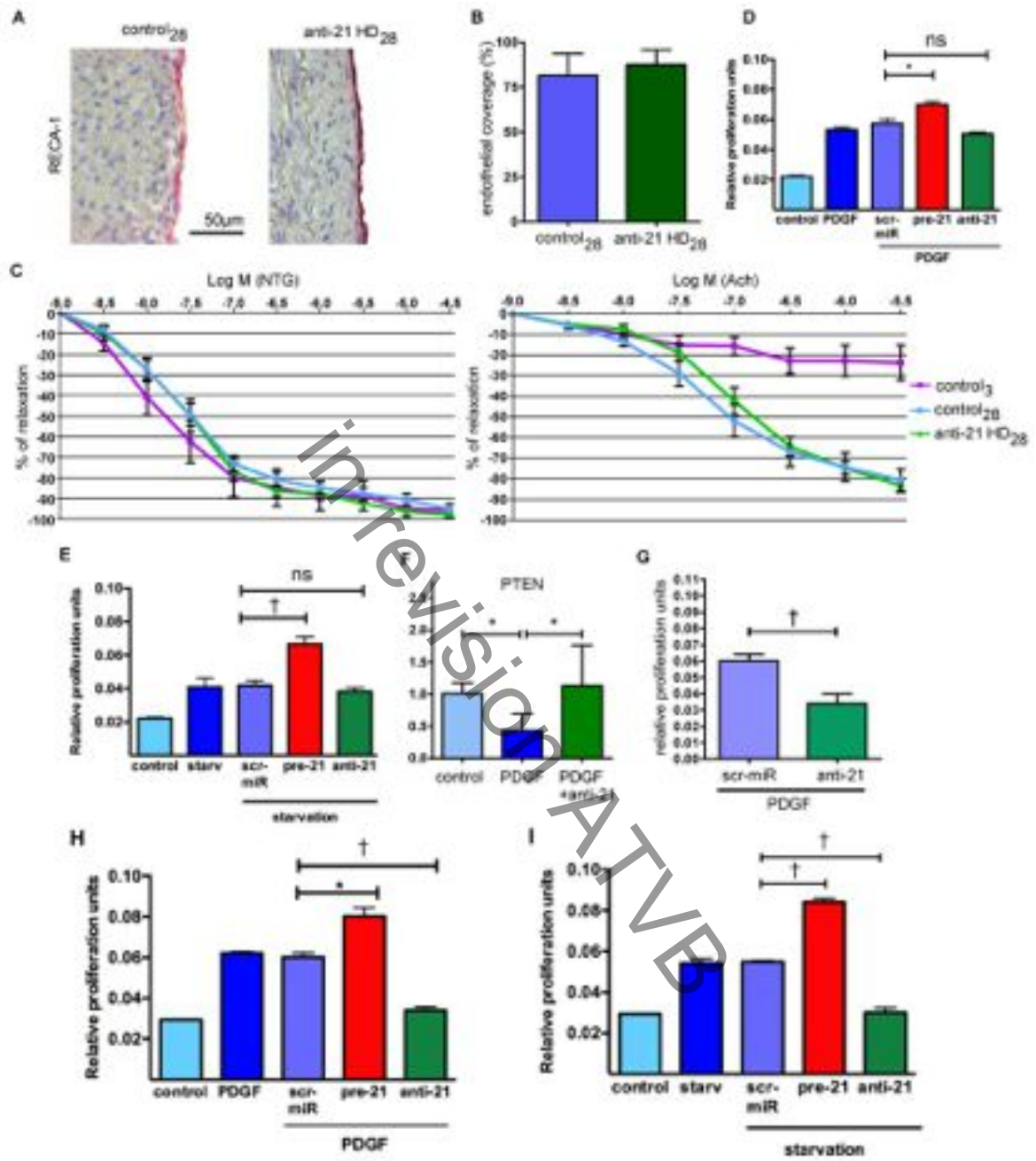


Figure 4.



Materials and Methods (Supplement Only)

Human sample acquisition

Remnant segments of human internal mammary arteries (IMAs) from routine coronary artery bypass surgeries, and stented coronary vessels retrieved from explanted native hearts of heart transplant recipients were obtained. Their use for research was approved by the Institutional Review Board (IRB), and patients gave written informed consent.

Rats

Male athymic RNU-rats (CrI:NIH-Foxn1^{nu}) and Lewis rats were purchased from Charles River (Sulzfeld, Germany). Animals were housed in the animal care facilities of the University Hospital Hamburg-Eppendorf and received humane care in compliance with the Guide for the Principles of Laboratory Animals, prepared by the Institute of Laboratory Animal Resources, and published by the National Institutes of Health. All animal protocols were approved by the local authority ("Amt für Gesundheit und Verbraucherschutz, Hansestadt Hamburg").

Humanized mammary artery denudation (hMA) and stent implantation model

IMA endothelium was removed by balloon injury using a 2-French (Fr) Fogarty catheter (Suppl. Fig. 3B) as described before^{1,2}. Briefly, a segment of the abdominal aorta of RNU-rats is removed and replaced by the denuded human IMA via end-to-end anastomosis using 8-0 sutures (Ethicon, Norderstedt, Germany). In this model we do not detect any signs of advanced cell death and/or proliferation, as well as altered inflammatory activation in the IMA-recipient RNU rats. Stent implantation was performed as indicated in Suppl. Fig. 3B, using either bare metal stents (BM-stent) or anti-miR-21-eluting stents (anti-21-stent). 2.75mmx8mm stents (Translumina, Hechingen, Germany) were deployed into balloon-injured IMAs, which were then implanted into the abdominal position of RNU rats as previously described by our group^{1,2}.

Rat aortic denudation model

To study vessel re-endothelialization after balloon injury with and without systemic anti-21 treatment, endothelial denudation in male Lewis rats was performed via balloon inflation as previously described¹. Vessels from all models described above were retrieved at the postoperative day indicated in the subscript number after the group name.

Systemic anti-21 treatment in vivo

FAM-tagged locked nucleic acid (LNA) anti-miR-21 (anti-21) (Exiqon, Vedbaek, Denmark; 5'-3': 56-FAM-/TCAGTCTGATAAGCT) was dissolved in PBS. Animals were treated with one dose of anti-21 via intravenous femoral vein injection, one day after vessel implantation. The concentration of anti-21 was 1mg/kg in the low-dose (LD) group and 5mg/kg in the high-dose (HD) group.

Anti-21 stent coating

The Translumina YUKON DES System with PEARL microporous surface was used as previously described³. Stents were coated with FAM-tagged-LNA-anti-miR-21 (Exiqon) in 70% isopropyl alcohol to a final drug amount of 5mg/kg animal weight. The coated stent surface was visualized with a fluorescence microscope (Leica, Wetzlar, Germany) and a Hitachi S-4800 scanning electron microscope (Hitachi, Düsseldorf, Germany).

Histological analysis

All arteries were perfusion fixed with 4% paraformaldehyde to ensure full distension before performing quantification if applicable. Tissues were then dehydrated, and embedded in paraffin. Stented grafts were fixed and dehydrated alike and infiltrated in a mixture (MMA I) of 59.3% methyl methacrylate, 34.6% butyl methacrylate, 4.9% methyl benzoate and 1.2% polyethylene glycol for 2 days, MMA I with 0.4% dry benzoyl peroxide for 2 days, and MMA I with 0.8% dry benzoyl peroxide (MMA III) for 2 days at 4°C. Subsequently, grafts were embedded on a pre-polymerized base in a solution of MMA III with N,N-dimethyl-p-toluidine. Continuous polymerization was conducted in a climate chamber (Binder, Tuttlingen, Germany). Slides of 5µm thickness were cut and stained with Masson's trichrome for morphometric analysis of myointimal lesion. Luminal obliteration was defined as the percentage of the cross-sectional area within the internal elastic lamina taken up by the intima. The endothelium was stained using antibodies against RECA-1 (HIS52; Serotec, Raleigh, NC) and the ZytoChem-Plus AP Polymer-Kit (Zytomed Systems, Berlin, Germany).

Immunofluorescence staining

Rehydrated tissue slides underwent heat-induced antigen retrieval with Dako antigen retrieval solution (Dako, Glostrup, Denmark) in a steamer, followed by antigen blocking with Image-iT® FX signal enhancer (Invitrogen, Carlsbad, CA). Antibodies against smooth-muscle-actin (SMA, ab5694; Abcam, Cambridge, UK), smooth-muscle-myosin-heavy-chain (EPR5335; Abcam), SMemb (3H2; Yamasa, Tokyo, Japan), fibroblast-activation-protein (FAP, ab28246; Abcam), human leukocyte antigen I (HLA I, 3F10; Santa Cruz, Santa Cruz, CA), and rat FITC-conjugated major histocompatibility complex I (MHC I, B5; BD Pharmingen, Franklin Lakes, NJ) were incubated for 1h at 37°C. After washing with PBS, sections were incubated for 1h at 37°C with a corresponding secondary antibody conjugated to Alexa Fluor 488 or Alexa Fluor 555 (Invitrogen). Cell nuclei were counterstained with DAPI and imaging was performed using a Nikon Eclipse TiE microscope (Nikon, Tokyo, Japan) equipped with the Perkin Elmer UltraVIEW VoX confocal imaging system (Perkin Elmer, Waltham, MA)

Fluorescence imaging

To demonstrate overall anti-21 distribution, freshly recovered organs (heart, lung, liver, kidney, stented or un-stented vessels) were washed in PBS and imaged using a Xenogen IVIS200 imaging system (Caliper Lifesciences, Hopkinton, MA). Fluorescent signal of FAM-tagged anti-21 was visualized at 488nm in relative light units (photons/s/cm²).

In situ hybridization

The miRCURY LNA microRNA ISH Optimization Kit (Exiqon) was used for *in situ* hybridization (ISH) of miR-21. Staining was performed according to manufacturer's instructions and as previously described⁴. In brief, tissue sections were treated with Proteinase K followed by a two-hour hybridization at the appropriate temperature. After washing in saline-sodium citrate buffers, we applied standard DIG blocking and staining procedures. Nuclear counterstaining was done with Nuclear Fast Red (Sigma Aldrich, St. Louis, MO).

Off-target effect screening

Rat blood was collected during vessel retrieval, and the following parameters were measured at University Hospital Hamburg-Eppendorf using routine techniques: aspartate aminotransferase (AST), alanine aminotransferase (ALT), blood urea nitrogen (BUN), creatinine, total cholesterol, low density lipoprotein (LDL), high density lipoprotein (HDL), and triglycerides. At sacrifice, rat hearts, lungs, livers, and kidneys were harvested for fluorescent microscopy, RNA extraction, and qRT-PCR.

Organ chamber and ex vivo IMA ring assays

Freshly harvested aortae were cut into rings of 4mm size, and endothelium-dependent and -independent relaxation was measured as previously described¹. Fresh pieces of IMA were denuded using 2-Fr Fogarty catheter, cut into rings of 2mm size, and kept in RPMI medium 1640 (Gibco, Carlsbad, CA) containing 10% fetal bovine serum. PDGF-BB (Sigma) at 200 ng/ml and/or anti-21 at 10µg/ml were added to the IMA-pieces and incubated for 24h at 4°C.

Optical coherence tomography (OCT) imaging

OCT images were recorded using the M2 OCT imaging system (LightLab Imaging, Westford, MA) as described previously⁵.

RNA extraction and quantitative real-time PCR

Total RNA was isolated using the miReasy mini kit (Qiagen, Hilden, Germany). Tissues were disrupted using a tissue homogenizer (ProScientific, Oxford, CT), or stainless steel beads (5mm) in combination with TissueLyser (Qiagen). RNA quantity and quality was assessed using the Nanodrop 1000 spectrophotometer (Thermo Scientific, Wilmington, DE; 260/280 ratio 1.9-2.1). RNA was reverse-transcribed using the TaqMan microRNA Reverse Transcription Kit (Life Technologies, Carlsbad, CA), according to the manufacturer's instructions. MicroRNA Assay Kits (Life Technologies) for hsa-miR-1 (UGGAAUGUAAAGAAGUAUGU AU), hsa-miR-21 (UAGCUUAUCAGACUGAUGUUGA), hsa-miR-29b (UAGCACCAUUUGAAAUCAGUGUU), hsa-miR-133a (UUUGGUCCCCU UCAACCAGCUG), hsa-miR-143 (UGAGAUGAAGCACUGUAGCUC), hsa-miR-145 (GUCCAGUUUCCAGGAAUCCCU), hsa-miR-221 AGCUACAUUG UCUGCUGGGUUUC, hsa-miR-222 (AGCUACAUCUGGCUACUGGGU) and U6, RNU44, RNU48 (endogenous controls for normalization in human) and U6 and U87 (endogenous controls for normalization in rat samples) were used. For mRNA, the High Capacity RT kit with Rnase out (Life Technologies) was used to synthesize first-strand cDNA according to the manufacturer's protocol. qRT-PCR was performed using rat and human specific primers for PTEN (Life Technologies). Probes were normalized to RPLP0 (human) or HPRT1 (rat) as internal controls. Amplification took place on an ABI PRISM 7900HT (Applied Biosystems, Carlsbad, CA). All data were calculated using the method of $\Delta\Delta C_t$ values and are expressed as mean \pm SD.

Proliferation assay

The MTT (3-[4,5-dimethyl-thiazol-2-yl]-2,5-diphenyltetrazolium bromide) assay (Vybrant, Life Technologies) was performed following the manufacturer's instructions. Anti-21 treatment group was compared to the scrambled miRNA control group. After cell transfection, cells were incubated for 4 h in the presence of 10 ml of MTT AB solution (Millipore, Billerica, MA). The formazan product was dissolved through adding 100 ml acidic isopropanol (0.04N HCl) and absorbance was measured at 570 nm (reference wavelength 630 nm) on an ELISA plate reader.

In vitro studies

Human coronary artery smooth muscle cells (hCASMCs) and human coronary artery endothelial cells (hCAECs) were propagated in appropriate growth media in standard culture conditions with 5% FBS (Lonza; passage 5 to 6). Cells were either serum-starved or treated with PDGF for 48 h prior to transfection. Cells were transfected at 70-80% confluency with anti-21, or mismatch (scrambled) miRNAs (Life Technologies) using Lipofectamine RNAiMAX (Life Technologies). Transfection followed manufacturer's protocol, allowing a 12h transfection time. Experiments were carried out in triplicates. Proliferation assays were performed as described in the Supplement.

Statistical analysis

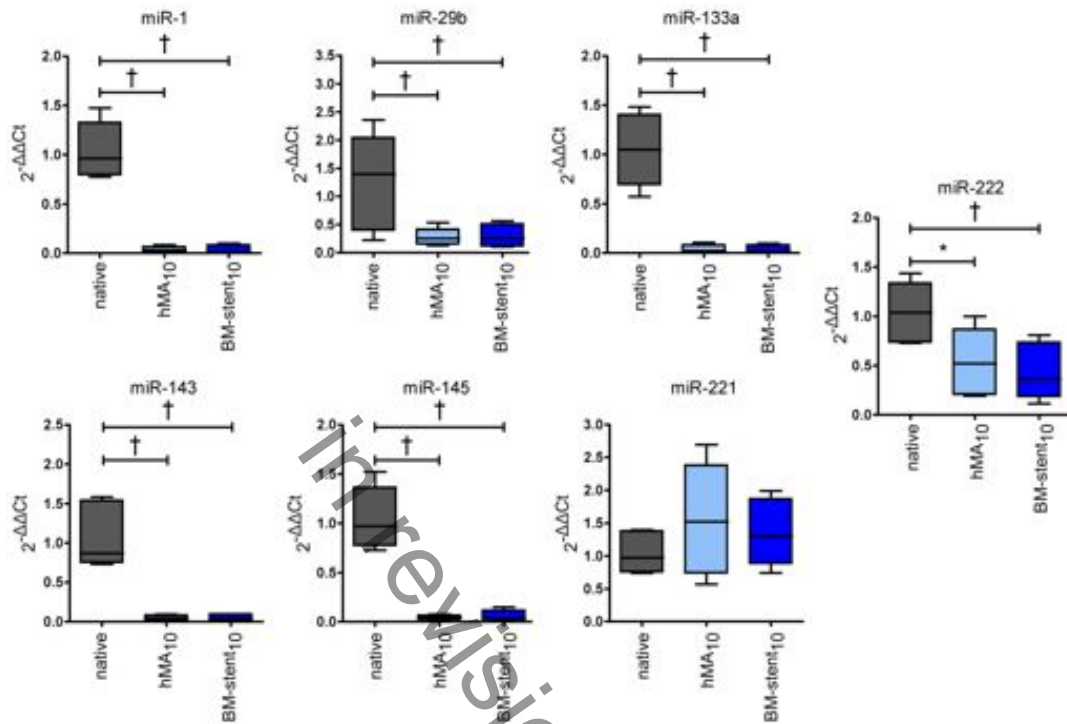
Data are presented as mean \pm standard deviation or mean \pm standard error of the mean as indicated. Analysis was carried out using SPSS statistical software package 22.0 (SPSS, Chicago, IL). Groups were compared with the unpaired Student's t-test, or analysis of variance (ANOVA) with Bonferroni's or LSD post-hoc test as indicated. Significance is displayed as * $p < 0.05$ and † $p < 0.01$.

References

1. Deuse T, Hua X, Wang D, Maegdefessel L, Heeren J, Scheja L, et al. Dichloroacetate prevents restenosis in preclinical animal models of vessel injury. *Nature*. 2014;509:641-644
2. Hua X, Deuse T, Michelakis ED, Haromy A, Tsao PS, Maegdefessel L, et al. Human internal mammary artery (ima) transplantation and stenting: A human model to study the development of in-stent restenosis. *Journal of visualized experiments : JoVE*. 2012:e3663
3. Deuse T, Erben RG, Ikeno F, Behnisch B, Boeger R, Connolly AJ, et al. Introducing the first polymer-free leflunomide eluting stent. *Atherosclerosis*. 2008;200:126-134
4. Maegdefessel L, Azuma J, Toh R, Deng A, Merk DR, Raiesdana A, et al. MicroRNA-21 blocks abdominal aortic aneurysm development and nicotine-augmented expansion. *Science translational medicine*. 2012;4:122ra122
5. Deuse T, Koyanagi T, Erben RG, Hua X, Velden J, Ikeno F, et al. Sustained inhibition of epsilon protein kinase c inhibits vascular restenosis after balloon injury and stenting. *Circulation*. 2010;122:S170-178

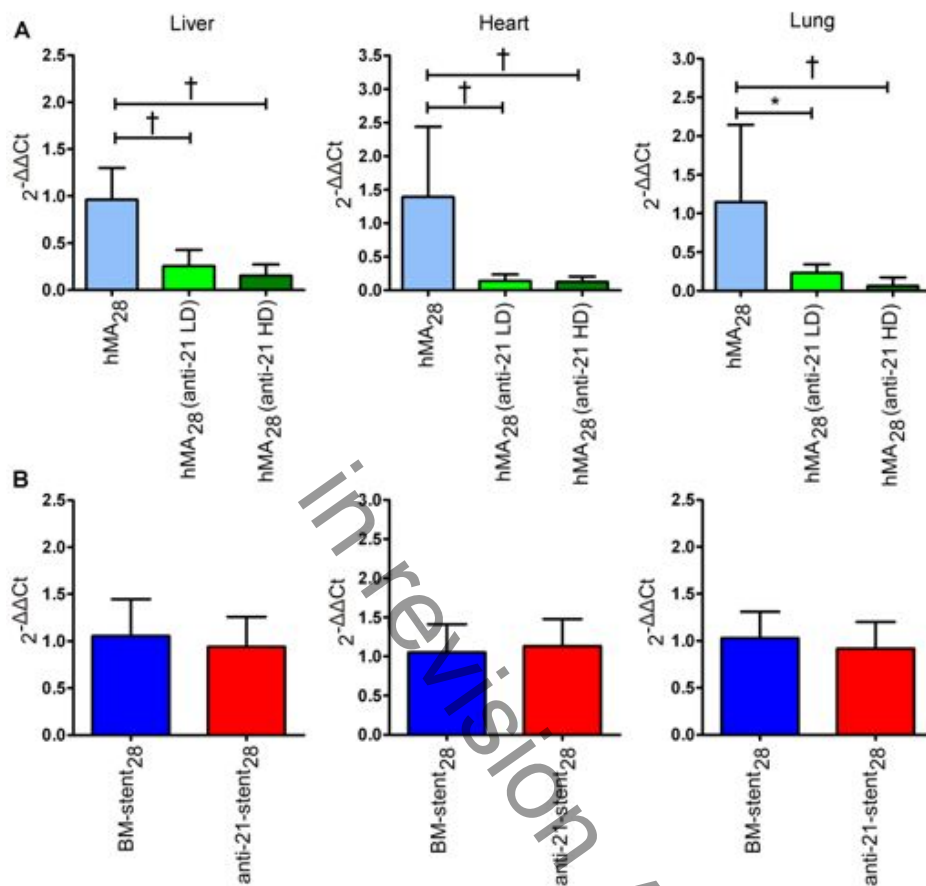
Supplementary Results

Supplemental Figure 1: miR qRT-PCR expression in the humanized balloon injury and stent-model.



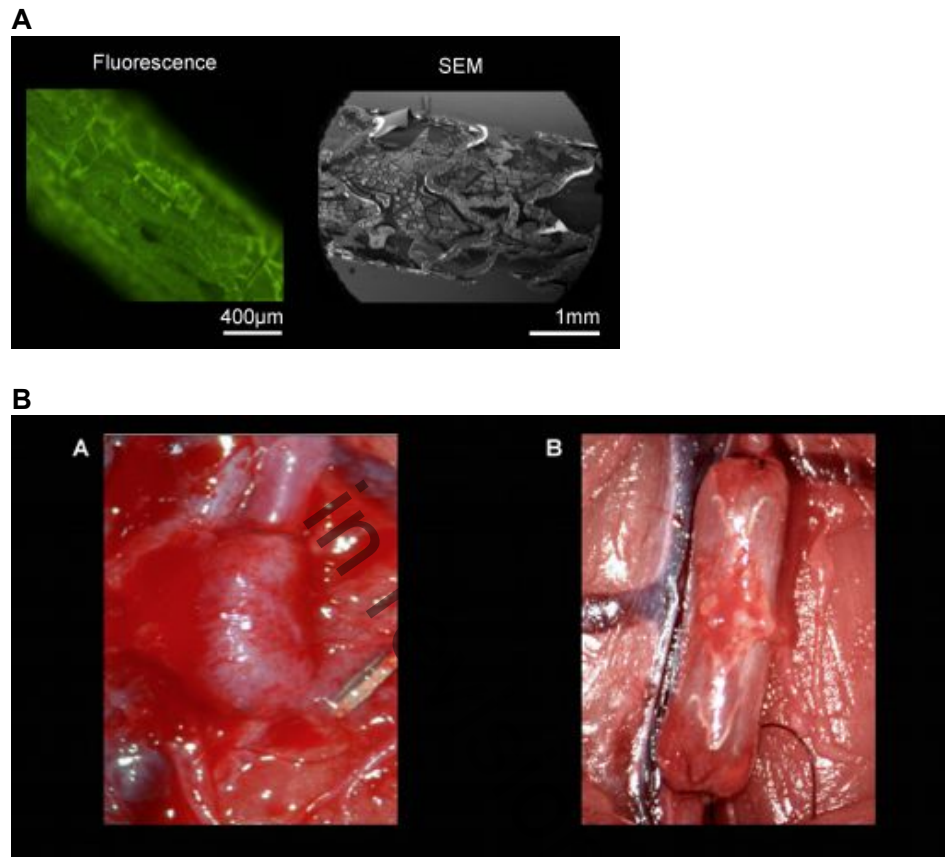
Human IMA were denuded with a 2 Fr. Catheter (hMA) or had a stent deployed (BM-stent), followed by implantation into the abdominal aorta of RNU rats. microRNA expression was measured using qRT-PCR 10 days after implantation. Six of the evaluated miRNAs were differentially expressed compared to native IMA vessels. Significantly down-regulated miRNAs included: miR -1, miR-29b, miR-133a, miR-143, miR-145 and miR-222. Notably, stented hMA-vessels had similar expression profiles to balloon-denuded vessels. Thus, vessel injury in the humanized model resulted in an similar dysregulation of miRNA expression, regardless of additional stenting (mean \pm s.d., n=6 animals per group, ANOVA with Bonferroni's post-hoc test). * p<0.05, † p<0.01.

Supplemental Figure 2: Off-target effects of systemic (A) and local (B) anti-21 treatment.



To evaluate potential off-target effects of anti-21 treatment, miR-21 expression in organs from systemically treated (A) and locally treated animals (B) were determined by qRT-PCR. Systemically treated animals showed considerably reduced miR-21 expression in the liver (mean± s.d., n=7 per group, ANOVA with Bonferroni's post-hoc test), heart (mean± s.d., n=6 (hMA), n=7 (anti-21 LD), n=6 (anti-21 HD), ANOVA with Bonferroni's post-hoc test) and lung (mean± s.d., n=7 per group, ANOVA with Bonferroni's post-hoc test). In contrast, no relevant differences were detected in the liver, heart and lung (mean± s.d., n=8 (BM-stent), n=6 (anti-21-stent), unpaired t-test) between the BM-stent group and the local anti-21-stent group, indicating no relevant off-target effects by local anti-21 delivery. *p<0.05, † p<0.01.

Supplemental Figure 3: Confirmation of successful stent coating and humanized balloon injury and stent model



(A) FAM-tagged-LNA-anti-miR-21 (anti-21) was dissolved in 70% isopropyl alcohol and coated onto stents. Fluorescence (left) and scanning electron (right) microscope images, confirm successful anti-21-coating onto the stent surface. (B) Surgical technique of the hMA model: Human internal mammary arteries (IMA) were balloon injured with a 2 French catheter and implanted into the abdominal aortic position of RNU rats via end-to-end anastomosis. (B) Surgical technique of BM-stent model: A stent was deployed into balloon-injured IMA, followed by implantation into the abdominal aorta of RNU rats.

Movie S1: Optical coherence tomography (OCT) imaging video showing in-stent restenosis in BM-stent versus anti-21-stent. Motorized OCT pullbacks were performed at a rate of 1 mm/s and images were acquired at 15 frames/s. Images revealed considerably less myointima formation in the anti-21-stent group (right) compared to BM-stent (left).

Dichloroacetate prevents restenosis in preclinical animal models of vessel injury

Tobias Deuse^{1,2,3}, Xiaoqin Hua^{1,2}, Dong Wang^{1,2}, Lars Maegdefessel⁴, Joerg Heeren⁵, Ludger Scheja⁵, Juan P. Bolaños⁶, Aleksandar Rakovic⁷, Joshua M. Spin⁸, Mandy Stubbendorff^{1,2}, Fumiaki Ikeno⁸, Florian Länger⁹, Tanja Zeller^{2,10}, Leonie Schulte-Uentrop^{2,11}, Andrea Stoehr^{2,12}, Ryo Itagaki^{1,2}, Francois Haddad⁸, Thomas Eschenhagen^{2,12}, Stefan Blankenberg^{2,10}, Rainer Kiefmann^{2,11}, Hermann Reichenspurner^{2,3}, Joachim Velden¹³, Christine Klein⁷, Alan Yeung⁸, Robert C. Robbins¹⁴, Philip S. Tsao^{8,15} & Sonja Schrepfer^{1,2,3,14}

Despite the introduction of antiproliferative drug-eluting stents, coronary heart disease remains the leading cause of death in the United States¹. In-stent restenosis and bypass graft failure are characterized by excessive smooth muscle cell (SMC) proliferation^{2,3} and concomitant myointima formation with luminal obliteration. Here we show that during the development of myointimal hyperplasia in human arteries, SMCs show hyperpolarization of their mitochondrial membrane potential ($\Delta\Psi_m$) and acquire a temporary state with a high proliferative rate and resistance to apoptosis. Pyruvate dehydrogenase kinase isoform 2 (PDK2) was identified as a key regulatory protein, and its activation proved necessary for relevant myointima formation. Pharmacologic PDK2 blockade with dichloroacetate or lentiviral PDK2 knockdown prevented $\Delta\Psi_m$ hyperpolarization, facilitated apoptosis and reduced myointima formation in injured human mammary and coronary arteries, rat aortas, rabbit iliac arteries and swine (pig) coronary arteries. In contrast to several commonly used antiproliferative drugs, dichloroacetate did not prevent vessel re-endothelialization. Targeting myointimal $\Delta\Psi_m$ and alleviating apoptosis resistance is a novel strategy for the prevention of proliferative vascular diseases.

Balloon injury of Lewis rat aortas triggered an inflammatory response and caused leukocyte infiltration in the SMC-rich media after 48 h, consisting mainly of CD68-positive (CD68⁺) macrophages and some myeloperoxidase-positive (MPO⁺) neutrophils; CD3⁺ lymphocytes were not observed (Extended Data Fig. 1a–c). Compared to healthy, non-injured aortas, we observed increased phosphorylation of AKT (pAKT), and ERK1, ERK2 (pERK1/2) and $\Delta\Psi_m$ hyperpolarization in media cells of injured vessels (Extended Data Fig. 1d, e). A myointima subsequently developed luminal to the internal elastic lamina, which caused progressive luminal obliteration over 28 days (Extended Data Fig. 1f, g). This process was accompanied by leukocyte infiltration and inflammatory cytokine release, which was strong after 7 days and markedly reduced at 28 days (Extended Data Fig. 1h, i).

A humanized model was subsequently developed to study myointima formation longitudinally in human arteries. Balloon-injured human internal mammary arteries (HMAs) were implanted into the abdominal aortic position of T-cell-deficient Rowett nude (RNU) rats (Supplementary Video 1). Myointimal hyperplasia rapidly developed over 4 weeks (Fig. 1a) causing progressive luminal obliteration (Fig. 1c). By histopathology (Fig. 1b) and confocal immunofluorescence (Extended Data Fig. 2a, b),

the myointima in the HMA model after 28 days or later closely resembled lesions of diseased human coronary arteries retrieved from autopsy samples. Using human leukocyte antigen class I (HLA I) and rat MHC I antibodies, the human origin of the SMCs within the myointima was confirmed (Extended Data Fig. 2c). Only the mechanical vessel injury was causally related to myointima formation and no relevant xenoantigen-triggered immune activation was observed (Extended Data Fig. 3a, b). Similar to the immunocompetent Lewis rat aortic injury model, we observed accumulation of CD68⁺ macrophages and MPO⁺ neutrophils in HMA vessels after 7 days, which was markedly attenuated by day 28 (Extended Data Fig. 3c). Immune cell infiltration was again accompanied by the elevation of inflammatory cytokines (Extended Data Fig. 3d).

Analysis of cell growth dynamics in HMAs showed a transient but strong increase in proliferative activity within the myointima between 7 and 21 days after injury, accompanied by a persistently low rate of apoptosis (Fig. 1d, e). Proliferation and apoptosis leveled off after 28 days when there was also no further progression of myointimal disease (Fig. 1c, e). Only during the time period of highly positive net proliferation did myointimal cells demonstrate $\Delta\Psi_m$ hyperpolarization (Fig. 1f). Within the myointima, cells in the luminal region showed higher proliferative activities and higher $\Delta\Psi_m$ than cells closer to the media (Extended Data Fig. 3e).

Platelet-derived growth factor (PDGF) was suspected to be the major driving factor promoting myointimal hyperplasia as it was temporarily increased in injured HMA vessels and PDGF receptor blockade prevented the development of relevant disease (Extended Data Fig. 3f, g). Human vascular SMCs were isolated from fresh HMAs and characterized (Extended Data Fig. 4a, b). PDGF was then shown to induce $\Delta\Psi_m$ hyperpolarization in cultured SMCs (Extended Data Fig. 4c), similar to the $\Delta\Psi_m$ hyperpolarization previously observed in injured HMAs (Fig. 1f). Thus, mitochondrial $\Delta\Psi_m$ hyperpolarization in myointimal SMCs and cultured SMCs coincided with the availability of PDGF. PDGF also caused a phenotype switch in SMCs from a contractile to a dedifferentiated state (Extended Data Fig. 4d).

Mitochondria have been shown to regulate apoptosis via their mitochondrial apoptotic pathway⁴. This involves mitochondrial permeability transition and the release of toxic components such as cytochrome C and caspases⁵. In this context, $\Delta\Psi_m$ has an important role in the control of the mitochondrial permeability transition pore, as $\Delta\Psi_m$

¹TSI-laboratory, University Heart Center Hamburg, Martinistraße 52, 20246 Hamburg, Germany. ²Cardiovascular Research Center Hamburg (CVRC) and DZHK (German Center for Cardiovascular Research), partner site Hamburg/Kiel/Luebeck, University Medical Center Hamburg-Eppendorf, Martinistraße 52, 20246 Hamburg, Germany. ³Cardiovascular Surgery, University Heart Center Hamburg, Martinistraße 52, 20246 Hamburg, Germany. ⁴Department of Medicine, Atherosclerosis Research Unit, Karolinska Institute, CMM L8:03, 17176 Stockholm, Sweden. ⁵Department of Biochemistry and Molecular Cell Biology, University Medical Center Hamburg-Eppendorf, Martinistraße 52, 20246 Hamburg, Germany. ⁶Institute of Functional Biology and Genomics, University of Salamanca-CSIC, Zacarias Gonzalez 2, 37007 Salamanca, Spain. ⁷Institute of Neurogenetics, University of Lübeck, Maria-Goeppert-Straße 1, 23562 Lübeck, Germany. ⁸Cardiovascular Medicine and Stanford Cardiovascular Institute, Stanford University, 300 Pasteur Drive, Stanford, California 94305, USA. ⁹Institute of Pathology, Hannover Medical School, Carl-Neuberg-Straße 1, 30625 Hannover, Germany. ¹⁰Department of General and Interventional Cardiology, University Heart Center Hamburg, Martinistraße 52, 20246 Hamburg, Germany. ¹¹Department of Anaesthesiology, University Medical Center Hamburg-Eppendorf, Martinistraße 52, 20246 Hamburg, Germany. ¹²Institute of Experimental Pharmacology and Toxicology, University Medical Center Hamburg-Eppendorf, Martinistraße 52, 20246 Hamburg, Germany. ¹³Department of Nephropathology, Institute of Pathology, University Hospital Erlangen, Krankenhausstraße 8-10, 91054 Erlangen, Germany. ¹⁴Department of Cardiothoracic Surgery and Stanford Cardiovascular Institute, Stanford University, 300 Pasteur Drive, Stanford, California 94305, USA. ¹⁵Veterans Affairs Palo Alto Health Care System, 3801 Miranda Avenue, Palo Alto, California 94304, USA.

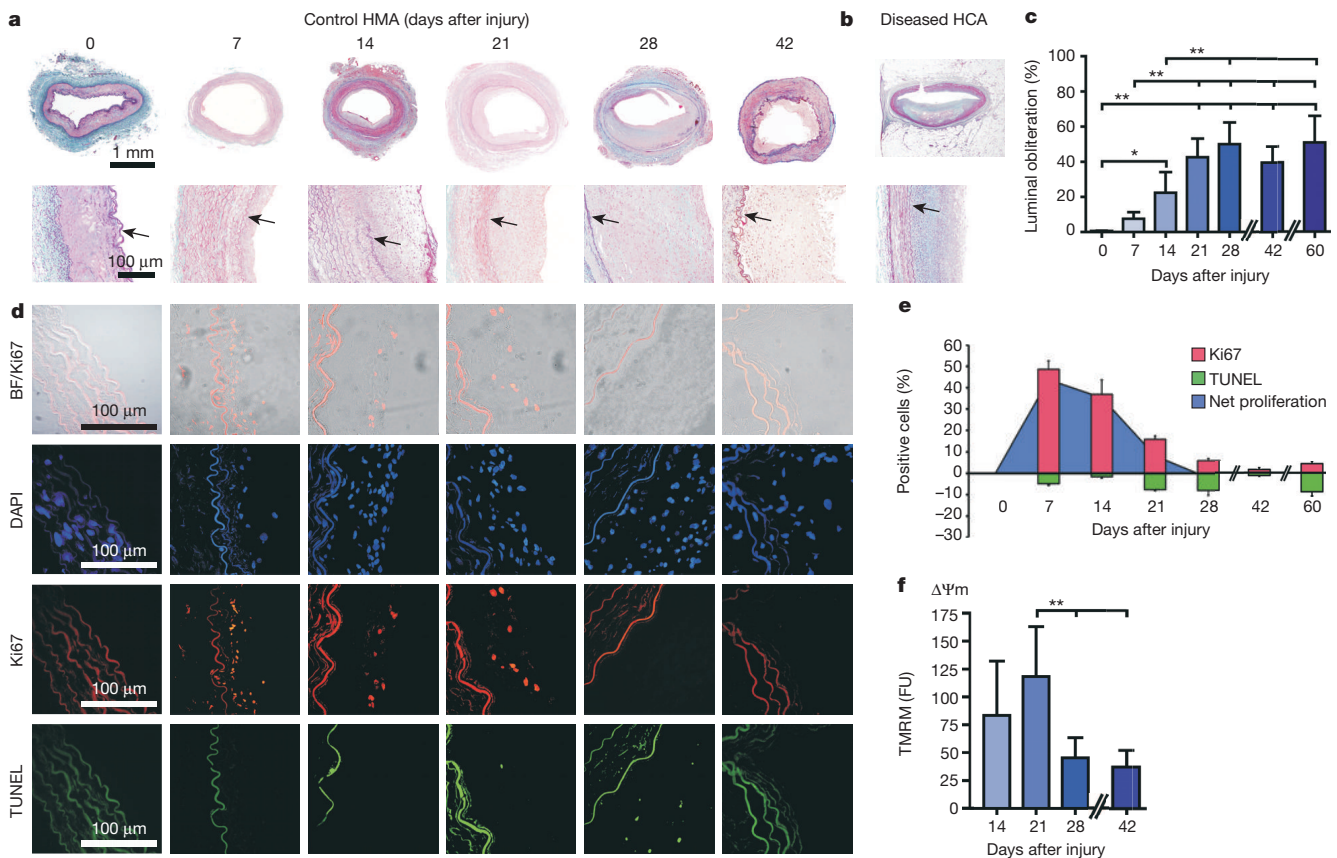


Figure 1 | Chronology and growth dynamics of myointima formation in the HMA model. **a**, Development of myointimal hyperplasia (trichrome; black arrows, internal elastic lamina). **b**, Non-calcified lesions in naturally diseased human coronary artery (HCA). **c**, Luminal obliteration over time (mean \pm s.d., $n = 5$ animals (days 0–28), 4 animals (days 42–60)), ANOVA with Bonferroni's post-hoc test). **d**, **e**, The timeline of proliferative (Ki67) and apoptotic activity (TUNEL, TdT-mediated dUTP nick end labelling) within the myointima was

monitored by immunofluorescence (**d**) and quantified (**e**, mean \pm s.e.m., $n = 7$ animals (day 7), 5 animals (day 14), 6 animals (days 21–60)). Net proliferation was calculated as the percentage of Ki67-positive minus TUNEL-positive cells. BF, brightfield. **f**, $\Delta\Psi_m$ in HMA myointima (mean \pm s.d., $n = 5$ animals (day 14), 9 animals (day 21), 6 animals (days 28–42)), ANOVA with Bonferroni's post-hoc test). FU, arbitrary fluorescence units; TMRM, tetramethylrhodamine methyl ester perchlorate assay. * $P < 0.05$, ** $P < 0.01$.

hyperpolarization has been suspected to impede pore opening^{6,7}. Dichloroacetate (DCA), a rapid-acting small molecule targeting mitochondrial PDKs, has previously been demonstrated to reduce $\Delta\Psi_m$ in A549 cells⁸. As elevated $\Delta\Psi_m$ and suppressed apoptosis have been observed after injury in our HMA model, we reasoned that DCA would prevent post-injury $\Delta\Psi_m$ hyperpolarization, facilitate apoptosis and reduce myointimal growth.

DCA effectively prevented $\Delta\Psi_m$ hyperpolarization in PDGF-treated SMCs isolated from either healthy or atherosclerotic vessels (Extended Data Fig. 5a, b). Previously, mitochondrial cytochrome C release and apoptosis induction were shown to be suppressed by hyperpolarized $\Delta\Psi_m$ ^{7,9}. Consistent with this observation, PDGF reduced staurosporine-induced mitochondrial cytochrome C leakage (Extended Data Fig. 5c, d) and rendered SMCs resistant to apoptosis (Extended Data Fig. 5e). DCA both increased cytochrome C release and restored the ability to enter apoptosis (Extended Data Fig. 5c–e).

In vivo, oral DCA did not affect leukocyte infiltration in the media of balloon-injured aortas in immunocompetent Lewis rats, but effectively lowered $\Delta\Psi_m$ in the media at 48 h (Extended Data Fig. 6a–d). The accumulation of CD68⁺ macrophages and MPO⁺ neutrophils in the developing myointima was also not affected by DCA (Extended Data Fig. 6e). However, at 7 days, DCA markedly reduced myointimal $\Delta\Psi_m$ and permitted apoptosis (Extended Data Fig. 6f, h). At 28 days, $\Delta\Psi_m$ in the developed control myointima had already lowered and DCA showed little effect (Extended Data Fig. 6g). Also, proliferation and apoptosis were low at that time point (Extended Data Fig. 6i).

The potential vasculoprotective effect of DCA was then tested in the HMA and human coronary artery (HCA) models (Fig. 2a–d). For the latter, HCAs with minor pre-existing disease, which underwent the same balloon injury and implantation procedure as described for HMA, were used to better reflect the coronary pathophysiology. Oral DCA administration strongly reduced the development of myointima and luminal narrowing in both HMAs (Fig. 2a) and HCAs (Fig. 2d). Similar to untreated HMA controls, the proliferative response to injury in DCA-treated vessels was strongest within the first 14 days and weakened thereafter (Fig. 2b). However, the apoptotic activity was also enhanced and mirrored the proliferative activity at each time point, resulting in a much lower net proliferation. In accordance with the *in vitro* data, we observed significantly lower $\Delta\Psi_m$ in the 21-day HMA specimens of the DCA group (Fig. 2c). To exclude the possibility that ischaemia-reperfusion injury or xenogeneic immune interactions might have affected our results, DCA was tested further in the rat aortic (Fig. 2e) and the rabbit iliac artery balloon injury models (Fig. 2f). Again, myointima formation after 28 days was remarkably reduced by DCA in both models. Interestingly, DCA neither demonstrated anti-migratory effects on endothelial cells *in vitro* nor inhibited vessel re-endothelialization *in vivo* (Extended Data Fig. 7 and Supplementary Video 2).

PDKs are the only known targets of DCA and PDKs exclusively phosphorylate and thus inactivate pyruvate dehydrogenase (PDH). It was therefore suspected that PDK knockdown would generate similar biological effects as PDK inhibition by DCA. Although SMCs express PDK1, PDK2 and PDK3 (Extended Data Fig. 8a), PDK2 has the highest affinity

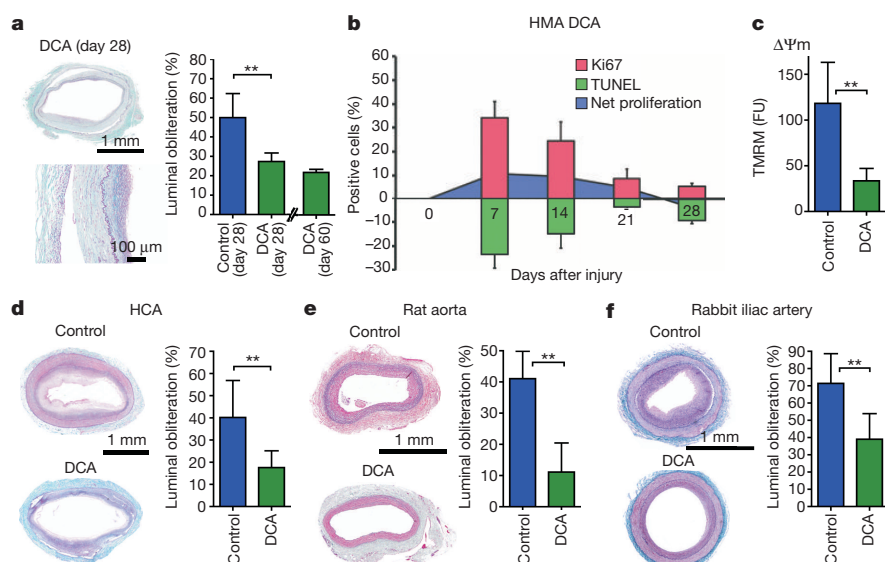


Figure 2 | DCA alleviates myointima formation *in vivo*. **a**, After 28 days, luminal obliteration was significantly less in the DCA group of the HMA model (mean \pm s.d., $n = 5$ animals per group, Student's *t*-test). In animals treated for 60 days ($n = 4$), there was no further disease progression. **b**, Myointimal growth dynamics in the HMA DCA group (mean \pm s.e.m., $n = 4$ animals (day 7), 5 animals (day 14), 3 animals (day 21), 6 animals (day 28)). **c**, At day 21, $\Delta\Psi_m$ was significantly lower in HMA DCA vessels than in control arteries (mean \pm s.d., $n = 9$ control animals, $n = 4$ DCA animals, Student's *t*-test). **d**, At day 28, DCA reduced luminal obliteration in the HCA model (mean \pm s.d., $n = 8$ control animals, $n = 14$ DCA animals, Student's *t*-test). **e**, **f**, At day 28, DCA effectively alleviated myointima formation in balloon-injured rat aortas (**e**, mean \pm s.d., $n = 6$ animals per group, Student's *t*-test) and rabbit iliac arteries (**f**, mean \pm s.d., $n = 12$ control animals, $n = 15$ DCA animals, Student's *t*-test). ** $P < 0.01$.

to DCA¹⁰ and is likely to mediate the vast majority of the DCA effect. Therefore, PDK2-knockdown SMCs were generated using PDK2 lentiviral short hairpin RNA (shRNA) (Extended Data Fig. 8b, c) to verify the mechanistic involvement of PDK2 in the DCA effect. Indeed PDK2-knockdown SMCs maintained steady low $\Delta\Psi_m$ (Extended Data Fig. 9a) under control conditions and with PDGF stimulation. Also, PDK2-knockdown SMCs maintained increased cytochrome C release and elevated apoptotic rates even during PDGF incubation (Extended Data Fig. 9b–d). In addition, DCA lost its ability to affect $\Delta\Psi_m$ in PDK2-knockdown SMCs (Extended Data Fig. 9a). As expected, when PDH (the primary inhibitory target of PDK2) was knocked down (Extended Data Fig. 9e) instead of PDK2, the opposite effect was observed: $\Delta\Psi_m$ was permanently elevated, even under control conditions (Extended Data Fig. 9f). DCA again lost its ability to depolarize $\Delta\Psi_m$, indicating that the DCA effect on $\Delta\Psi_m$ depended on both PDK2 and PDH.

To assess whether arteries with *ex vivo* PDK2 knockdown would develop similarly reduced myointima as arteries under DCA treatment, PDK2 knockdown was induced in HMAs and HCAs before implantation (Extended Data Fig. 8d–f). Comparable to the DCA group, PDK2-knockdown HMAs showed low net proliferation throughout the 28-day study period (Fig. 3a). $\Delta\Psi_m$ hyperpolarization was also effectively prevented and the low $\Delta\Psi_m$ of PDK2 knockdown HMAs at day 21 (Fig. 3b) closely resembled the $\Delta\Psi_m$ values of DCA-treated HMAs

(Fig. 2c). Reduced luminal obliteration was observed in both PDK2-knockdown HMAs (Fig. 3c) and HCAs (Fig. 3d) at day 28.

DCA was ultimately evaluated in a translationally relevant swine model of coronary artery restenosis. Yorkshire swine underwent standardized coronary artery balloon injury under fluoroscopic guidance. After 28 days, DCA-treated animals showed significantly reduced luminal obliteration, proliferation area, and max. proliferation thickness (Fig. 4a–d). In summary, DCA reduced myointima formation in five different pre-clinical *in vivo* models.

Upon PDGF stimulation of cultured SMCs, we observed an activation of the downstream PI(3)K (phosphatidylinositol-3-OH kinase) and MEK (MAPK kinase) pathways with AKT phosphorylation, ERK1 and ERK2 phosphorylation, hexokinase 2 (HK2) upregulation, and increased HK2-mitochondrial association (Extended Data Fig. 10a–d). HK2 has previously been shown to have a binding site close to VDAC (voltage-dependent anion-selective channel), the most abundant protein of the outer mitochondrial membrane, and HK2 binding was reported to reduce channel conductance^{11,12}. Consistent with this previous work, we show that HK2-mitochondrial association coincides with $\Delta\Psi_m$ hyperpolarization and apoptosis resistance in our study. Furthermore, displacement of HK2 from its mitochondrial VDAC binding site both reduced $\Delta\Psi_m$ and restored the susceptibility to apoptosis (Extended Data Fig. 10e). VDAC closure using the inhibitor DIDS also increased SMC $\Delta\Psi_m$ and reduced

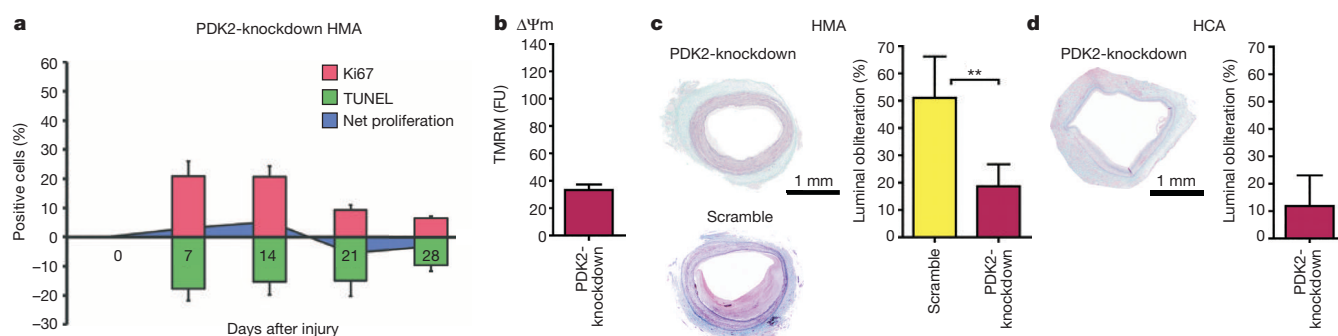


Figure 3 | PDK2 knockdown alleviates myointima formation *in vivo*. **a**, PDK2-knockdown HMAs showed elevated apoptosis rates during the early time points of increased proliferative activity resulting in low myointimal net proliferation (mean \pm s.e.m., $n = 3$ (day 7), 4 (day 14), 3 (day 21), 8 (day 28) animals). **b**, At day 21, $\Delta\Psi_m$ in PDK2-knockdown HMA vessels was approximately as low as in DCA HMA vessels (mean \pm s.d., $n = 4$ animals;

see Fig. 2c). **c**, At day 28, luminal obliteration was significantly reduced in PDK2-knockdown HMA compared to scrambled shRNA controls (mean \pm s.d., $n = 4$ animals (scramble) and $n = 9$ animals (PDK2-knockdown, Student's *t*-test). **d**, Luminal obliteration was low in PDK2-knockdown HCA vessels at day 28 (mean \pm s.d., $n = 3$ animals). ** $P < 0.01$.

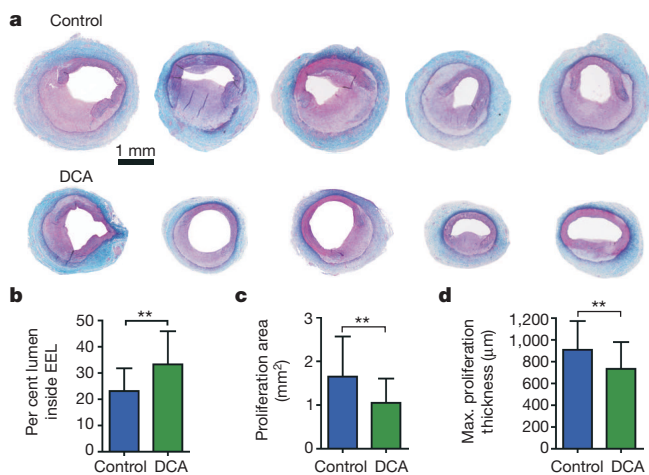


Figure 4 | DCA effectively reduces balloon-injury-induced myointima formation in swine coronary arteries *in vivo*. **a**, After 28 days, the coronary arteries of untreated and DCA-treated Yorkshire swine were retrieved (trichrome). One representative vessel per animal is presented. **b**, The patent lumen inside the external elastic lamina (EEL) was significantly larger in the DCA group (mean \pm s.d., $n = 45$ sections per group (three sections per vessel, three coronary arteries per pig, five pigs per group), Student's *t*-test). Thus, DCA significantly alleviated myointima formation. **c**, **d**, In the region of a ruptured internal elastic lamina, the proliferation area (**c**) and the maximal proliferation thickness (**d**) were significantly smaller with DCA (mean \pm s.d., $n = 42$ control sections, $n = 31$ DCA sections, Student's *t*-test). ** $P < 0.01$.

apoptosis (Extended Data Fig. 10f), further supporting the direct mechanistic involvement of VDAC in the regulation of both $\Delta\Psi_m$ and apoptosis.

DCA and PDK2 knockdown diminished HK2 elevation (Extended Data Fig. 10b) and HK2-mitochondrial association (Extended Data Fig. 10c, d), and maintained low $\Delta\Psi_m$ despite PDGF (Extended Data Fig. 10g). Notably, it was confirmed that the depolarizing effects of DCA and PDK2 knockdown on $\Delta\Psi_m$ were ultimately mediated through VDAC, because inhibition of VDAC opening by DIDS was found to neutralize these effects (Extended Data Fig. 10g). However, the mechanistic link between PDK2 inhibition and the decrease in HK2-VDAC binding and reversal of $\Delta\Psi_m$ hyperpolarization remains elusive.

In healthy vessels, proliferation and apoptosis are very low and balanced¹³. Vessel injury disrupts this homeostasis and triggers an inflammatory state^{14–16}, which induces temporary $\Delta\Psi_m$ hyperpolarization in SMCs and drives myointima formation. As shown here, PDK2 repression counteracts temporarily acquired apoptosis resistance and may be a well-tolerated strategy for the prevention of restenosis without interfering with re-endothelialization.

METHODS SUMMARY

Myointimal hyperplasia was induced in HMAs and HCAs by balloon injury and the human arteries were implanted into athymic RNU rats (CrI:NIH-*Foxn1*tm). Lewis rats and New Zealand rabbits underwent balloon injury of their abdominal aorta or their iliac arteries, respectively. Yorkshire swine underwent percutaneous transluminal coronary angioplasty to achieve a 1.3–1.35:1 balloon-artery overstretch. Rats and rabbits were treated with DCA 0.75 g l⁻¹ in drinking water; swine received DCA at 25 mg kg⁻¹ three times a day. Confluent SMCs were incubated with PDGF (50 ng ml⁻¹) for 48 h and/or DCA (5 mM; starting 2 days before PDGF) if not indicated otherwise. PDK2 shRNA lentiviral particles (Santa Cruz) were used to knock down PDK2 in SMCs *in vitro* or *in vivo* in HMAs or HCAs before implantation. PDH was knocked down in SMCs using short interfering RNA (siRNA) (Santa Cruz). For organ chamber experiments, fresh vascular rings were pre-constricted with prostaglandin F₂ α and nitroglycerin or acetylcholine was added for relaxation studies. To measure $\Delta\Psi_m$, freshly isolated tissues or cells were incubated with tetramethylrhodamine methyl ester perchlorate (TMRM, Invitrogen) and Hoechst 33342 (Invitrogen). Fluorescence signals were quantified by confocal microscopy (Perkin Elmer). SMCs were treated with staurosporine (50 nM, Sigma) for 18 h to induce apoptosis. ApopTag apoptosis detection kit (Merck Millipore) was then used to label apoptotic cells.

Online Content Any additional Methods, Extended Data display items and Source Data are available in the online version of the paper; references unique to these sections appear only in the online paper.

Received 4 October 2013; accepted 6 March 2014.

Published online 20 April 2014.

- Lloyd-Jones, D. *et al.* Heart disease and stroke statistics—2009 update: a report from the American Heart Association Statistics Committee and Stroke Statistics Subcommittee. *Circulation* **119**, 480–486 (2009).
- Dzau, V. J., Braun-Dullaeus, R. C. & Sedding, D. G. Vascular proliferation and atherosclerosis: new perspectives and therapeutic strategies. *Nature Med.* **8**, 1249–1256 (2002).
- Novak, K. Cardiovascular disease increasing in developing countries. *Nature Med.* **4**, 989–990 (1998).
- Green, D. R. & Reed, J. C. Mitochondria and apoptosis. *Science* **281**, 1309–1312 (1998).
- Hengartner, M. O. The biochemistry of apoptosis. *Nature* **407**, 770–776 (2000).
- Zamzami, N. & Kroemer, G. The mitochondrion in apoptosis: how Pandora's box opens. *Nature Rev. Mol. Cell Biol.* **2**, 67–71 (2001).
- Halestrap, A. P. What is the mitochondrial permeability transition pore? *J. Mol. Cell. Cardiol.* **46**, 821–831 (2009).
- Bonnet, S. *et al.* A mitochondria-K⁺ channel axis is suppressed in cancer and its normalization promotes apoptosis and inhibits cancer growth. *Cancer Cell* **11**, 37–51 (2007).
- Bernardi, P. Modulation of the mitochondrial cyclosporin A-sensitive permeability transition pore by the proton electrochemical gradient. Evidence that the pore can be opened by membrane depolarization. *J. Biol. Chem.* **267**, 8834–8839 (1992).
- Roche, T. E. & Hiromasa, Y. Pyruvate dehydrogenase kinase regulatory mechanisms and inhibition in treating diabetes, heart ischemia, and cancer. *Cell. Mol. Life Sci.* **64**, 830–849 (2007).
- Azoulay-Zohar, H., Israelson, A., Abu-Hamad, S. & Shoshan-Barmatz, V. In self-defence: hexokinase promotes voltage-dependent anion channel closure and prevents mitochondria-mediated apoptotic cell death. *Biochem. J.* **377**, 347–355 (2004).
- Pastorino, J. G., Shulga, N. & Hoek, J. B. Mitochondrial binding of hexokinase II inhibits Bax-induced cytochrome c release and apoptosis. *J. Biol. Chem.* **277**, 7610–7618 (2002).
- Clarke, M. C. *et al.* Apoptosis of vascular smooth muscle cells induces features of plaque vulnerability in atherosclerosis. *Nature Med.* **12**, 1075–1080 (2006).
- Bernal-Mizrachi, C. *et al.* Vascular respiratory uncoupling increases blood pressure and atherosclerosis. *Nature* **435**, 502–506 (2005).
- Mitra, A. K., Del Core, M. G. & Agrawal, D. K. Cells, cytokines and cellular immunity in the pathogenesis of fibroproliferative vasculopathies. *Can. J. Physiol. Pharmacol.* **83**, 701–715 (2005).
- Newby, A. C. & Zaltsman, A. B. Molecular mechanisms in intimal hyperplasia. *J. Pathol.* **190**, 300–309 (2000).

Supplementary Information is available in the online version of the paper.

Acknowledgements We thank C. Pahrman for performing all cell cultures and for her technical assistance. We thank J. Thoms for performing immunoblots, H. Wiebold for assistance in organ chamber experiments, J. Lyons and her team for her assistance with the swine study, and S. Ehret, A. Deng and M. Resch for their technical assistance. We thank the UKE Imaging Facility (UMIF, B. Zobiak) and the UKE Animal Facility. Ethicon (Norderstedt, Germany) provided surgical suture materials. We also thank A. Treszl and G. Schoen for their statistical analyses. This study was funded by the German Research Foundation (Deutsche Forschungsgemeinschaft (DFG), SCHR992/3-1 and SCHR992/4-1 to S.S.), the International Society for Heart and Lung Transplantation (ISHLT, to S.S.), the Förderverein des Universitären Herzzentrums Hamburg (to S.S.), the Hermann and Lilly Schilling Foundation (to C.K.), the MINECO (SAF2013-41177-R, to J.P.B.) and the NIH (NIH 1R01HL105299, to P.S.T.).

Author Contributions T.D. designed the studies, performed surgical procedures, analysed the data and wrote the manuscript. X.H. and D.W. performed confocal immunofluorescence, immunohistochemistry, TMRM assays *in vivo* and *in vitro*, endothelial cell assays, the histopathological studies, analysed data and edited the manuscript. L.M. participated in designing experiments, analysed data, edited the manuscript and secured funding. J.H., L.S., J.P.B., A.R., J.M.S. and C.K. participated in designing experiments, analysed data and edited the manuscript. M.S. performed surgical procedures in rats, contributed to molecular biology experiments and flow cytometry. F.I. and A.Y. contributed to the swine coronary artery procedures and edited the manuscript. F.L. contributed to human coronary artery pathology data. T.Z. performed organ chamber experiments. L.S.-U. and R.K. contributed to the rabbit experiments. A.S. performed PCR experiments and analysed data. R.I. performed histology and immunological experiments. F.H. edited the manuscript. T.E., S.B. and H.R. edited the manuscript. J.V. performed histologic analyses. R.C.R. contributed to the study design and edited the manuscript. P.S.T. designed experiments, analysed data and edited the manuscript. S.S. designed the studies, performed surgical procedures in rats and rabbits, ran molecular biology experiments *in vitro* and *in vivo*, edited the manuscript and secured the funding.

Author Information Reprints and permissions information is available at www.nature.com/reprints. The authors declare no competing financial interests. Readers are welcome to comment on the online version of the paper. Correspondence and requests for materials should be addressed to S.S. (schrepfer@stanford.edu).

METHODS

Animal models. HMAs were obtained during routine coronary artery bypass surgery and HCAs without stenotic disease or calcifications were obtained from patients <50 years of age undergoing heart transplantation for dilated cardiomyopathy. The use of leftover arteries from the operating room for research was approved by the Institutional Review Board (IRB) and patients gave their written informed consent. Human myointimal hyperplasia was induced in HMAs and HCAs by balloon injury using a 2-French Fogarty catheter and the human arteries were implanted into the abdominal aortic position of male athymic RNU rats (8 weeks old; Crl:NIH-Foxn1tm; Charles River, Sulzfeld, Germany). Male Lewis rats (8 weeks old) and male New Zealand rabbits (12 weeks old, Charles River) underwent balloon injury of their abdominal aortas or their iliac arteries, respectively, using Fogarty catheters. Rats and rabbits in the DCA groups were treated with DCA (0.75 g l⁻¹ in drinking water, Sigma, Munich, Germany). The PDGF-R blocker imatinib (50 mg kg⁻¹ day⁻¹, oral) was administered in one experiment. Animals were excluded if they died prematurely or became sick, as diagnosed by a veterinarian. Vessels in the PDK2-knockdown HMA or HCA groups underwent *ex vivo* PDK2 knockdown on the day before implantation. Rat and rabbit studies were approved by the Hamburg Amt für Gesundheit und Verbraucherschutz. Naturally diseased human coronary artery samples were recovered at autopsy from patients with myointimal hyperplasia at 54 to 63 years of age.

Swine study. Swine experiments were performed according to the protocol approved by the Stanford University Administrative Panel on Laboratory Animal Care (APLAC). A total of 10 female juvenile Yorkshire swine (40–50 kg, 12–14 weeks old) were used for this study. Swine were pretreated with aspirin (650 mg) and nifedipine (30 mg) orally at least 12 h before the injury procedure. The animals were sedated with telazol (6 mg kg⁻¹, intramuscular), followed by inhalant mask induction (isoflurane 4–5%). Following intubation, anaesthesia was maintained with 1–3% isoflurane in a mixture of oxygen and air. Animals were placed in the supine position and continuous electrocardiography and haemodynamic monitoring were performed throughout all procedures.

Vascular access was obtained using a standard 6-French vascular sheath placed in the right or left carotid and/or femoral arteries, as necessary. All animals received pre-procedural heparin (300 IU kg⁻¹, intra-arterial) and an activated clotting time was maintained at >300 s.

After advancing a 6-French guiding catheter through the aorta into the coronary ostia, an intracoronary injection of 0.2 mg nitroglycerin was administered and baseline coronary angiography was performed to identify the desirable location for the lesion based on coronary artery size and anatomy. A 0.014-inch percutaneous transluminal coronary angioplasty guidewire was advanced through the guiding catheter into the coronary artery. A bare metal coronary stent was implanted distal to the target lesion site to achieve a 1.05–1.15:1 stent–artery ratio as a marker. Balloon injury was induced at 10–20 mm proximal from the marker stent to achieve a 1.3–1.35:1 balloon–artery overstretch. The balloon was inflated for 30 s twice with a 30-s interval. Three coronary arteries, the left anterior descending artery, the circumflex artery and the right coronary artery were used in all animals. Subsequently, coronary artery patency was confirmed by coronary artery angiography. The animals were weaned from mechanical ventilation and allowed to recover in their normal housing at the animal care facility. Swine in the treatment group received DCA at 25 mg kg⁻¹ three times a day. The animals were monitored daily until the time of coronary artery retrieval at 4 weeks after euthanasia. A total of 45 sections were analysed per group (three sections per vessel, three coronary arteries per pig, five pigs per group).

Histology and immunohistochemistry. Vessels were stained with Masson's trichrome for quantification of the luminal obliteration, which was defined as the percentage of the cross-sectional area within the internal elastic lamina taken up by the myointima. The overview vessel images in the figures show cropped vessels without surrounding tissue. RECA-1 (HIS52, Serotec, Raleigh, North Carolina) was used to stain endothelium. CD3 (SP7), CD68 (ED1, Abcam) and MPO (no. 475915, Calbiochem) staining characterized leukocyte infiltration.

Cytokine antibody array. Injured rat aortas or HMAs were recovered and homogenized in cell lysing buffer (including proteinase inhibitor) using the Qiagen Tissue Lyser. Tissue lysate (400 µg) was diluted in 1 ml assay buffer and membranes were incubated for 2 h at 20–25 °C followed by antibody incubation according to the protocol. Cytokine antibody arrays for PDGF, IFN γ , MCP-1, MIP-3 α , and IL-1 β (Raybiotech, Norcross, Georgia, USA) were performed according to the manufacturer's protocol. The membranes were digitized using bioluminescence imaging and quantified using NIH ImageJ. Cytokine concentration is expressed in arbitrary units (AU).

Cell culture. Human vascular SMCs were freshly isolated from HMA or atherosclerotic coronary arteries using papain (1 mg ml⁻¹), dithiothreitol (0.5 mg ml⁻¹), collagenase (0.6 mg ml⁻¹) and bovine serum albumin (0.6 mg ml⁻¹, Sigma). SMCs were used for experiments when they were 70–80% confluent. SMCs were incubated

with PDGF (50 ng ml⁻¹) for 48 h and/or DCA (5 mM; DCA treatment was started 2 days before PDGF) if not indicated otherwise. The VDAC inhibitor diisothiocyanatostilbene-2,2'-disulfonic acid (DIDS, 0.5 mM for 24 h, Sigma) or HXK2VBD-cpm, a cell-permeable peptide analogue of the HK2-VDAC binding domain (100 µM, Advanced Peptide, Boston, MA), were used in some assays.

PDK2 knockdown. Lentiviral shRNA particles targeting *PDK2* (Santa Cruz, Santa Cruz, California) were used to knock down *PDK2* *ex vivo* before HMA or HCA implantation, and *in vitro* using human SMCs. Lentiviral particles were a pool of three different shRNA plasmids: 5'-GATCCCCAAGTACATAGAGCACTTTTC AAGAGAAAGTGCTCTATGTACTTGGTTTTT-3', 5'-GATCCGACCGATGCTGTCATCTATTCAAGAGAATAGATGACAGCATCGGTTCTTTTT-3', 5'-GATCCCCCAACTCTAAAGTGGAAAGATTCAAGAGATCTCCACTTTAGAGT TGGTTTTT-3'.

shRNA lentiviral particles containing an shRNA construct encoding a scrambled sequence served as control. Vessels were inflated with lentiviral-particle-containing medium (1 × 10⁶ infectious units of virus per 200 µl); human SMCs were transduced at a multiplicity of infection of 50. Successfully transduced *PDK2*-knockdown SMCs were purified using puromycin.

PDH knockdown. SMCs (3 × 10⁴) were transfected with 80 pmol of siRNA targeting *PDH* (Santa Cruz) in OptiMem (Gibco, Grand Island, New York) supplemented with transfection reagent (Santa Cruz) at 37 °C and 5% CO₂. *PDH* siRNA was a pool of three different siRNA duplexes: sense, 5'-CAGAUCAGCUGUAUA AACATT-3'; antisense, 5'-UGUUUAUACAGCUGAUCUGTT-3'; sense, 5'-GG AUUGCUCUAGCCUGUAATT-3'; antisense, 5'-UUACAGGCUAGAGCAAU CCTT-3'; sense, 5'-CUGUCACAUUCCUUAUUUCUTT-3', antisense: 5'-AGAA AUAGGAAUGUGACAGTT-3'.

After 6 h, the same volume of normal growth medium containing two times the normal serum and antibiotics concentration was added without removing the transfection mixture. After an additional 24 h, medium was replaced and cells were used for experiments 48 h after the transfection.

Elispot assays. For uni-directional Elispot assays, recipient splenocytes were isolated from fresh spleen 7 days after HMA or aortic transplantation and used as responder cells. Donor-specific non-transplanted HMA or aortic tissues were homogenized and single cells were mitomycin-inhibited and served as stimulator cells. Stimulator cells (10⁵) were incubated with 10⁶ recipient responder splenocytes for 24 h and IFN γ spot frequencies were automatically counted using an Elispot plate reader.

Endothelial-cell scratch assay. Endothelial cells (5 × 10⁵ per well) were plated onto 6-well plates. When cells reached confluence, a scratch was made across the cell monolayer using a pipette tip (scratch width, 338 µm). Time to closure was monitored by living cell imaging (Improvision Spinning Disk; Perkin Elmer, Waltham, Massachusetts, magnification × 100) for 24 h. In addition, endothelial cells that migrated into the 340 µm × 338 µm scratch area were counted after 5 h.

Organ chamber experiments. Fresh vascular rings of rat aorta were cut into 4-mm segments and mounted in phosphate-buffer-filled organ chambers gassed with 95% oxygen and 5% carbon dioxide. After pre-constriction with prostaglandin F_{2 α} (15 µl 10⁻² M in 25 ml buffer) to achieve 50–80% of the maximal KCl-induced tone, increasing concentrations of nitroglycerin (NTG, 10⁻⁹ M to 10^{-4.5} M) or acetylcholine (10⁻⁹ M to 10^{-5.5} M) were added for relaxation studies. Endothelium-dependent (acetylcholine) and -independent (NTG) vasodilator responses were assessed with denuded aortic rings serving as negative controls for endothelial function.

Immunoblot analysis. Proteins were separated on SDS-PAGE gels (Invitrogen, Carlsbad, California) and western blot analyses were conducted with specific antibodies to pAKT (D9E), pERK1/2 (#9101), GAPDH (14C10, Cell Signaling, Irvine, California), HK2 (1A7), PDH (9H9), PDK1 (C20), PDK2 (N20), PDK3 (N14), PDK4 (C16, Santa Cruz), SMA (ab5694), CV (ab110415), β -actin (ACTN05 (C4), Abcam), cytochrome C (6H2.B4, Calbiochem, Darmstadt, Germany), myocardin (355521, R+D Systems, Minneapolis, Minnesota), and SMemb (3H2, Yamasa, Tokyo, Japan). The membranes were digitized using bioluminescence imaging and quantified using NIH ImageJ. GAPDH or β -actin served as housekeeping control.

RNA quantification and PCR. Total RNA was isolated with a TRIzol-based (Invitrogen) RNA isolation protocol and RNA was quantified by NanoDrop (NanoDrop ND-1000, Peqlab, Erlangen, Germany). Samples required 260:280 ratios of >1.8 for inclusion. RNA was reverse-transcribed with the High Capacity cDNA Reverse Transcription Kit (Applied Biosystems, Foster City, California) according to the manufacturer's instructions. Quantitative determination of RNA was performed by real-time RT-PCR with POWER SYBR Green PCR Master Mix (Applied Biosystems) according to the manufacturer's instructions. Primers were used specific for every human sequence. Particularly, the primers used to amplify *PDK1-4* were: *PDK1* forward, 5'-AGTGCCTCTGGCTGGTTTTGG-3' and reverse, 5'-CGTGGTTG GTGTTGTAATGCTTCC-3'; *PDK2* forward, 5'-GCAAGTTCTCCCGTCCCC G-3' and reverse, 5'-GGACATACCAGCTCTGCCACAG-3'; *PDK3* forward, 5'-CAGAGCTGCCCTTGGCTGG-3' and reverse, 5'-TGGCCGATCGCGGAC TTATT-3' and *PDK4* forward, 5'-TGGTAGCAGTGGTCCAAGATGCC-3' and

reverse, 5'-CAACTGTTGCCCGCATTGCAT-3'. Absolute and relative RNA levels of *PDK1*, *PDK2*, *PDK3* and *PDK4* were determined to endogenous *GAPDH*. *c-KIT* RNA was amplified using primers forward, 5'-CACCGAAGGAGGCATTACAC-3' and reverse, 5'-GGAATCCTGTGCCACACA-3'. *SMA* RNA was amplified using primers forward, 5'-GCGTGGCTATTCTTCGTTA-3' and reverse, 5'-ATGAAGGATGGCTGGAACAG-3'. *SM22* RNA was amplified using primers forward, 5'-AACAGCCTGTACCCTGATGG-3' and reverse, 5'-CGGTAGTGCCCATCATCTT-3'. Experiments were performed on the 7900 HT Sequence Detection System (Applied Biosystems). The amount of RNA was estimated according to the comparative Ct method with the $2^{-\Delta\Delta Ct}$ formula.

Immunofluorescence staining. Tissues were fixed with 4% paraformaldehyde, dehydrated and embedded in paraffin. After heat-induced antigen retrieval with Dako antigen retrieval solution (Dako, Glostrup, Denmark) in a steamer for 20 min, 3- μ m paraffin sections were blocked with Image-iT FX signal enhancer (Invitrogen) for 30 min. Primary antibodies of following sources were used: SMA (ab5694), SM heavy chain (EPR5335), SM22 (ab10135), calponin (CALP), smoothelin (R4A, Abcam), Ki67 (SP6), CD3 (SP7), PDK1 (C20), PDK2 (N20), human leukocyte antigen I (HLA I, 3F10, Santa Cruz), myocardin (355521, R+D Systems), and rat major histocompatibility complex I (MHC I, B5) conjugated with FITC (BD Pharmingen). Except for MHC I staining, all other studies included incubation with a corresponding secondary antibody conjugated to Alexa Fluor 488, Alexa Fluor 555, or Alexa Fluor 647 (Invitrogen). Sections were incubated with antibodies for 1 h at 37 °C, followed by cell nucleus staining with DAPI for 10 min. Imaging was performed using a Nikon Eclipse TiE microscope (Nikon, Tokyo, Japan) equipped with the Perkin Elmer UltraVIEW VoX confocal imaging system (Perkin Elmer, Waltham, Massachusetts). Analysis was carried out with Velocity 6.1.1 (Perkin Elmer).

For co-localization of HK2 and mitochondria, confocal images stained for HK2 (1A7, Santa Cruz), MitoTracker (Invitrogen), and DAPI were obtained with the confocal Nikon Eclipse TiE microscope.

Flow cytometry by FACS. Primary antibodies used to characterize SMCs were SMA (ab5694), SM22 (ab10135), calponin (CALP), smoothelin (R4A, Abcam), and myocardin (355521, R+D Systems). Samples were measured on a FACSCalibur system (Becton Dickinson, Heidelberg, Germany) and analysed using FlowJo (Tree Star, Ashland, Oregon). In the histograms, the isotype controls are displayed in grey and the antigens of interest in green.

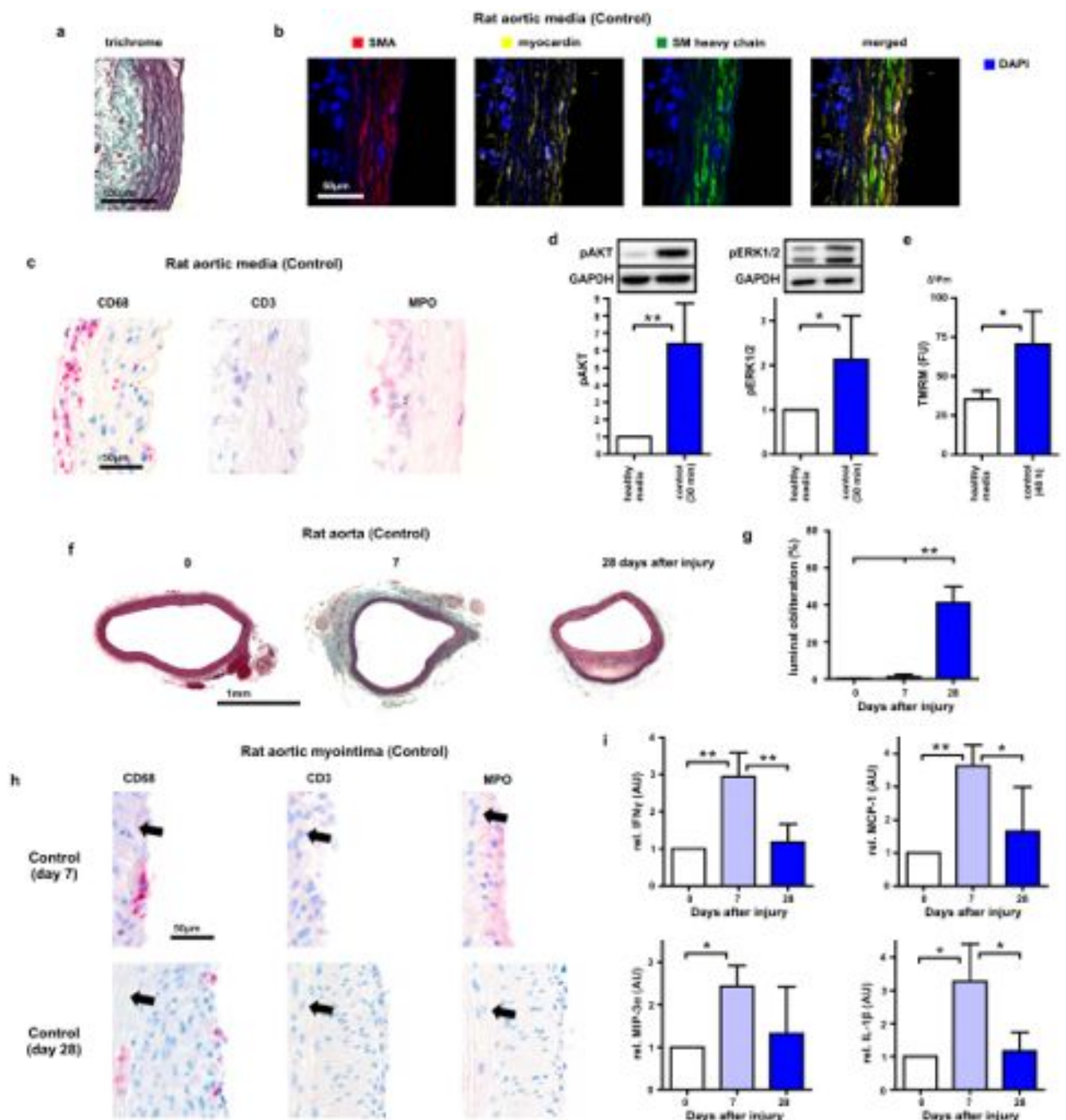
TMRM staining. To measure $\Delta\Psi_m$, freshly isolated tissues or cells were incubated with tetramethylrhodamine methyl ester perchlorate (TMRM, 10 nM; Invitrogen) and Hoechst 33342 (0.3 μ M; Invitrogen) for 30 min at 37 °C. Subsequently, samples were washed to remove unbound dye and immediately imaged. *In vitro*, 5×10^4 SMCs were plated on confocal dishes and cells were stimulated according to their

group-specific protocol. Vessels were freshly cut under the microscope into thin slices and were timely stained and analysed. Fluorescence signal was measured using a Nikon Eclipse TiE microscope equipped with Perkin Elmer UltraVIEW VoX confocal imaging system. Analysis was carried out on Velocity 6.1.1. For analysis, mean TMRM-fluorescence intensity was calculated by dividing individual object fluorescence intensities by sizes (number of voxels) and is expressed in arbitrary fluorescence units (FU).

Cytochrome C staining. To measure cytochrome-C-related apoptosis, cells were stained for cytochrome C after staurosporine treatment (50 nM; Sigma) for 18 h. Cells were then fixed in 4% paraformaldehyde, permeabilized with Permeabilization Solution (Applied StemCell, Menlo Park, California), and blocked with Blocking Solution (Applied StemCell). After incubation with a mouse antibody against cytochrome C (6H2.B4, Calbiochem) for 16 h at 4 °C, a goat anti-mouse antibody conjugated with Alexa Fluor 488 (Invitrogen) was used as the secondary antibody (1 h, 37 °C). Cell nuclei were counterstained with DAPI. Examination was carried out with a Nikon Eclipse TiE microscope equipped with Perkin Elmer UltraVIEW VoX confocal imaging system, followed by analysis with Velocity 6.1.1. For analysis, cells showing diffuse cytoplasmatic cytochrome C staining overlying the nucleus were counted and divided by the number of DAPI positive cells to obtain the percentage of cells with cytochrome C leakage.

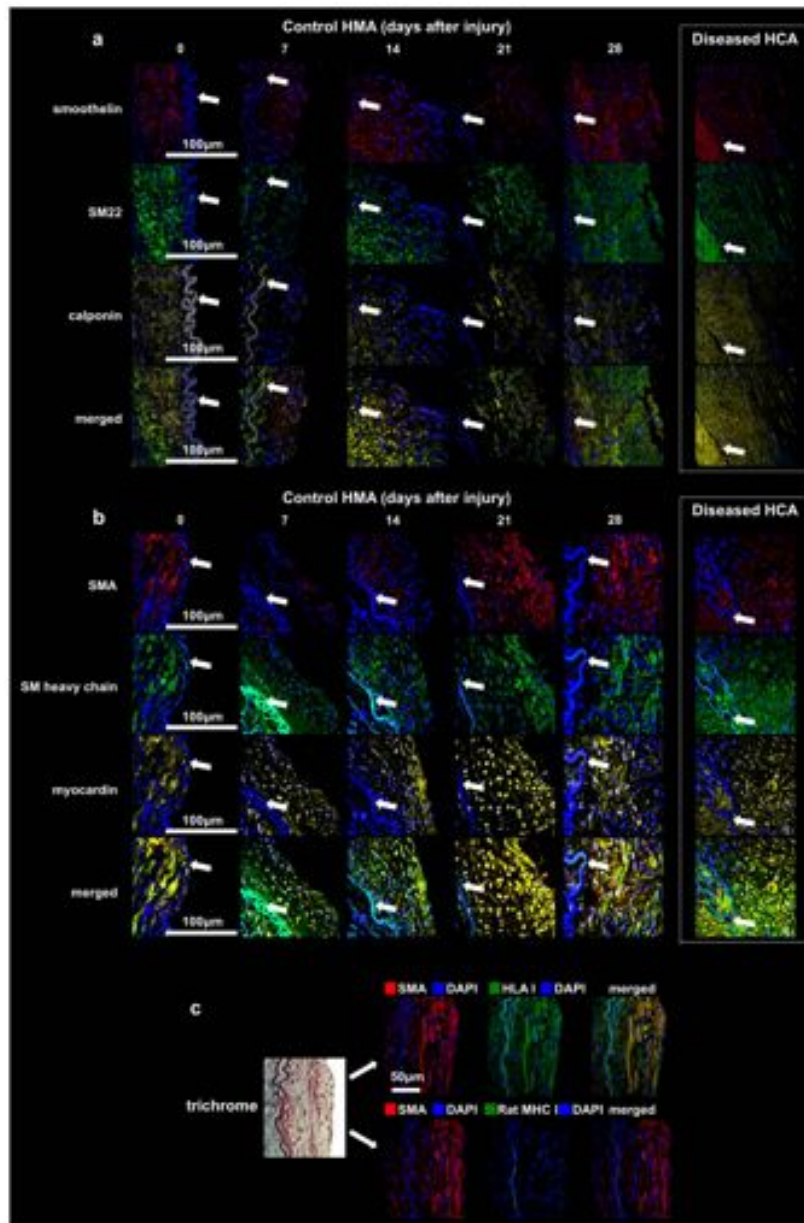
TUNEL staining. SMCs were treated with staurosporine (50 nM; Sigma) for 18 h to induce apoptosis. ApoptTag apoptosis detection kit (TUNEL; Merck Millipore, Darmstadt, Germany) was then used according to manufacturer's instructions to label apoptotic cells. Similarly, tissue sections, processed as described in "Immunofluorescence staining", underwent heat-induced antigen retrieval with Dako antigen retrieval solution (Dako) in a steamer for 20 min, followed by blocking with Image-iT FX signal enhancer (Invitrogen) for 30 min. Staining was performed according to manufacturer's instructions using the ApoptTag apoptosis detection kit. Nuclei were counterstained with DAPI. The percentage of TUNEL-positive cells was calculated.

Statistics. Owing to the exploratory character of this study and the fact that an inhibitory effect of DCA on myointima formation has not been described yet, there were no data for an initial power analysis. Usually, five to seven animals were randomized to one group. All samples were number coded until the readout was finalized. The numbers were assigned before the experiment and determined the group, treatment and condition. The surgeons performing the procedures and the scientists performing the readouts were blinded. All values are expressed as mean \pm s.d. or mean \pm s.e.m. as indicated. Intergroup differences were appropriately assessed by either unpaired two-tailed Student's *t*-test or one-way analysis of variance (ANOVA) with Bonferroni's post-hoc test. If data were normalized to the control group, one-sample *t*-tests against 1.0 were used for study groups. * $P < 0.05$, ** $P < 0.01$.



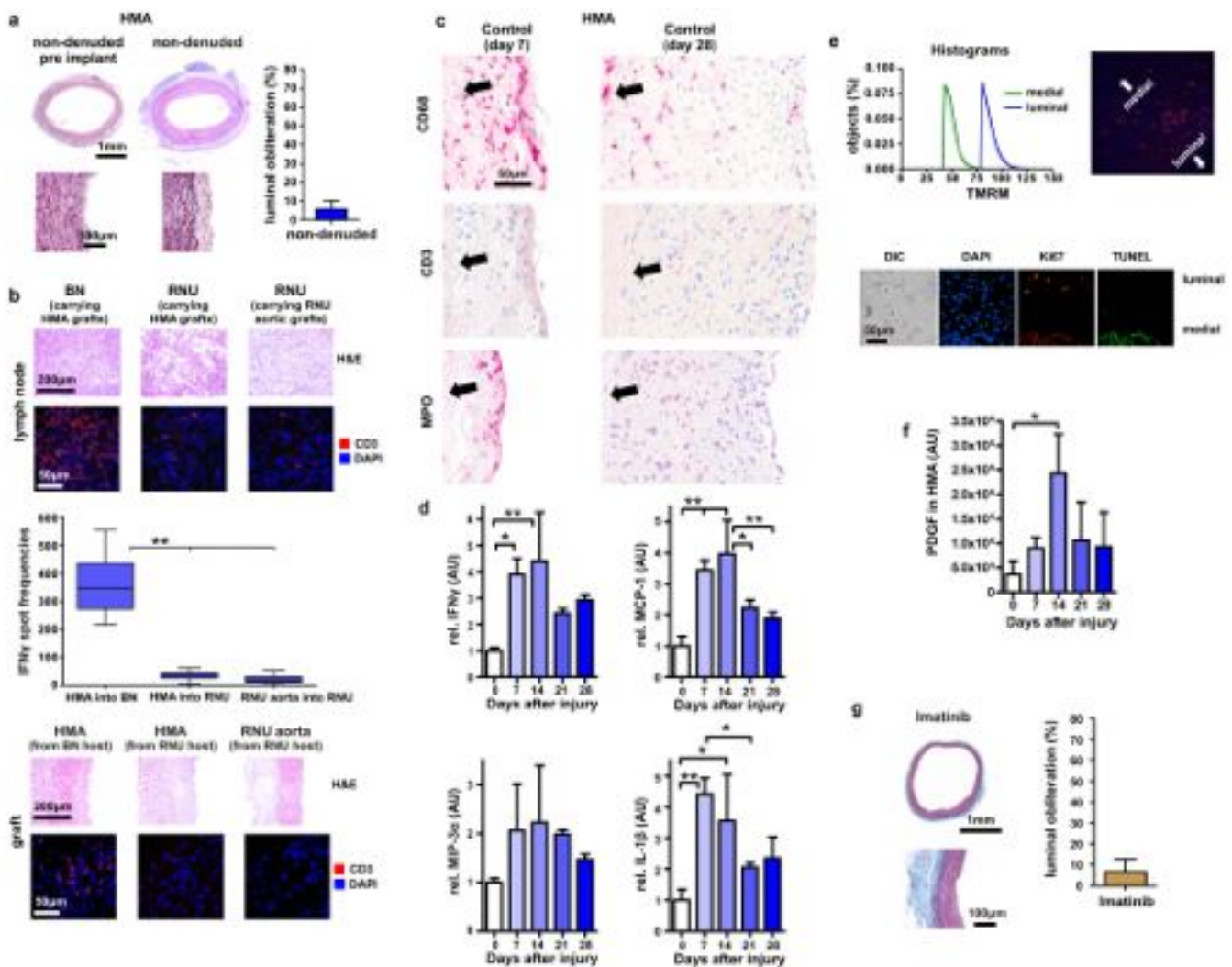
Extended Data Figure 1 | Myointima formation in balloon-injured rat aortas. **a, b**, Forty-eight hours after mechanical injury, trichrome (**a**) and immunofluorescence for SMC-markers (**b**) identified abundant SMCs in the aortic media. **c**, The infiltrate at 48 h was composed of CD68⁺ macrophages, some MPO⁺ neutrophils, and no CD3⁺ lymphocytes. **d**, Phosphorylation of AKT (pAKT), and ERK1 and ERK2 (pERK1/2), was markedly increased as early as 30 min after injury (mean \pm s.d., $n = 6$ animals per group, control after 30 min normalized to healthy media, one-sample t -tests). **e**, Media cells of injured aortas showed $\Delta\Psi_m$ hyperpolarization after 48 h (mean \pm s.d., $n = 4$ animals (healthy media), 6 animals (control after 48 h), Student's t -test).

f, g, A myointima developed over 28 days in injured rat aortas (**f**, trichrome) and caused luminal obliteration (**g**, mean \pm s.d., $n = 5$ animals (day 0), 4 animals (day 7), 6 animals (day 28), ANOVA with Bonferroni's post-hoc test). **h**, Many infiltrating macrophages and very few neutrophils were observed in the myointima at 7 days. Leukocyte infiltration was sparse at 28 days; no lymphocytes were found (black arrows, internal elastic lamina). **i**, Tissue IFN γ , MCP-1, MIP-3 α , and IL-1 β levels were markedly increased at 7 days and were diminished after 28 days (mean \pm s.d., $n = 3$ animals (day 0), 4 animals (day 7 and 28), days 7 and 28 normalized to day 0, one-sample t -test (day 0 versus day 7), Student's t -test (day 7 versus day 28)). * $P < 0.05$; ** $P < 0.01$.



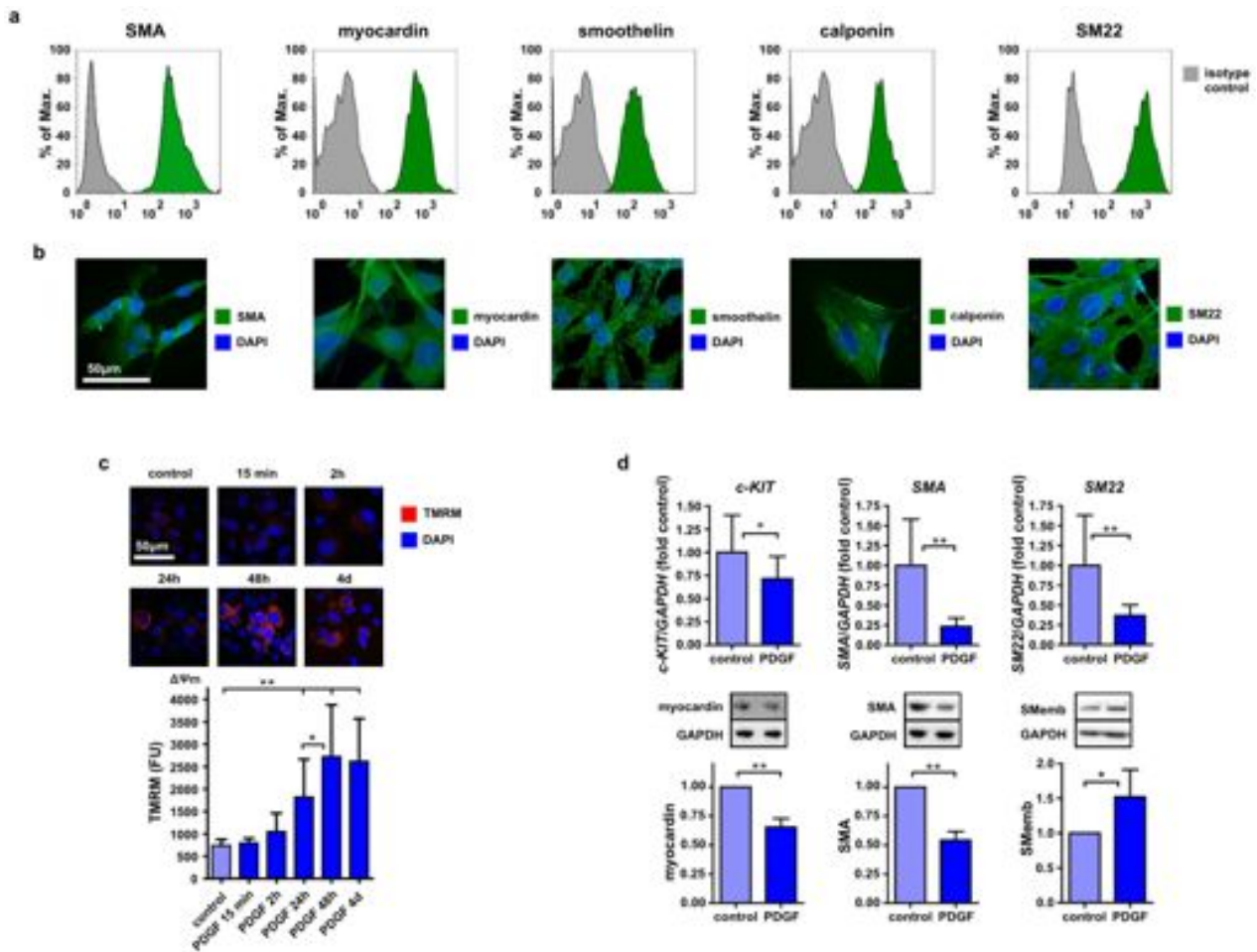
Extended Data Figure 2 | Characterization of the human internal mammary artery model. **a, b,** Sections were co-stained for the SMC markers smoothelin, SM22, and calponin (**a**) or SMA, smooth muscle myosin (SM) heavy chain and myocardin (**b**). Co-localization could be observed in the merged pictures (white arrows, internal elastic lamina, pictures are representative of two replicates). Direct comparison between the HMA myointima on day 28 with the myointima in diseased human coronary artery (HCA) samples illustrated close similarities in immunofluorescence

morphology. **c,** The human origin of myointimal cells in 21-day control HMAs was confirmed. Trichrome showed the development of a cell-rich myointima with mild fibrosis. Specimens were stained for SMA, DAPI and human leukocyte antigen class I (HLA I, upper row) or rat major histocompatibility complex class I (rat MHC I, lower row). Cells expressing SMA (red) co-expressed HLA I (green), which resulted in a yellow staining in the merged picture. No co-expression of SMA and rat MHC I was observed.



Extended Data Figure 3 | The central role for PDGF in advancing myointima formation. **a**, After 28 days, non-deneduded HMAs in RNU rats showed only minor myointimal lesions (trichrome, mean \pm s.d., $n = 5$ animals). **b**, To evaluate a possible rejection process in the xenogeneic HMA setting, host immune activation and graft infiltration were assessed. In the HMA model, xenogeneic HMA were transplanted into RNU rats (middle column). Xenogeneic HMA transplants into immunocompetent hosts (Brown Norway rats; BN, left column) and syngeneic RNU aortic transplants into RNU recipients (right column) served as controls; all analyses were performed after 7 days. Para-aortic BN lymph nodes harboured huge amounts of CD3⁺ lymphocytes, whereas the number was low in RNU lymph nodes. In IFN γ -Elispot assays with homogenized graft cells and recipient splenocytes, only BN recipients showed strong immune activation, whereas RNU recipients failed to mount a relevant immune response (box 25th to 75th percentile with median, whiskers min-max, quadruplicates of 5 animals (columns 1 and 2) and 4 animals (column 3), ANOVA with Bonferroni's post-hoc test). Dense CD3⁺ infiltrates were found in HMA grafts of BN recipients, but not in HMA

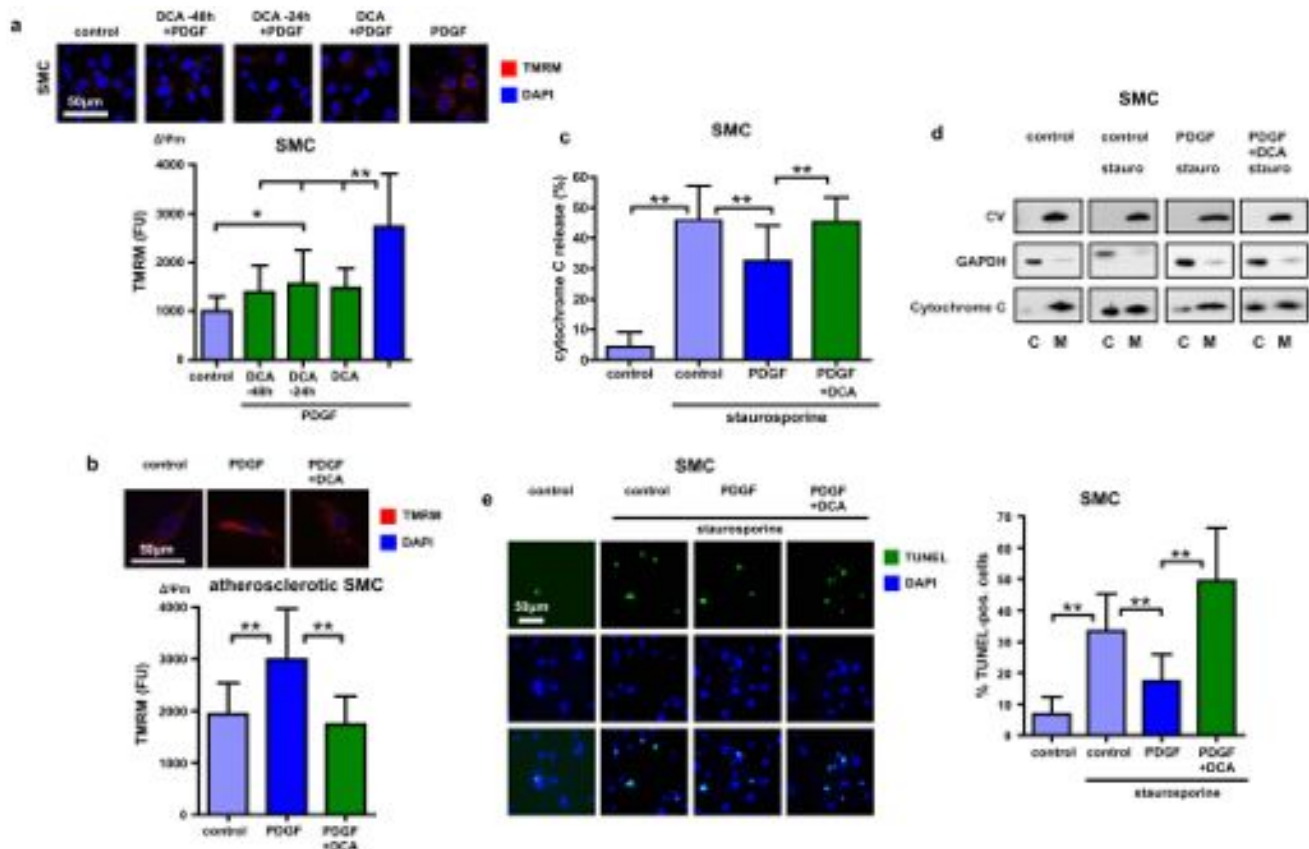
or RNU aortic grafts in RNU recipients. **c**, Immunohistochemistry identified myointimal macrophages and neutrophils in HMA control specimens on day 7 and reduced leukocyte infiltration in control specimens on day 28. Lymphocytes were not observed (black arrows, internal elastic lamina). **d**, HMA tissue levels of the inflammatory cytokines IFN γ , MCP-1, MIP-3 α , and IL-1 β were elevated during the first 14 days (mean \pm s.d., $n = 3$ animals per group, ANOVA with Bonferroni's post-hoc test). **e**, In HMA day 21 vessels, spatial differences of SMC $\Delta\Psi_m$ with higher TMRM fluorescence in the luminal areas compared to the areas adjacent to the media were observed. SMC proliferation also mainly occurred in these luminal regions of elevated $\Delta\Psi_m$. DIC, differential interference contrast. **f**, Tissue PDGF was increased in HMA after injury and peaked after 14 days (mean \pm s.d., $n = 3$ animals per time point, ANOVA with Bonferroni's post-hoc test). **g**, Compared to untreated control vessels at day 28 in the rat aortic balloon injury model (Extended Data Fig. 1g), imatinib (PDGF-R blocker)-treated 28-day vessels showed only minor lesions (mean \pm s.d., $n = 8$ animals). * $P < 0.05$; ** $P < 0.01$.



Extended Data Figure 4 | SMC characterization and response to PDGF.

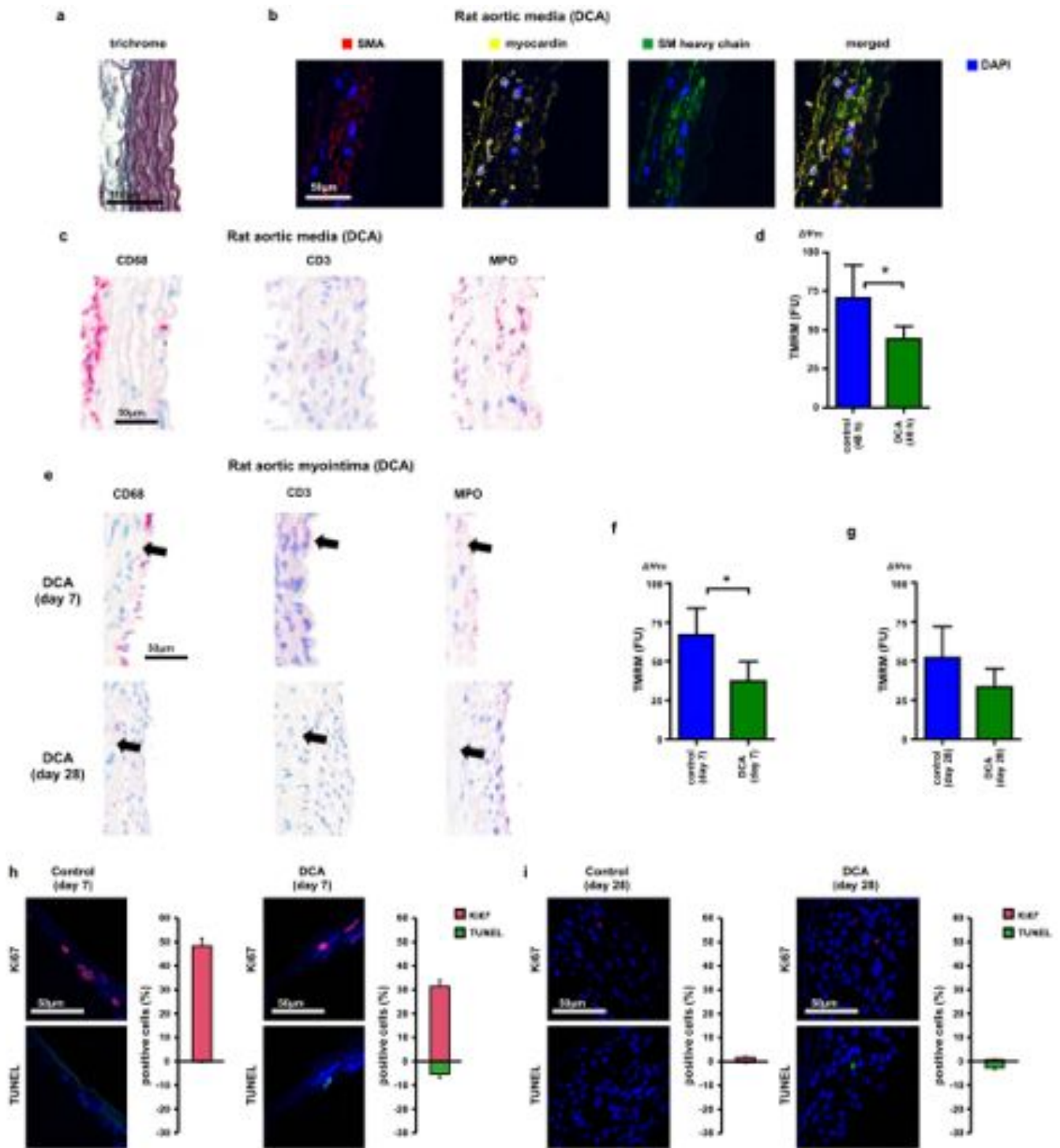
a, b, Cells isolated from fresh HMA were positive for SMA, myocardin, smoothelin, calponin, and SM22 α (SM22) as detected by FACS (**a**, pictures are representative of three replicates) and immunofluorescence (**b**, pictures are representative of three replicates). Thus, cells were identified as SMCs, but we cannot rule out that cells from other sources (for example, vessel wall stem cells with smooth muscle characteristics) were also involved. **c**, $\Delta\Psi_m$ hyperpolarization, a phenomenon observed at times of maximized net proliferative activity in HMA (Fig. 1f), could be linked to PDGF. When SMCs were incubated with PDGF, $\Delta\Psi_m$ hyperpolarization steadily increased over time, reaching its maximum after 48 h (mean \pm s.d., 5 replicates of

2 (15 min, 2 h) or 3 (all other groups) independent experiments, ANOVA with Bonferroni's post-hoc test). **d**, We found a significant downregulation of *c-KIT*, *SMA* and *SM22* mRNA versus *GAPDH* mRNA after incubation with PDGF, all maturity markers for contractile SMCs (mean \pm s.d., 13 independent experiments, Student's *t*-test). Western blot analysis further revealed a downregulation of myocardin and confirmed SMA reduction. In contrast, SMemb, the embryonic form of smooth muscle myosin heavy chain and a marker for dedifferentiated SMCs, was increased, indicating a PDGF-induced phenotype switch (mean \pm s.d., 5 (myocardin and SMA) and 6 (SMemb) independent experiments, PDGF normalized to control, one-sample *t*-tests). * $P < 0.05$; ** $P < 0.01$.



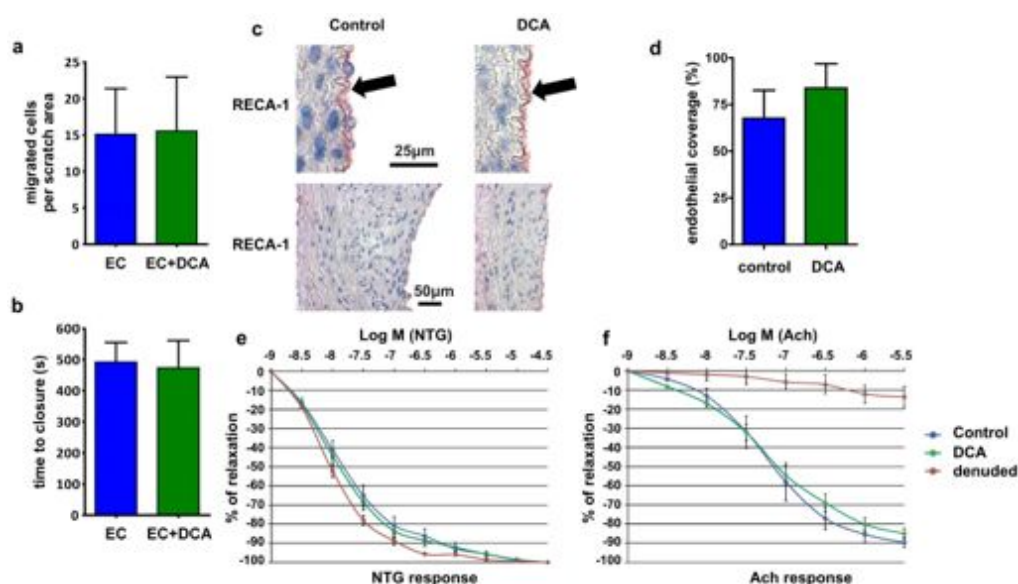
Extended Data Figure 5 | DCA reduces $\Delta\Psi_m$ hyperpolarization and facilitates apoptosis in SMCs. **a**, To assess the kinetics of DCA action *in vitro*, SMCs were pre-incubated with DCA for different time periods and then stimulated with PDGF for 48 h (mean \pm s.d., 10 replicates of 3 independent experiments per group, ANOVA with Bonferroni's post-hoc test). DCA reduced PDGF-induced $\Delta\Psi_m$ hyperpolarization irrespective of the pre-incubation period. **b**, Atherosclerotic plaques from heavily calcified and atherosclerotic human coronary arteries were scraped off the media and cultured in SMC medium. Outgrowing SMCs were picked and expanded. PDGF significantly increased $\Delta\Psi_m$, an effect that was prevented by DCA (mean \pm s.d., 10 replicates of 3 independent experiments, ANOVA with Bonferroni's post-hoc test). **c–e**, Apoptosis induction with staurosporine significantly increased the number of control SMCs that showed cytochrome C leakage, as identified by diffuse cytochrome C staining throughout the cell (c, mean \pm s.d., 10 replicates of 2 independent experiments per group, ANOVA

with Bonferroni's post-hoc test). PDGF significantly reduced cytochrome C release in SMCs and DCA counteracted this PDGF effect. Cytoplasmatic (C) and mitochondrial fractions (M) were isolated for immunoblotting (d, data are representative of 3 independent experiments). Separation was confirmed by the contents of mitochondrial complex V (CV) and cytosolic GAPDH. Cytochrome C was retained inside the mitochondria in control SMCs and was released with staurosporine. PDGF reduced the cytoplasmatic fraction, indicating reduced cytochrome C release, and DCA reversed the PDGF effect. SMC apoptosis was detected by TUNEL staining (e, mean \pm s.d., 10 replicates of 2 (column 1) or 3 (columns 2–4) independent experiments, ANOVA with Bonferroni's post-hoc test). Staurosporine significantly increased the number of apoptotic control SMCs. PDGF treatment decreased the percentage of apoptotic SMCs and DCA reversed this anti-apoptotic effect. * $P < 0.05$; ** $P < 0.01$.



Extended Data Figure 6 | DCA lowers medial and myointimal $\Delta\Psi_m$ and facilitates apoptosis in balloon-injured rat aortas. **a, b**, Trichrome (**a**) and immunofluorescence (**b**) confirmed abundant SMCs in the aortic media of DCA-treated animals 48h after injury. **c**, Similar to control vessels, the infiltrate mainly contained macrophages and neutrophils, but no CD3⁺ lymphocytes. **d**, DCA reduced $\Delta\Psi_m$ of medial cells (mean \pm s.d., $n = 6$ animals (control at 48 h) and 4 animals (DCA at 48 h), Student's *t*-test). **e**, Macrophages were the main inflammatory cell population in the developing myointima of immunocompetent DCA animals at 7 days. Very few neutrophils and no lymphocytes were observed. Leukocyte infiltration was markedly alleviated at 28 days (black arrows, internal elastic lamina). **f, g**, DCA effectively lowered the

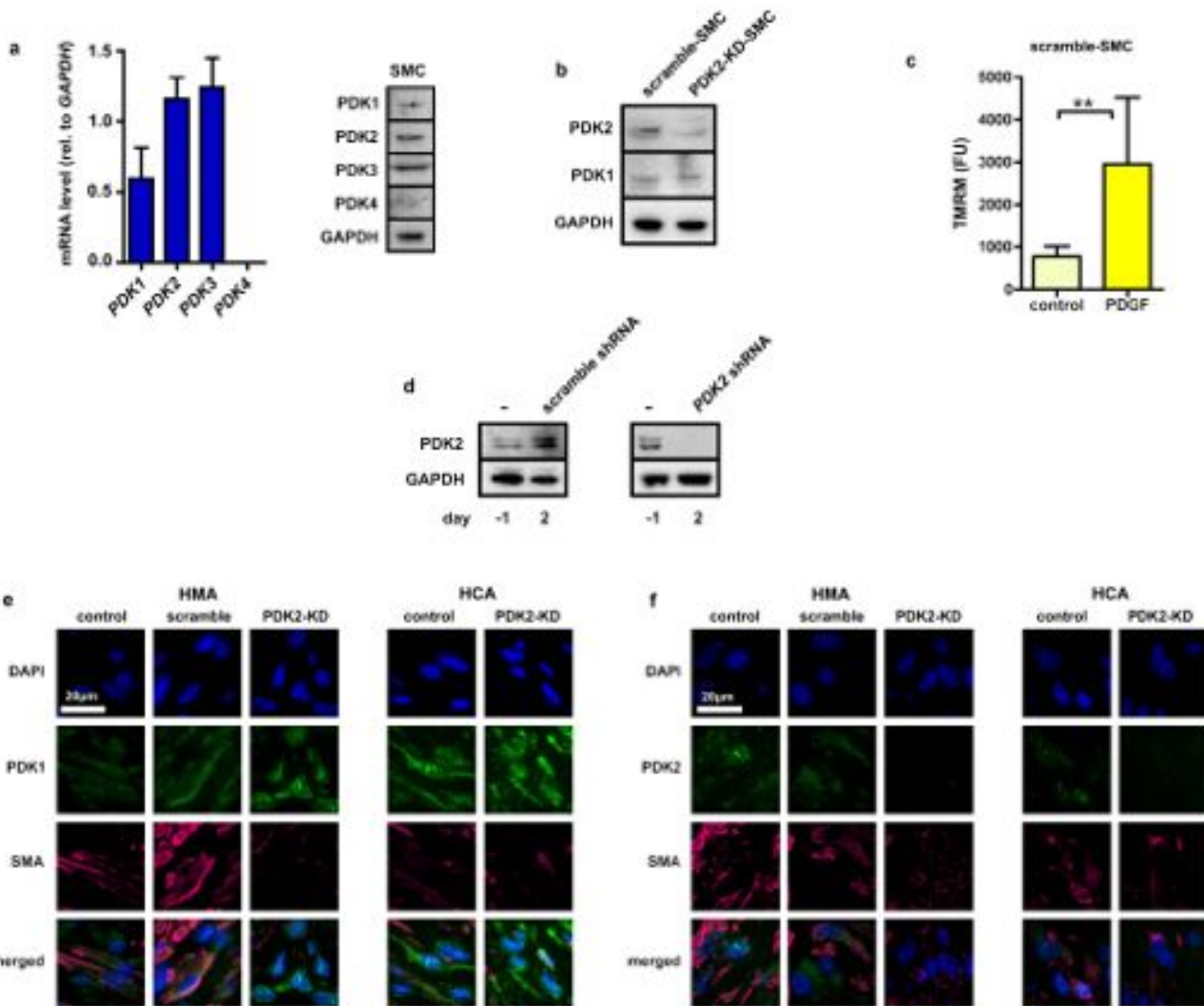
elevated $\Delta\Psi_m$ of myointimal cells on day 7 (**f**, mean \pm s.d., $n = 4$ animals per group, Student's *t*-test), but had little effect on the already reduced $\Delta\Psi_m$ at 28 days (**g**, mean \pm s.d., $n = 6$ animals per group, Student's *t*-test). **h, i**, The percentages of proliferating (Ki67⁺) and apoptotic (TUNEL⁺) cells in the myointima were calculated (representative cropped pictures of the myointima are presented). The few myointimal cells in control- and DCA-vessels at 7 days showed high proliferative activity (red, positive *y* axis), but apoptosis (green, negative *y* axis) was only observed in DCA-treated animals (**h**, mean \pm s.e.m., $n = 4$ animals per group). Proliferation and apoptosis were low after 28 days in both groups (**i**, mean \pm s.e.m., $n = 5$ animals (control at day 28) and 7 animals (DCA at day 28)). * $P < 0.05$.



Extended Data Figure 7 | DCA does not impair endothelial cell migration or vessel re-endothelialization. The effect of DCA on endothelial cell (EC) migration was assessed *in vitro*. **a, b**, A scratch (width 338 µm) was made across a confluent human EC monolayer. The number of cells that migrated into a 340 µm × 338 µm scratch rectangle within 5 h was counted (**a**, mean ± s.d., triplicates of 3 independent experiments, Student's *t*-test) and the time needed to close the scratch was recorded (**b**, mean ± s.d., *n* = 5 (EC), 4 (EC + DCA) independent experiments, Student's *t*-test). There were no differences between untreated and DCA-treated ECs. **c, d**, To evaluate vessel re-endothelialization, rat aortas underwent mechanical endothelial denudation by balloon injury. Aortas were recovered after 28 days and stained for rat endothelial cell antigen (**c**, black arrows, RECA-1). Re-endothelialization was quantified (**d**, mean ± s.d., *n* = 5 animals (control at day 28) and 6 animals

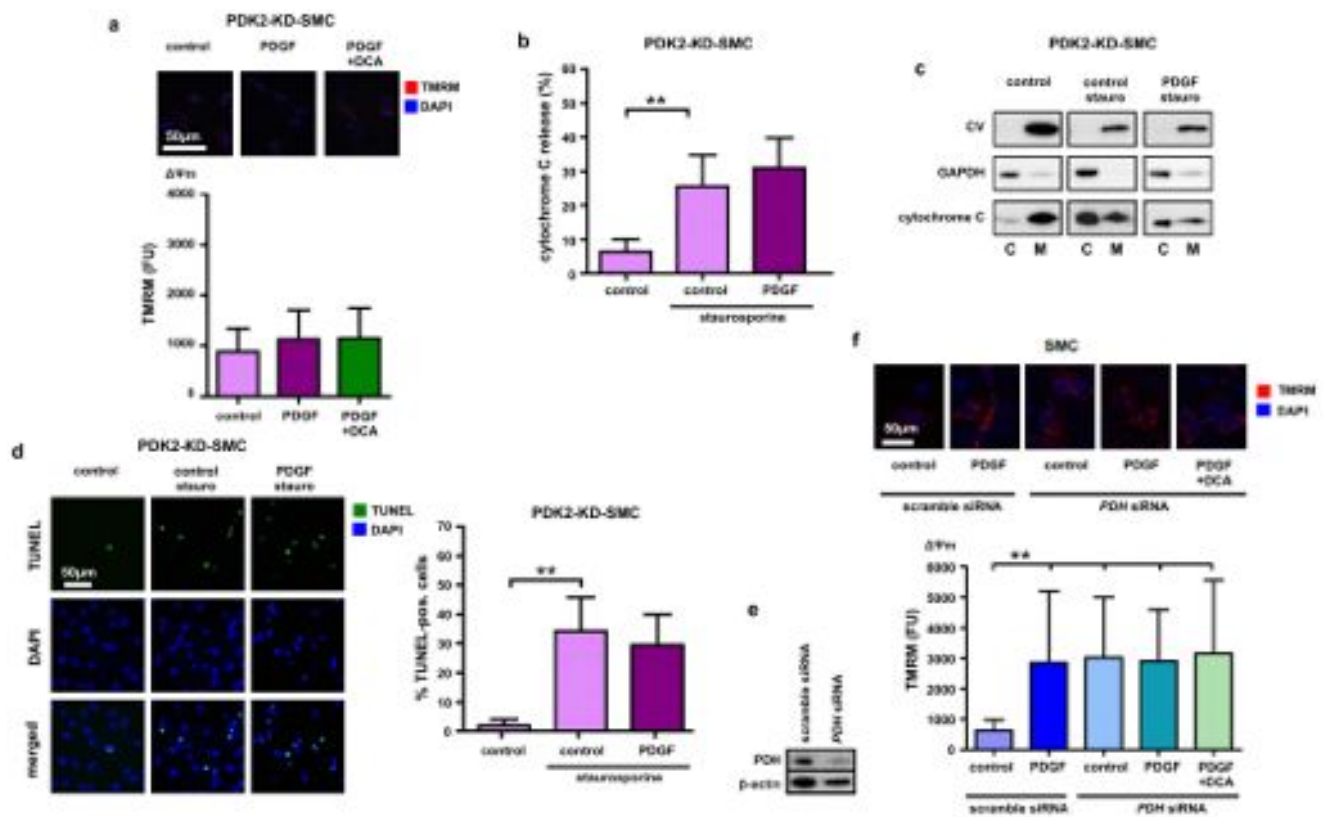
(DCA at day 28), Student's *t*-test) and was similar in both groups.

e, f, Endothelial function in both 28-day groups was further assessed in relaxation studies and compared to denuded aortas three days after balloon injury (mean ± s.e.m., *n* = 9 animals (control at day 28), 11 animals (DCA at day 28) and 3 animals (denuded at day 3)). Freshly recovered aortic segments were pre-constricted and DCA-treated and control vessels, as well as denuded aortas, showed similar endothelium-independent relaxation capacities using nitroglycerin (NTG) as vasodilator (**e**). However, denuded aortas largely failed to show endothelium-dependent relaxation with acetylcholine (Ach; **f**). Both DCA-treated and control vessels demonstrated similar and physiologic endothelium-dependent relaxation, indicating functional integrity of the vascular endothelium.



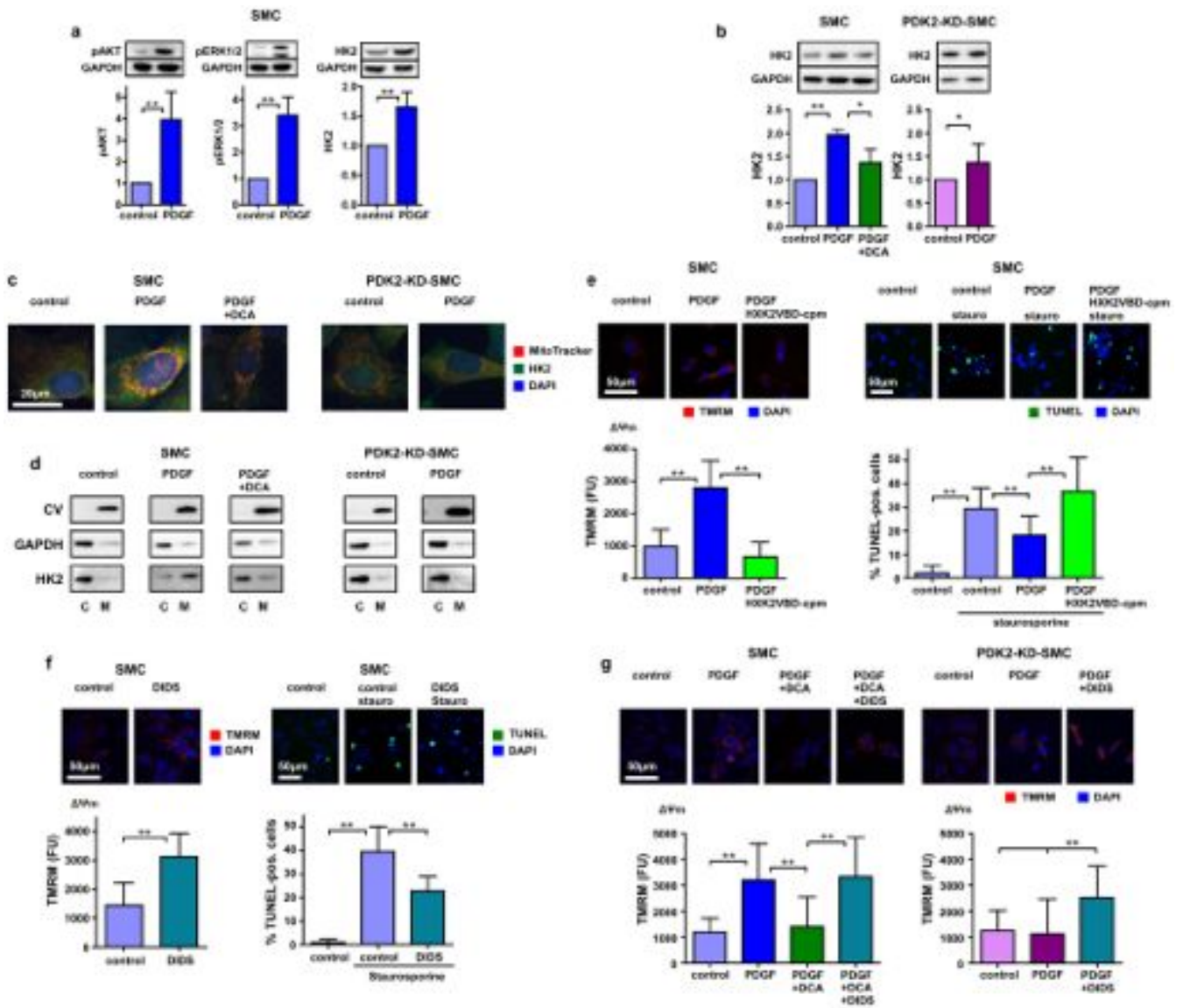
Extended Data Figure 8 | PDK2 knockdown in SMCs, HMAs and HCAs. **a**, *PDK1*, *PDK2*, *PDK3* and *PDK4* mRNA expression was assessed in control SMCs and normalized to *GAPDH* (mean \pm s.d., 3 independent experiments). *PDK1*, *PDK2* and *PDK3* mRNA was detected as shown. Also, *PDK1*, *PDK2* and *PDK3* but not *PDK4* were detectable in immunoblot analyses (data are representative of 3 independent experiments). **b**, To confirm *in vitro* *PDK2* knockdown, *PDK1* and *PDK2* expressions were assessed in immunoblot analyses (data are representative of 3 independent experiments). *PDK2* was markedly reduced in *PDK2*-knockdown SMCs (*PDK2*-KD-SMC), but not in scramble shRNA-transduced SMCs (scramble-SMC). *PDK1* expression remained unaffected by *PDK2*- or scramble-shRNA constructs. **c**, To exclude that lentiviral shRNA transduction changed the $\Delta\Psi_m$ response to PDGF, scramble-SMCs were stimulated with PDGF (mean \pm s.d., 10 replicates of 2 independent experiments, Student's *t*-test). Both the baseline potential and the PDGF-triggered increase in $\Delta\Psi_m$ were similar to SMCs (see Extended Data

Fig. 5a). **d**, Fresh HMA vessels underwent balloon injury, were divided, and one half was sampled (day -1). The other half was incubated with lentiviral particles containing *PDK2* or scrambled shRNA. On the next day, transduced vessels were transplanted into RNU rats. Two days later, vessels were recovered (day 2) for immunoblotting. *PDK2* could be detected in untreated HMA vessels (day -1). On day 2, only scrambled control HMAs, but not *PDK2*-KD vessels showed a *PDK2* signal (data are representative of 3 independent experiments). **e**, **f**, After 28 days, HMA and HCA samples were stained for DAPI, *PDK1*, *PDK2* and SMA. *PDK1* was similarly detectable in all control, scramble and *PDK2*-KD sections at day 28 (**e**, pictures are representative of 3 independent experiments). At day 28, HMA control and scramble as well as HCA control showed detectable *PDK2* protein, whereas *PDK2* fluorescence in HMA and HCA *PDK2*-KD at day 28 was negligible (**f**, pictures are representative of 3 independent experiments), demonstrating selective knockdown. *******P* < 0.01.



Extended Data Figure 9 | PDK2 knockdown mimics the DCA effect on SMC $\Delta\Psi_m$ and apoptosis. **a**, PDK2-KD-SMCs were pre-incubated with DCA and/or stimulated with PDGF. PDK2-KD-SMCs maintained low $\Delta\Psi_m$ despite PDGF stimulation and DCA did not further depolarize $\Delta\Psi_m$ (mean \pm s.d., 10 replicates of 3 (columns 1 and 3) or 4 (column 2) independent experiments, ANOVA with Bonferroni's post-hoc test). **b**, **c**, Apoptosis was induced with staurosporine. Control PDK2-KD-SMCs showed mainly mitochondria-housed cytochrome C in fluorescence stainings (**b**, mean \pm s.d., 10 replicates of 2 independent experiments, ANOVA with Bonferroni's post-hoc test) and compartment-separated immunoblot analyses (**c**, data are representative of

2 independent experiments). After induction of apoptosis, cytochrome C leaked into the cytoplasm and PDGF did not suppress cytochrome C leakage. **d**, PDGF did not induce resistance to apoptosis in PDK2-KD-SMCs (mean \pm s.d., 10 replicates of 2 independent experiments per group, ANOVA with Bonferroni's post-hoc test). **e**, To establish a link between PDH and $\Delta\Psi_m$, PDH was knocked down (data are representative of 2 independent experiments). **f**, $\Delta\Psi_m$ was significantly increased in PDH siRNA-transfected SMCs and PDGF and DCA no longer affected $\Delta\Psi_m$ (mean \pm s.d., 10 replicates of 2 (column 2) or 3 (columns 1, 3, 4 and 5) independent experiments, ANOVA with Bonferroni's post-hoc test). ** $P < 0.01$.



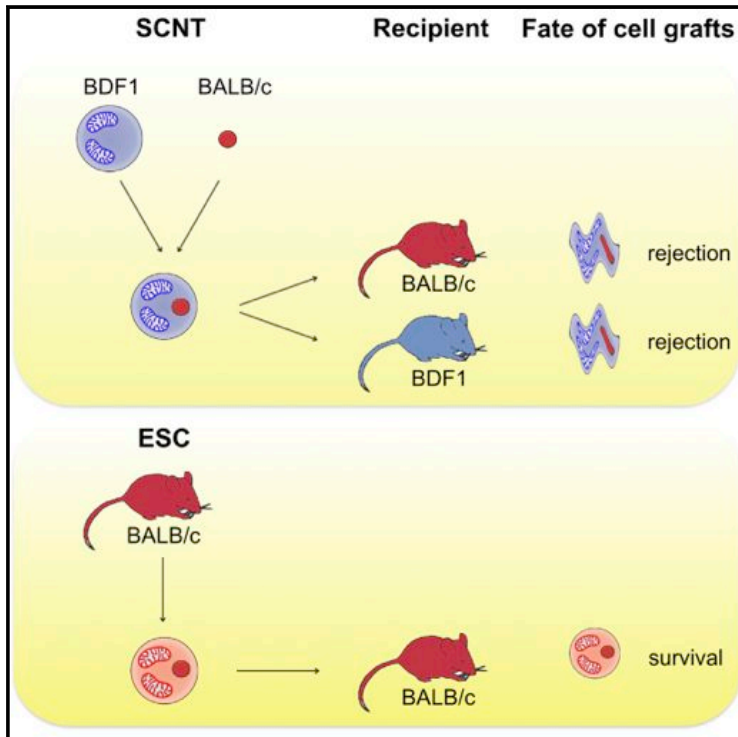
Extended Data Figure 10 | VDAC controls $\Delta\Psi_m$ and apoptosis. **a**, PDGF stimulation of SMCs significantly increased phosphorylated AKT, and ERK1 and ERK2, and increased the expression of HK2 (mean \pm s.d., 5 (pAKT and pERK1/2) and 8 (HK2) independent experiments, PDGF normalized to control, one-sample *t*-tests). **b**, Immunoblot analysis revealed PDGF-induced upregulation of HK2 expression in SMCs (mean \pm s.d., 3 (SMC) independent experiments, data normalized to control, one-sample *t*-test (control versus PDGF), Student's *t*-test (PDGF versus PDGF + DCA)). HK2 upregulation was alleviated by DCA or PDK2-KD (mean \pm s.d., 8 (PDK2-KD-SMC) independent experiments, PDGF normalized to control, one-sample *t*-test). **c**, Confocal images with mitochondrial (MitoTracker, red), HK2 (green), and nuclear staining (DAPI, blue, data are representative of 2 independent experiments) were captured. Co-localization of green HK2 with red mitochondria generated a yellow colour. SMCs incubated with PDGF increased their yellow signal, an effect that was prevented by DCA. PDGF did not induce HK2-mitochondrial association in PDK2-KD-SMCs. **d**, Cytoplasmic (C) and mitochondrial fractions (M) were isolated for immunoblotting (data are representative of 2 independent experiments). In control SMCs and

PDK2-KD-SMCs, HK2 was mainly detected in the cytoplasmic fraction. In SMCs, PDGF caused a partial translocation of HK2 to the mitochondrial compartment. DCA markedly alleviated this translocation. PDGF did not induce HK2 translocation in PDK2-KD-SMCs. **e**, In the presence of HXX2VBD-cpm, PDGF failed to induce both $\Delta\Psi_m$ hyperpolarization (mean \pm s.d., 10 replicates of 3 independent experiments, ANOVA with Bonferroni's post-hoc test) and apoptosis resistance (mean \pm s.d., 10 replicates of 3 independent experiments, ANOVA with Bonferroni's post-hoc test). **f**, VDAC inhibition by DIDS caused $\Delta\Psi_m$ hyperpolarization (mean \pm s.d., 10 replicates of 2 independent experiments, Student's *t*-test) and rendered SMCs resistant to staurosporine-induced apoptosis (mean \pm s.d., 10 replicates of 3 independent experiments, ANOVA with Bonferroni's post-hoc test). **g**, The depolarizing effect of DCA on PDGF-treated SMCs was counteracted by DIDS (mean \pm s.d., 10 replicates of 3 independent experiments, ANOVA with Bonferroni's post-hoc test). Although PDGF did not increase $\Delta\Psi_m$ in PDK2-KD-SMC, DIDS caused marked mitochondrial hyperpolarization (mean \pm s.d., 10 replicates of 2 independent experiments, ANOVA with Bonferroni's post-hoc test). **P* < 0.05; ***P* < 0.01.

Cell Stem Cell

SCNT-Derived ESCs with Mismatched Mitochondria Trigger an Immune Response in Allogeneic Hosts

Graphical Abstract



Authors

Tobias Deuse, Dong Wang, ..., Irving L. Weissman, Sonja Schrepfer

Correspondence

schrepfer@stanford.edu

In Brief

Deuse et al. report that SCNT-derived mouse ESCs trigger an immune rejection in spite of their matching with the entire nuclear genome of the recipient mouse strain. Their findings reveal that mismatched mitochondria can be sufficient to elicit an allogeneic response.

Highlights

NT-ESCs with mismatched mitochondria possess alloantigenicity

This alloantigenicity is weaker than that of an MHC mismatch

The provoked alloimmune response is adaptive and amenable for tolerance induction

SCNT-Derived ESCs with Mismatched Mitochondria Trigger an Immune Response in Allogeneic Hosts

Tobias Deuse,^{1,2,3} Dong Wang,^{1,2} Mandy Stubbendorff,^{1,2} Ryo Itagaki,^{1,2} Antje Grabosch,^{1,2} Laura C. Greaves,⁴ Malik Alawi,^{5,6} Anne Grünewald,⁷ Xiaomeng Hu,^{1,2} Xiaojin Hua,^{1,2} Joachim Velden,⁸ Hermann Reichenspurner,^{2,3} Robert C. Robbins,⁹ Rudolf Jaenisch,¹⁰ Irving L. Weissman,^{11,12} and Sonja Schrepfer^{1,2,9,12,*}

¹TSI Laboratory, University Heart Center Hamburg, Martinistrasse 52, 20246 Hamburg, Germany

²Cardiovascular Research Center Hamburg (CVRC) and DZHK (German Center for Cardiovascular Research), partner site Hamburg/Kiel/Luebeck, Martinistrasse 52, 20246 Hamburg, Germany

³Cardiovascular Surgery, University Heart Center Hamburg, Martinistrasse 52, 20246 Hamburg, Germany

⁴Newcastle University Centre for Brain Ageing and Vitality, Newcastle University, Newcastle upon Tyne, NE2 4HH, UK

⁵Bioinformatics Service Facility, University Medical Center Hamburg-Eppendorf, Martinistrasse 52, 20246 Hamburg, Germany

⁶Heinrich-Pette Institute, Leibniz Institute for Experimental Virology, Virus Genomics, Martinistrasse 52, 20246 Hamburg, Germany

⁷Wellcome Trust Centre for Mitochondrial Research, Institute of Neuroscience, Newcastle University, Newcastle upon Tyne, NE2 4HH, UK

⁸Department of Nephropathology, Institute of Pathology, University Hospital Erlangen, Maximiliansplatz 2, 91054 Erlangen, Germany

⁹Stanford Cardiovascular Institute and Department of Cardiothoracic Surgery, Stanford University School of Medicine, 300 Pasteur Drive, Stanford, CA 94305, USA

¹⁰Whitehead Institute for Biomedical Research, Massachusetts Institute of Technology, 9 Cambridge Center, Cambridge, MA 02142, USA

¹¹Department of Developmental Biology, Stanford Institute for Stem Cell Biology and Regenerative Medicine, Stanford University School of Medicine, 300 Pasteur Drive, Stanford, CA 94305, USA

¹²Co-senior author

*Correspondence: schrepfer@stanford.edu

<http://dx.doi.org/10.1016/j.stem.2014.11.003>

SUMMARY

The generation of pluripotent stem cells by somatic cell nuclear transfer (SCNT) has recently been achieved in human cells and sparked new interest in this technology. The authors reporting this methodical breakthrough speculated that SCNT would allow the creation of patient-matched embryonic stem cells, even in patients with hereditary mitochondrial diseases. However, herein we show that mismatched mitochondria in nuclear-transfer-derived embryonic stem cells (NT-ESCs) possess alloantigenicity and are subject to immune rejection. In a murine transplantation setup, we demonstrate that allogeneic mitochondria in NT-ESCs, which are nucleus-identical to the recipient, may trigger an adaptive alloimmune response that impairs the survival of NT-ESC grafts. The immune response is adaptive, directed against mitochondrial content, and amenable for tolerance induction. Mitochondrial alloantigenicity should therefore be considered when developing therapeutic SCNT-based strategies.

In somatic cell nucleus transfer (SCNT), the nucleus of a somatic cell is transplanted into an enucleated oocyte (Noggle et al., 2011). It has been envisioned that by this means, autologous pluripotent stem cells can be generated for specific patient-matched therapies. Embryonic stem cells by nuclear transfer (NT-ESCs) were first successfully generated from mice (Munsie et al., 2000) and primates (Byrne et al., 2007). After substantial

optimization of the SCNT technique, the derivation of NT-ESCs from human fetal fibroblasts (Tachibana et al., 2013), and most recently, from adult somatic cells (Chung et al., 2014; Yamada et al., 2014), was reported. These latter studies suggest that age-associated changes in the nucleus donor cell are not necessarily an impediment to generating human NT-ESCs (Chung et al., 2014). Furthermore, the differentiation of insulin-producing beta cells derived from NT-ESCs generated from a subject with longstanding diabetes proved that specialized cell types that are lost in diseased patients can be reestablished (Yamada et al., 2014). Because NT-ESCs acquire healthy mitochondria from the selected oocyte donor, inherited or acquired mtDNA diseases are most amenable for correction using the SCNT technology (Tachibana et al., 2013). The recent advancements in SCNT methodology have increased expectations for this approach to lead to human-assisted reproductive technologies (Cibelli, 2014).

A so far underappreciated obstacle for clinical application of SCNT-derived cell therapy may be the immunogenicity of mismatched mitochondria in NT-ESCs. After transplantation of NT-ESC-derived cells or tissue back into the nucleus donor, mismatched mtDNA-coded proteins may induce alloimmunity. We here show that allogeneic mitochondria in murine NT-ESCs may trigger an adaptive immune response that impairs the survival of NT-ESC grafts.

To assess mitochondria-specific alloantigenicity, transplantation studies with SCNT-derived murine NT-ESCs were conducted across defined immunological barriers. NT-ESCs were produced previously by Kirak et al. (2010) using enucleated BDF1 (B6D2F1/J) oocytes (C57BL/6J × DBA/2NcrI) F1 and isolated BALB/c (BALB/cAnNcrI; major histocompatibility complex [MHC] H2^d) fibroblast nuclei (Figure 1A). Both oocytes and NT-ESCs demonstrated high mitochondrial abundance (Figure S1A

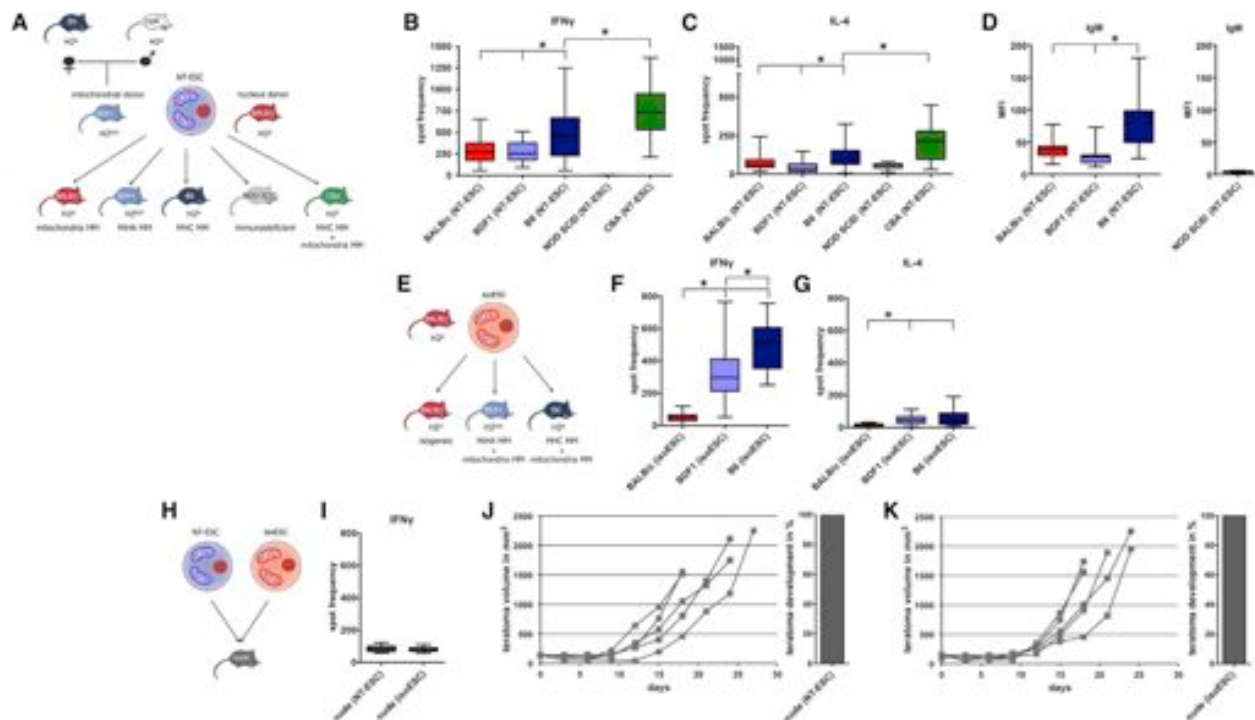


Figure 1. NT-ESCs Possess Mitochondria-Related Antigenicity

(A) NT-ESCs were generated using enucleated BDF1 oocytes and isolated BALB/c fibroblast nuclei. NT-ESCs were transplanted into mitochondria-mismatched (MM) BALB/c, MiHA-MM BDF1, MHC-MM B6, immunodeficient NOD SCID, or combined MHC-MM and mitochondria-MM CBA. See also Figure S1.

(B) Recipient-specific Th1 ELISPOT results against NT-ESCs showed significantly lower IFN γ spot frequencies for BALB/c (n = 18) and BDF1 (n = 17) recipients compared to B6 (n = 24). Overall, the CBA IFN γ response (n = 15) was the strongest and the NOD SCID response (n = 6) was negligible.

(C) IL-4 (Th2) ELISPOT responses revealed similar relations among groups (BALB/c, n = 12; BDF1, n = 17; B6, n = 24; NOD SCID, n = 8; CBA, n = 10) as described in (B) for Th1 response.

(D) The NT-ESC-specific IgM antibody production after 5 days was significantly stronger in B6 (n = 22) than in BALB/c (n = 31) or BDF1 (n = 15). No IgM antibodies against NT-ESCs were detected in NOD SCID (n = 6).

(E) Isogenic BALB/c ESCs (isoESCs) were transplanted either into isogenic BALB/c or recipients with combined mitochondria- and MiHA-MM (BDF1) or mitochondria- and MHC-MM (B6).

(F) The IFN γ ELISPOT responses against isoESC grafts were negligible in BALB/c (n = 5) and significantly stronger in BDF1 (n = 22) or B6 (n = 6). Th1 activation in MHC-MM B6 was significantly stronger than in MiHA-MM BDF1.

(G) The isoESC-specific IL-4 ELISPOT responses were significantly stronger in BDF1 (n = 23) and B6 (n = 10) than in BALB/c (n = 5).

(H) BALB/c nude mice received NT-ESC (mitochondria-MM) or isoESC grafts. Because of the T cell deficiency, the nude model assesses NK cell responses.

(I) The IFN γ NK cell response against NT-ESCs (n = 9) was low, similar to the response against isoESCs (n = 8).

(J and K) Teratoma growth diagrams for NT-ESCs (J, n = 5) and isoESCs (K, n = 5) in BALB/c nude mice are shown. The overall teratoma development is depicted in separate adjacent graphs.

On each box blot, the central mark is the median, the edges of the box are the 25th and 75th percentiles, and the whiskers extend to the most extreme data points. MM, mismatch; *p < 0.05.

available online). The high repetition of mtDNA copies and the high amount of mitochondrial proteins contribute to their relevance as possible immunogenic antigens. Culture-expanded NT-ESCs expressed markers related to pluripotency (Figure S1B). NT-ESCs grew tumors in immunodeficient NOD SCID mice (NOD.CB17-Prkdc^{scid}/J). These tumors contained tissues of endodermal, ectodermal, and mesodermal origin (Figures S1C and S1D), thus meeting the criteria for teratomas. The generated NT-ESCs thus contain maternally inherited C57BL/6J (B6) mitochondria and BALB/c nuclei of the H2^d haplotype. Suspensions of 10⁶ NT-ESCs were intramuscularly injected into the thighs of recipient mice. BALB/c recipients are matched for the entire nuclear genome but are mitochondria mismatched.

mtDNA sequence analysis comparing B6 mitochondria of the NT-ESCs with BALB/c mitochondria revealed two nonsynonymous nucleotide substitutions within the *mt-Co3* and *mt-Cytb* genes, which resulted in amino acid substitutions in the associated proteins (Figure S2A). These two nonsynonymous single nucleotide polymorphisms (SNPs) were therefore the only differences in the entire cellular DNA between donor cells and recipient. According to dbSNP (Sherry et al., 2001), both variants are common in mouse. The affected loci are conserved among vertebrates (Figure S2B) and for one of the two observed variants a human counterpart is described in dbSNP. BDF1 (H2^{b/d}) recipients share the H2^d alleles with the NT-ESCs and are mitochondria matched but minor histocompatibility antigen (MiHA)

mismatched (Figure 1A). B6 recipients possess the H2^b haplotype and are therefore MHC mismatched but mitochondria matched to the NT-ESCs. The severely immunodeficient NOD SCID strain was used as a negative control because it cannot mount any antigen-specific cellular immune response. The CBA (CBA/J; H2^k) strain is both MHC and mitochondria mismatched to the NT-ESCs. mtDNA sequencing revealed identical mtDNA genomes for CBA and BALB/c (not shown), as was previously reported in the context of mouse mtDNA phylogeny (Goios et al., 2007). Therefore, besides the MHC differences, NT-ESC transplantations into BALB/c and CBA cross the same mitochondrial mismatch.

Previous studies on the immunogenicity of murine mitochondrial peptides were mostly restricted to cytotoxic T lymphocytes (CTLs) and MHC class Ia and Ib presentation (Dabhi and Lindahl, 1995). We herein used assays that quantify activation of T helper cells (Th) because this entity plays a central role in activating CTLs and B cells, thus orchestrating graft rejection. Five-day ELISPOT assays for Th1-specific γ -interferon (IFN γ) showed a substantial immune activation in the MHC-mismatched B6 recipients, which was significantly stronger than those in mitochondria-mismatched BALB/c or MiHA-mismatched BDF1 (Figure 1B). The MHC- and mitochondria-mismatched CBA strain demonstrated the highest spot frequencies of all strains, which were approximately additive of the frequencies of the isolated MHC-mismatched B6 and the isolated mitochondria-mismatched BALB/c. The immunodeficient NOD SCID recipients showed immunological Th1 anergy. The Th2 response, although generally generating lower IL-4 spot frequencies, showed a similar relation between the recipient strains (Figure 1C). There was also a surge in NT-ESC-specific IgM antibodies in B6 recipients 5 days after immunization, which was significantly stronger than that in BALB/c or BDF1 (Figure 1D). There were no NT-ESC-specific IgM antibodies in NOD SCID.

In an additional experiment, we could exclude that there were general differences among BALB/c, BDF1, and B6 in the degree of immune responsiveness (Figure S2C). Splenocytes of these three strains were unspecifically stimulated and ELISPOT assays demonstrated similar Th1 and Th2 activation. This result permits us to attribute the above ELISPOT results to the mismatched proteins.

To exclude methodological bias caused by the state of pluripotency, isogenic BALB/c ESCs (isoESCs) were used (Figure 1E). Transplantation experiments were performed with fully nuclear DNA- and mtDNA-matched, isogenic BALB/c recipients, MiHA- and mitochondria-mismatched BDF1, and MHC- and mitochondria-mismatched B6. There was negligible Th1 and Th2 activation in isogenic BALB/c recipients (Figures 1F and 1G). Between mitochondria-mismatched recipients, an additional MHC mismatch (B6) generated a significantly stronger Th1 activation than an additional MiHA mismatch (BDF1, Figure 1F). Together, these results demonstrate that an isolated mitochondria mismatch is sufficient to initiate marked Th activation and NT-ESC-directed antibody production. These immune responses are not caused by pluripotency features themselves. Second, an MHC mismatch causes a significantly stronger immune activation than a MiHA mismatch, in the setting of both additional mitochondrial match and mismatch.

And third, the Th1 activation is additive for an MHC and a mitochondria mismatch.

Based on the results by Ishikawa (Ishikawa et al., 2010), which assumed that the innate immunity was responsible for rejection of mitochondria-mismatched cell grafts, the T cell-deficient nude mouse model was used to study the NK cell response. BALB/c nude (BALB/c nu/nu, CAnN.Cg-Foxn1^{-/-}/Cr; H2^d) mice were used as recipients for either mitochondria-mismatched NT-ESCs or fully isogenic isoESCs (H2^d, Figure 1H). Our results show that there was no increase in NK-cell-driven IFN γ ELISPOT frequency in response to NT-ESCs as compared to the response to isoESCs (Figure 1I). Also, the survival of cell grafts was similar for NT-ESCs and isoESCs and all animals formed teratomas, thus excluding relevant innate rejection processes (Figures 1J and 1K). Importantly, the transplantation experiment by Ishikawa was specifically designed to be mismatched for the maternally transmitted mitochondrial antigen (Mta) previously described by Fischer Lindahl (Fischer Lindahl et al., 1980). Our transplant setting avoids this incompatibility and, as a consequence, we did not observe relevant innate immunity-driven rejection.

Survival of NT-ESC grafts and teratoma development were assessed in the transplantation settings of Figure 1A. As expected, all NT-ESC transplants survived and formed teratomas in NOD SCID recipients (Figure 2A), whereas all grafts were rejected in fully mismatched CBAs (Figure 2B). The rather mild Th1 activation in MiHA-mismatched BDF1 still allowed 90% teratoma development of rapidly proliferating NT-ESC grafts (Figure 2C), whereas there was only 20% teratoma growth in MHC-mismatched B6 (Figure 2D). In mitochondria-mismatched BALB/c, teratomas developed in 60% of the recipients, but the tumor growth was markedly slowed (Figure 2E). Half of the tumors did not develop until day 50 to 90. Interestingly, there was a strong correlation between graft survival and Th1 activation in individual BALB/c animals (Figure 2F). Only BALB/c recipients with very low spot frequencies developed teratomas, whereas animals with at least moderate Th1 activation rejected their grafts. This further supports the notion of a T cell-mediated rejection process of mitochondria-mismatched grafts.

To confirm a mitochondrial location of the immunogenic peptides, mitochondria of NT-ESCs were separated from the remainder of the cell (cytosol) and splenocytes of NT-ESC-immunized BALB/c were restimulated *in vitro* with either mismatched mitochondria or isogenic cytosol (Figure 2G). Only the mismatched mitochondria caused an IFN γ response, whereas the spot frequencies with the isogenic cytosol fractions were low, similar to those of unstimulated responder splenocytes (Figure 2H). Of note, the ELISPOT frequencies of the separated cell compartments were markedly lower than those involving whole cells. Although their precise presentation mechanism remains elusive, the detection of mitochondrial peptides in the context of MHC (Dabhi and Lindahl, 1995; Duvvuri et al., 2014) suggests that they enter conventional MHC antigen presentation pathways. The dependence on indirect antigen presentation in this assay may explain this observation. In accordance with the ELISPOT results, in a delayed-type hypersensitivity test, only mismatched mitochondria generated paw swelling, whereas isogenic cytosol did not (Figure 2I). The location of the

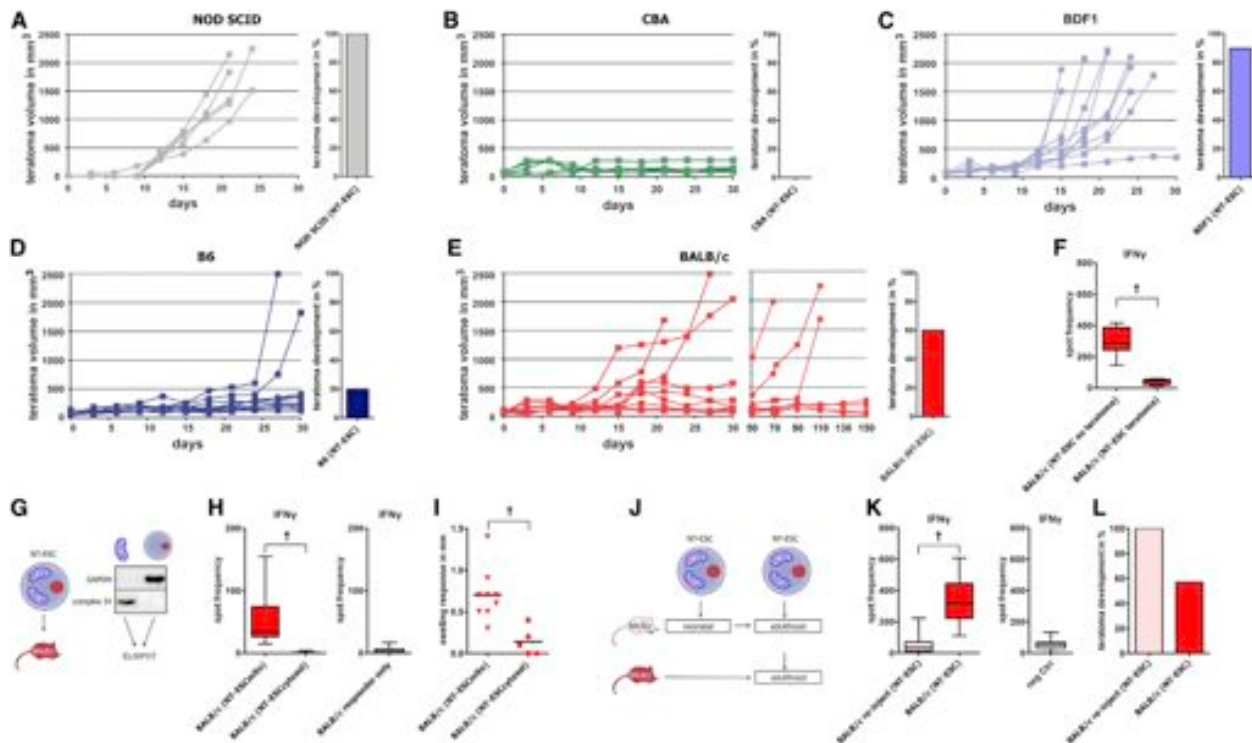


Figure 2. The Rejection of Mitochondria-MM NT-ESCs Is Adaptive, Directed against Mitochondrial Content, and Amenable for Tolerance Induction

(A–E) Teratoma growth diagrams for NT-ESC grafts in immunodeficient NOD SCID (A, $n = 5$), combined MHC- and mitochondria-MM CBA (B, $n = 5$), MIHA-MM BDF1 (C, $n = 10$), MHC-MM B6 (D, $n = 10$), and mitochondria-MM BALB/c (E, $n = 10$) recipients. The overall teratoma development is depicted in separate adjacent graphs. See also Figure S2.

(F) Within the BALB/c recipient group, the IFN γ ELISPOT frequencies of animals that did not (no teratoma, $n = 20$) or did (teratoma, $n = 8$) show teratoma growth were compared.

(G) BALB/c received mitochondria-MM NT-ESC grafts. Subsequent ELISPOT assays did not use NT-ESCs but used isolated mitochondria or the remainder of the cells (referred to as cytosol) for stimulation.

(H) IFN γ ELISPOT analyses show some BALB/c response against isolated NT-ESC mitochondria (NT-ESCmito, $n = 8$), whereas no reactivity against the mitochondria-depleted NT-ESC remnants (NT-ESCcytosol, $n = 4$) was detectable.

(I) There also was a paw swelling response in BALB/c recipients challenged with cutaneous injections of isolated NT-ESC mitochondria ($n = 9$), but not in BALB/c challenged with the mitochondria-depleted NT-ESC remnants ($n = 5$).

(J) One group of BALB/c mice received their first NT-ESC grafts at neonatal stage and were re-injected during adulthood (BALB/c_{reinject}). The other group received NT-ESC grafts only after entering adulthood (BALB/c).

(K) In ELISPOT assays, BALB/c_{reinject} ($n = 14$) showed a significantly lower IFN γ response than BALB/c ($n = 7$).

(L) The overall teratoma development of NT-ESC grafts in BALB/c_{reinject} ($n = 27$) and BALB/c animals ($n = 7$) is presented.

On each box in ELISPOT blots, the central mark is the median, the edges of the box are the 25th and 75th percentiles, and the whiskers extend to the most extreme data points. In each scatter blot, the central mark is the mean. MM, mismatch; [†] $p < 0.01$.

antigens for BALB/c immune activation against NT-ESCs was thus restricted to the mitochondrial fraction.

We next tested whether acquired immunological tolerance against allogeneic mitochondria can be induced. In accordance with the Medawar experiments (Billingham et al., 1953), neonatal BALB/c mice were immunized with mitomycin-inhibited NT-ESCs (Figure 2J). In adulthood, these animals were re-injected with NT-ESCs (BALB/c_{reinject}). In contrast to adult BALB/c recipients that received their first NT-ESC grafts, BALB/c_{reinject} showed no IFN γ response in ELISPOT assays and all animals developed teratomas (Figures 2K and 2L). This experiment not only shows that tolerance against allogeneic mitochondria can reliably be induced, it is also further proof for the relevance of

the adaptive immune system in rejecting mitochondria-mismatched grafts.

There have been few publications on the transplantation of mitochondria-mismatched cells or tissues with conflicting results. Although prolonged hematopoietic chimerism (Lanza et al., 2005) and acceptance of cardiac and renal cell transplants (Lanza et al., 2002) in cows receiving SCNT-derived mitochondria-mismatched cells was reported, this may not guarantee universal success. Pigs rejected kidney grafts from SCNT-derived mitochondria-mismatched clones (Kwak et al., 2013). In mice and rats, it was shown that a single nonsynonymous nucleotide substitution in the mitochondrial ND1 gene or the ATPase 6 gene, respectively, generated an aberrant peptide and resulted

in the loss of histocompatibility (Bhuyan et al., 1997; Davies et al., 1991; Loveland et al., 1990). Neopeptides from human mtDNA harboring large-scale frameshift deletions were recently reported to bind to MHC molecules and can be recognized by T cells from other individuals (Duvvuri et al., 2014). Interestingly, the Duvvuri et al. results further suggest that some neopeptides could bind promiscuously to both MHC class I and class II alleles, activate CD4 and CD8 T cells, and be recognized by CD8 memory T cells. Aberrant mitochondrial peptides may even provoke MHC overexpression and thus amplify their immunogenicity. In both mice and humans, increased MHC class I expression in cells harboring mtDNA deletions was shown (Gu et al., 2003). Mitochondrial peptides can thus serve as immunogens (Morse et al., 1996) and the recipient immune response may depend on the alloantigenicity of the aberrant mitochondrial protein. Although thought to be beneficial for immune surveillance and clearance of cells with mitochondrial mutations (Duvvuri et al., 2014; Gu et al., 2003), this immune feature is potentially hazardous in the context of SCNT-derived cell transplantation.

Artificial reprogramming using viral or nonviral plasmid-based approaches seems to alter the expression of a multitude of genes in induced pluripotent stem cells (iPSCs) that are differentially expressed in ESCs (de Almeida et al., 2014; Zhao et al., 2011). Specific factors being suppressed (de Almeida et al., 2014) or overexpressed (Zhao et al., 2011) in the pluripotent state have been suggested to contribute to the antigenicity of iPSCs. With differentiation, the antigenicity was reported to vanish as transcriptome profile and surface antigen expression converged with those of corresponding somatic cells (de Almeida et al., 2014). Terminally differentiated cells derived from iPSCs are now believed to possess no or negligible immunogenicity (Araki et al., 2013). The described immunogenicity is therefore differentiation dependent and not due to antigenic somatic coding mutations, which have recently been reported to occur during reprogramming (Gore et al., 2011). When compared to autologous iPSCs that are fully matched for both nuclear and mitochondrial DNA, NT-ESCs with mtDNA differences to the nucleus donor possess additional allogeneic peptides that may potentially be antigenic. These antigenic proteins in mitochondria-mismatched NT-ESCs are maintained with differentiation and the mtDNA copies, if anything, are increased in energy-consuming differentiated cells like cardiomyocytes. However, it remains to be determined if the results presented herein are transferrable to differentiated cells and tissues from NT-ESCs.

The level of heterogeneity in human mitochondria is considerably higher than that in laboratory mice (Goios et al., 2007); dbSNP lists 2,066 active human mitochondrial RefSNPs. At least 64 of these are common (global minor allele frequency 1% or higher) and nonsynonymously coding. *MT-CYTB* is affected by 26 such variants and *MT-CO3* by two, including the human counterpart of the murine variant we observed. A recent study hints at the level of heterogeneity in human mitochondrial genomes (Ridge et al., 2014). Within a data set of 1,007 full mitochondrial genomes, 899 single nucleotide variants, 26 insertions, and 20 deletions were identified. Compared to the human reference sequence, each individual carried on average 25.3 variants. Single individuals marked the extremes with 2 and 52 variants, respectively.

In the field of xenotransplantation, the immunity against the α Gal-antigen was long considered to be the one obstacle that needed to be overcome to clear the path for subsequent clinical application. However, when α Gal was knocked out, xenimmune responses were still evident and new immune targets surfaced that previously were overshadowed by the strong α Gal response (Miyata and Platt, 2003). Similarly, when nuclear DNA is matched in SCNT-derived cells, antigenic competition (Johnson et al., 1981) may allow mitochondrial antigens to emerge as immunogens. The immunogenicity of mitochondria should thus not be neglected when advancing SCNT technology.

SUPPLEMENTAL INFORMATION

Supplemental Information for this article includes two figures and Supplemental Experimental Procedures and can be found with this article online at <http://dx.doi.org/10.1016/j.stem.2014.11.003>.

AUTHOR CONTRIBUTIONS

T.D., R.C.R., R.J., I.L.W., and S.S. designed the study. T.D., D.W., M.A., and S.S. analyzed the data and performed the statistics. D.W. performed the live cell mitochondrial staining, characterized the cells, and provided all confocal data. M.S., R.I., A. Grabosch., and X. Hu performed the ELISPOT assays and/or generated the cell survival data. M.S. contributed to the FACS and DTH data. L.C.G. and A. Grünwald performed the mtDNA sequencing. M.A. performed bioinformatics analyses of mtDNA sequences. X. Hua and J.V. generated the teratoma data. R.J. generated the SCNT cells and ESCs. H.R. edited the manuscript. S.S. performed or supervised cell transplantation and all immunologic assays. T.D., D.W., M.A., I.L.W., and S.S. wrote the manuscript and all authors edited the manuscript.

ACKNOWLEDGMENTS

We thank Kirsten Fischer Lindahl for her critical comments and editing of the manuscript. We further thank Christiane Pahrman for performing all cell cultures and for her overall technical assistance and Oktay Kirak and Hidde Ploegh for generating the experimental cells. We extend special thanks to the UKE Imaging Facility (UMIF, Bernd Zobiak) and the UKE Animal Facility. This study was supported by the Else-Kröner-Fresenius-Stiftung (2012_EKES.04; T.D.), a grant from the Fondation Leducq (CDA 2013-2015; S.S.), and the German Research Foundation (Deutsche Forschungsgemeinschaft; DFG: SCHR992/3-1 and SCHR992/4-1; S.S.).

Received: July 6, 2014

Revised: September 27, 2014

Accepted: November 7, 2014

Published: November 20, 2014

REFERENCES

- Araki, R., Uda, M., Hoki, Y., Sunayama, M., Nakamura, M., Ando, S., Sugiura, M., Ideno, H., Shimada, A., Nifuji, A., and Abe, M. (2013). Negligible immunogenicity of terminally differentiated cells derived from induced pluripotent or embryonic stem cells. *Nature* 494, 100–104.
- Bhuyan, P.K., Young, L.L., Lindahl, K.F., and Butcher, G.W. (1997). Identification of the rat maternally transmitted minor histocompatibility antigen. *J. Immunol.* 158, 3753–3760.
- Billingham, R.E., Brent, L., and Medawar, P.B. (1953). Actively acquired tolerance of foreign cells. *Nature* 172, 603–606.
- Byrne, J.A., Pedersen, D.A., Clepper, L.L., Nelson, M., Sanger, W.G., Gokhale, S., Wolf, D.P., and Mitalipov, S.M. (2007). Producing primate embryonic stem cells by somatic cell nuclear transfer. *Nature* 450, 497–502.

- Chung, Y.G., Eum, J.H., Lee, J.E., Shim, S.H., Sepilian, V., Hong, S.W., Lee, Y., Treff, N.R., Choi, Y.H., Kimbrel, E.A., et al. (2014). Human somatic cell nuclear transfer using adult cells. *Cell Stem Cell* *14*, 777–780.
- Cibelli, J.B. (2014). Human somatic cell nuclear transfer is alive and well. *Cell Stem Cell* *14*, 699–701.
- Dabhi, V.M., and Lindahl, K.F. (1995). MtDNA-encoded histocompatibility antigens. *Methods Enzymol.* *260*, 466–485.
- Davies, J.D., Wilson, D.H., Hermel, E., Lindahl, K.F., Butcher, G.W., and Wilson, D.B. (1991). Generation of T cells with lytic specificity for atypical antigens. I. A mitochondrial antigen in the rat. *J. Exp. Med.* *173*, 823–832.
- de Almeida, P.E., Meyer, E.H., Kooreman, N.G., Diecke, S., Dey, D., Sanchez-Freire, V., Hu, S., Ebert, A., Odegaard, J., Mordwinkin, N.M., et al. (2014). Transplanted terminally differentiated induced pluripotent stem cells are accepted by immune mechanisms similar to self-tolerance. *Nat. Commun.* *5*, 3903.
- Duvvuri, B., Duvvuri, V.R., Wang, C., Chen, L., Wagar, L.E., Jamnik, V., Wu, J., Yeung, R.S., Grigull, J., Watts, T.H., and Wu, G.E. (2014). The human immune system recognizes neopeptides derived from mitochondrial DNA deletions. *J. Immunol.* *192*, 4581–4591.
- Fischer Lindahl, K., Bocchieri, M., and Riblet, R. (1980). Maternally transmitted target antigen for unrestricted killing by NZB T lymphocytes. *J. Exp. Med.* *152*, 1583–1595.
- Goios, A., Pereira, L., Bogue, M., Macaulay, V., and Amorim, A. (2007). mtDNA phylogeny and evolution of laboratory mouse strains. *Genome Res.* *17*, 293–298.
- Gore, A., Li, Z., Fung, H.L., Young, J.E., Agarwal, S., Antosiewicz-Bourget, J., Canto, I., Giorgetti, A., Israel, M.A., Kiskinis, E., et al. (2011). Somatic coding mutations in human induced pluripotent stem cells. *Nature* *471*, 63–67.
- Gu, Y., Wang, C., Roifman, C.M., and Cohen, A. (2003). Role of MHC class I in immune surveillance of mitochondrial DNA integrity. *J. Immunol.* *170*, 3603–3607.
- Ishikawa, K., Toyama-Sorimachi, N., Nakada, K., Morimoto, M., Imanishi, H., Yoshizaki, M., Sasawatari, S., Niikura, M., Takenaga, K., Yonekawa, H., and Hayashi, J. (2010). The innate immune system in host mice targets cells with allogeneic mitochondrial DNA. *J. Exp. Med.* *207*, 2297–2305.
- Johnson, L.L., Bailey, D.W., and Mobraaten, L.E. (1981). Antigenic competition between minor (non-H-2) histocompatibility antigens. *Immunogenetics* *13*, 451–455.
- Kirak, O., Frickel, E.M., Grotenbreg, G.M., Suh, H., Jaenisch, R., and Ploegh, H.L. (2010). Transnuclear mice with predefined T cell receptor specificities against *Toxoplasma gondii* obtained via SCNT. *Science* *328*, 243–248.
- Kwak, H.H., Park, K.M., Teotia, P.K., Lee, G.S., Lee, E.S., Hong, S.H., Yang, S.R., Park, S.M., Ahn, C., Park, C.K., et al. (2013). Acute rejection after swine leukocyte antigen-matched kidney allo-transplantation in cloned miniature pigs with different mitochondrial DNA-encoded minor histocompatibility antigen. *Transplant. Proc.* *45*, 1754–1760.
- Lanza, R.P., Chung, H.Y., Yoo, J.J., Wettstein, P.J., Blackwell, C., Borson, N., Hofmeister, E., Schuch, G., Soker, S., Moraes, C.T., et al. (2002). Generation of histocompatible tissues using nuclear transplantation. *Nat. Biotechnol.* *20*, 689–696.
- Lanza, R., Shieh, J.H., Wettstein, P.J., Sweeney, R.W., Wu, K., Weisz, A., Borson, N., Henderson, B., West, M.D., and Moore, M.A. (2005). Long-term bovine hematopoietic engraftment with clone-derived stem cells. *Cloning Stem Cells* *7*, 95–106.
- Loveland, B., Wang, C.R., Yonekawa, H., Hermel, E., and Lindahl, K.F. (1990). Maternally transmitted histocompatibility antigen of mice: a hydrophobic peptide of a mitochondrially encoded protein. *Cell* *60*, 971–980.
- Miyata, Y., and Platt, J.L. (2003). Xeno—still stuck without alphaGal. *Nat. Biotechnol.* *21*, 359–360.
- Morse, M.C., Bleau, G., Dabhi, V.M., Héту, F., Drobetsky, E.A., Lindahl, K.F., and Perreault, C. (1996). The COI mitochondrial gene encodes a minor histocompatibility antigen presented by H2-M3. *J. Immunol.* *156*, 3301–3307.
- Munsie, M.J., Michalska, A.E., O'Brien, C.M., Trounson, A.O., Pera, M.F., and Mountford, P.S. (2000). Isolation of pluripotent embryonic stem cells from reprogrammed adult mouse somatic cell nuclei. *Curr. Biol.* *10*, 989–992.
- Noggle, S., Fung, H.L., Gore, A., Martinez, H., Satriani, K.C., Prosser, R., Oum, K., Paull, D., Druckenmiller, S., Freeby, M., et al. (2011). Human oocytes reprogram somatic cells to a pluripotent state. *Nature* *478*, 70–75.
- Ridge, P.G., Maxwell, T.J., Foutz, S.J., Bailey, M.H., Corcoran, C.D., Tschanz, J.T., Norton, M.C., Munger, R.G., O'Brien, E., Kerber, R.A., et al. (2014). Mitochondrial genomic variation associated with higher mitochondrial copy number: the Cache County Study on Memory Health and Aging. *BMC Bioinformatics* *15* (7), S6.
- Sherry, S.T., Ward, M.H., Kholodov, M., Baker, J., Phan, L., Smigielski, E.M., and Sirotkin, K. (2001). dbSNP: the NCBI database of genetic variation. *Nucleic Acids Res.* *29*, 308–311.
- Tachibana, M., Amato, P., Sparman, M., Gutierrez, N.M., Tippner-Hedges, R., Ma, H., Kang, E., Fulati, A., Lee, H.S., Sritanandomchai, H., et al. (2013). Human embryonic stem cells derived by somatic cell nuclear transfer. *Cell* *153*, 1228–1238.
- Yamada, M., Johannesson, B., Sagi, I., Burnett, L.C., Kort, D.H., Prosser, R.W., Paull, D., Nestor, M.W., Freeby, M., Greenberg, E., et al. (2014). Human oocytes reprogram adult somatic nuclei of a type 1 diabetic to diploid pluripotent stem cells. *Nature* *510*, 533–536.
- Zhao, T., Zhang, Z.N., Rong, Z., and Xu, Y. (2011). Immunogenicity of induced pluripotent stem cells. *Nature* *474*, 212–215.

Cell Stem Cell, Volume 16

Supplemental Information

SCNT-Derived ESCs with Mismatched Mitochondria Trigger an Immune Response in Allogeneic Hosts

Tobias Deuse, Dong Wang, Mandy Stubbendorff, Ryo Itagaki, Antje Grabosch, Laura C. Greaves, Malik Alawi, Anne Grünewald, Xiaomeng Hu, Xiaoqin Hua, Joachim Velden, Hermann Reichenspurner, Robert C. Robbins, Rudolf Jaenisch, Irving L. Weissman, and Sonja Schrepfer

Supplemental Information

Inventory of Supplemental Information:

Figure S1, related to Figure 1

Figure S2, related to Figure 2

Experimental Procedures

Supplemental References

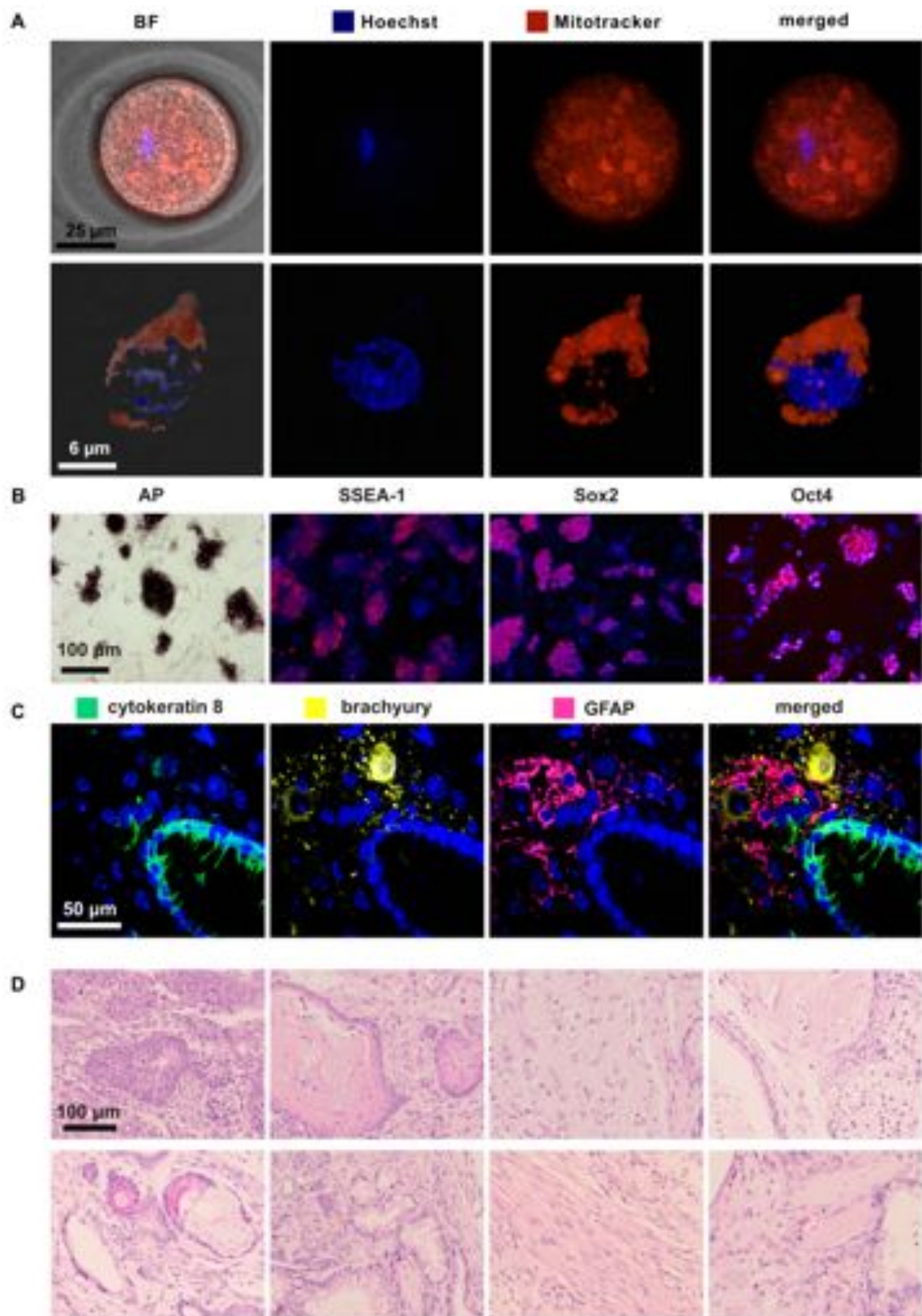


Figure S1: *Characterization of SCNT-derived NT-ESCs and proof of pluripotency, Related to Figure 1.*


(A) A murine oocyte (upper row) and an NT-ESC (lower row) were stained for nuclear (Hoechst) and mitochondrial content (Mitotracker). Confocal immunofluorescence shows the defined nucleus and the great abundance of mitochondria throughout the cells.

(B) SCNT-derived NT-ESCs demonstrated pluripotency markers as they were positive for alkaline phosphatase (AP), and expressed SSEA-1, Sox2, and Oct4.

(C) NT-ESCs were transplanted into immunodeficient NOD SCID mice and grew tumors within 3-4 weeks. Recovered tumors stained positive for tissues of all three germ layers and were thus identified as teratomas. Endodermal (cytokeratin 8), mesodermal (brachyury), and ectodermal (GFAP) lineages were demonstrated by confocal immunofluorescence microscopy.

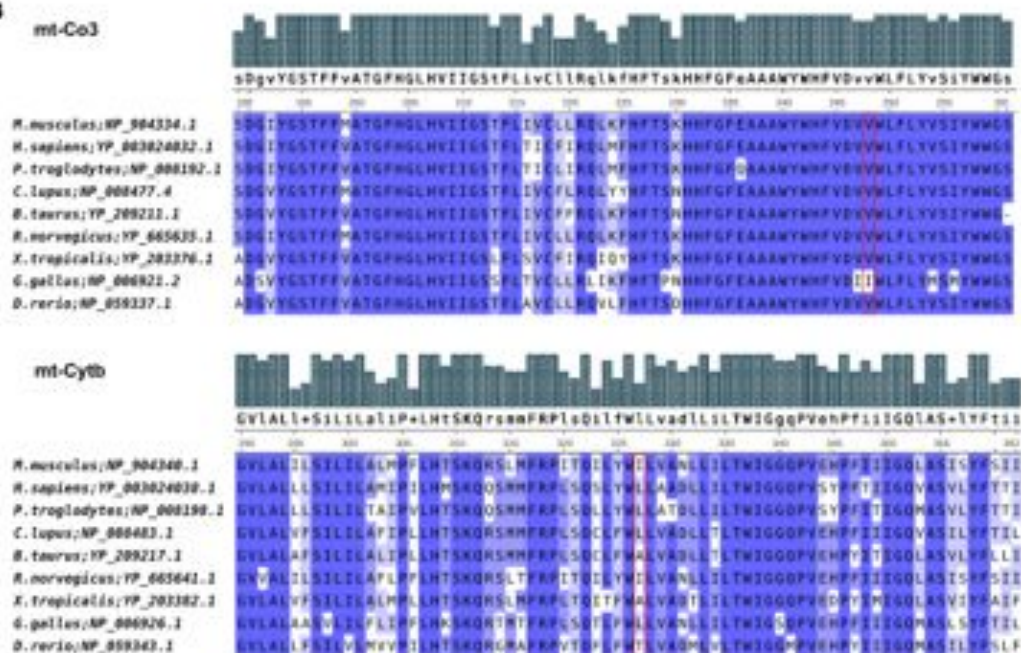
(D) Hematoxylin-eosin staining of NT-ESC-derived teratomas revealed their composition of various types of tissues. Upper row (left to right): primitive neural tube differentiation (ectoderm), squamous epithelium (ectoderm), brain tissue (ectoderm), bronchial and clear cell bronchogenic epithelium and bone (endoderm and mesoderm). Lower row (left to right): hair follicles with sebaceous glands (ectoderm), intestine (endoderm), smooth muscle (mesoderm), striated muscle (mesoderm).

A



Position	Gene	Protein	Nucleotide	AA	Nucleotide	AA	RefSNP ID	RefSNP Allelic Frequency	RefSNP ID (human counterpart)
m.9348	mt-Co3	cytochrome c oxidase III	G	V	A	I	rs8281486	G: 61.111% (22 / 36) A: 38.889% (14 / 36)	rs370688668
m.15123	mt-Cytb	cytochrome b	G	V	A	I	rs33258689	G: 8.333% (2 / 24) A: 91.667% (22 / 24)	-

B



C

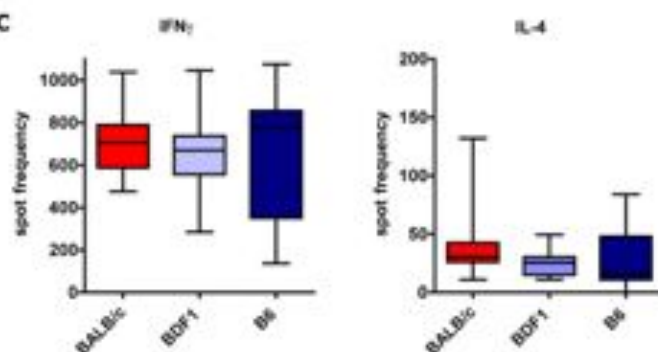


Figure S2: *Mitochondrial DNA (mtDNA) sequencing, level of conservation among vertebrates, and unspecific immune responsivenesses of different mouse strains, Related to Figure 2.*

(A) The comparison of mtDNA sequences between isolated B6 mitochondria and BALB/c mitochondria revealed two non-synonymous nucleotide substitutions.

(B) Multiple sequence alignments of mt-Co3 (upper part) and mt-Cytb (lower part). The level of conservation for each position is indicated by bars and background colors. The positions affected by variants observed in this study are highlighted. Alignments were calculated using Muscle (v3.8.31) (Edgar, 2004) with default parameters. For visualization, UGENE (v1.11.5) (Okonechnikov et al., 2012) was employed.

(C) BALB/c (n=10), BDF1 (n=10 for IFN γ and n=5 for IL-4), and B6 (n=10) splenocytes were stimulated with PMA and ionomycin for 24h. The IFN γ and IL-4 ELISPOT frequencies were similar among the mouse strains. In box blot graphs, the median is shown, the edges of the box are the 25th and 75th percentiles, and the whiskers extend to the most extreme data points.

Experimental Procedures

Generation and culture of NT-ESCs and isoESCs

Somatic cell nuclear transfer (SCNT)

Oocytes from superovulated BDF1 mice were metaphase-II arrested and enucleated. Nuclei from BALB/c were transferred into the enucleated oocytes to create NT-ESCs.

isoESCs

The BALB/c ESC line V39.7 was previously generated as described (Eggan et al., 2001).

Cell culture

NT-ESCs and isoESCs were cultured on mitomycin-inhibited CF1 feeders using standard ES cell media (Gibco, Darmstadt, Germany) containing LIF (Millipore, Billerica, MA). Before in vivo cell injection and in vitro immunology experiments, NT-ESCs and isoESCs were cultured on gelatin (Millipore) without feeders using standard media containing LIF. Cell cultures were regularly screened for mycoplasma infections (Lonza, Cologne, Germany).

Mice

BALB/c (BALB/cAnNCrl, H2^d), BDF1 (B6D2F1/J, H2^{b/d}), C57BL/6 (C57BL/6J, B6, H2^b), NOD SCID (NOD.CB17-Prkdc^{scid}/J), CBA (CBA/J, H2^k), and BALB/c nude (BALB/c NU/NU, CAnN.Cg-Foxn1^{nu}/Crl, H2^d) (all 6-10 weeks of age) were used as recipients for NT-ESC or isoESC grafts. Mice were purchased from Charles River Laboratories (Sulzfeld, Germany) and received humane care in compliance with the Guide for the Principles of Laboratory Animals. Mouse studies were approved by the Hamburg "Amt für Gesundheit und Verbraucherschutz". The numbers of mice per experimental group are presented with each figure.

Immunostaining in vitro

The mouse ESC/iPSC Characterization Kit (Applied StemCell, Sunnyvale, CA) was used to demonstrate the expression of the pluripotency markers alkaline phosphatase (AP), SSEA-1, Sox2, and Oct4. Staining was performed according to the manufacturer's protocol.

In vivo teratoma assay

Teratoma formation was observed within 4 weeks after injecting 10⁷ NT-ESCs intramuscularly into NOD SCID mice and teratomas were fixed with 4% paraformaldehyde and paraffin-embedded for confocal immunofluorescence and histopathology.

To demonstrate pluripotency using immunostainings, 5µm sections underwent heat-induced antigen retrieval with Dako antigen retrieval solution (Dako, Glostrup, Denmark) in a steamer

followed by blocking with Image-iT® FX signal enhancer (Invitrogen, Carlsbad, CA). Sections were incubated with a primary antibody against brachyury (ab20680, Abcam, Cambridge, England). For detection, a goat anti-rabbit antibody labeled with Alexa Fluor 555 (Invitrogen) was used. Subsequently, sections were incubated with FITC- and Alexa Fluor 647-conjugated antibodies against cytokeratin 8 (SB37b, Abcam) and GFAP (GA5, Cell signaling, Cambridge, UK), respectively. After nuclei staining with DAPI, images were obtained and analyzed using the Nikon Eclipse TiE microscope (Nikon, Tokyo, Japan) equipped with Perkin Elmer UltraVIEW VoX confocal imaging system (Perkin Elmer, Waltham, MA). Hematoxylin and eosin (H&E) stained slides were interpreted by an expert pathologist (J.V.) blinded to the study.

Live cell mitochondrial staining

Living cells were incubated in Mitotracker FM staining solution (0.1µM; Invitrogen) for 15 min at 37°C. Cell nuclei were stained with Hoechst 33342 (0.3µM; Invitrogen). Immediately after staining, images were taken with a Nikon Eclipse TiE microscope equipped with Perkin Elmer UltraVIEW VoX confocal imaging system (Perkin Elmer). Cropped pictures of single cells are presented.

mtDNA sequencing

B6, BALB/c, and CBA mtDNA sequencing was performed as previously described (Trifunovic et al., 2004). Sequence data reported in this publication have been submitted to the European Nucleotide Archive (ENA) and are available at <http://www.ebi.ac.uk/ena/data/view/PRJEB7710>. Results were compared to known SNPs in the Database of Single Nucleotide Polymorphisms (dbSNP; National Center for Biotechnology Information, National Library of Medicine, Bethesda, MD). dbSNP build IDs: 141 (human) and 140 (mouse) are available from <http://www.ncbi.nlm.nih.gov/SNP/>.

Cell transplantation

Before transplantation, NT-ESCs and isoESCs were cultured off-feeder for 1 passage to avoid contamination with feeder cells. NT-ESCs and isoESCs were trypsinated and re-suspended in sterile saline for immunobiology experiments (10^6 cells per 80µl saline for ELISPOT, 10^7 cells per 80µl saline for DTH) and NT-ESC graft survival studies (10^6 cells per 80µl saline). Cell viability was approximately 95% as determined by trypan blue staining. Cell transplantation was performed by direct injection of cell suspensions into the right thigh muscle of recipient mice using a 27-gauge syringe.

ELISPOT assays

For uni-directional Enzyme-Linked ImmunoSpot (ELISPOT) assays, recipient splenocytes were isolated from fresh spleen 5 days after NT-ESC or isoESC injection and used as responder cells. NT-ESCs or isoESCs were mitomycin-inhibited and served as stimulator cells. 10^5 stimulator cells were incubated with 5×10^5 recipient responder splenocytes for 24h and IFN γ and IL-4 spot frequencies were automatically enumerated using an ELISPOT plate reader. Duplicates or quadruplicates were performed in most assays.

To measure the ELISPOT response to cell compartments (mitochondria or cytosol), mitochondria were isolated from 3×10^7 NT-ESCs and served as stimulators. The remainder of the cells comprised the cytosol fraction. Successful separation of mitochondria and mitochondria-depleted cytosol was confirmed by immunoblots. Mitochondrial complex IV and GAPDH were used to confirm mitochondrial and cytosol content, respectively, and to rule out cross-contamination.

In accordance to the Medawar experiments, neonatal BALB/c mice were immunized with 10^5 mitomycin-inhibited NT-ESCs. In adulthood, the animals were re-injected with 10^6 NT-ESCs (Balb/C_{re-inject}) and uni-directional ELISPOT assays were performed as describe above.

Unspecifically stimulated BALB/c, BDF1, and B6 splenocytes served as ELISPOT controls. For these assays, 3×10^4 responder splenocytes were stimulated with PMA (phorbol 12-myristate 13-acetate, Sigma, 1ng/ml) and ionomycin (Sigma, 500ng/ml) for 24 h.

Delayed-type hypersensitivity response (DTH)

DTH is a rapid T cell-dependent in vivo immune response to a foreign antigen, which the host immune system has experienced in the recent past. In the sensitization phase, 2×10^6 NT-ESCs were injected subcutaneously into the flank of BALB/c mice. Seven days after sensitization, heated mitochondria or cytosol fractions, obtained from 10^6 NT-ESCs, were intradermally injected into the footpad during the challenge phase and paw swelling was measured after 24h using a digimatic micrometer (Mitutoyo, Aurora, IL). Results are demonstrated as swelling response to the antigen challenge in comparison to the PBS-injected contralateral control footpad of the animals.

NT-ESC-specific antibody assay using flow cytometry (FACS)

NT-ESC-specific mouse antibodies were detected by FACS analysis as previously described (Deuse et al., 2008). Briefly, the serum of BALB/c, BDF1, and B6 mice 5 days after

transplantation of NT-ESC grafts was incubated with NT-ESCs and the binding of antibodies was quantified. Only IgM antibodies were analyzed because of their known rapid surge within 5 days after allogeneic stimulation. IgM antibodies were stained by incubation of the cells with a PE-conjugated goat antibody specific for the Fc portion of mouse IgM (BD Biosciences, Franklin Lakes, NJ). Cells were washed and then analyzed on a FACSCalibur system (BD Biosciences). Fluorescence data were expressed as mean fluorescence intensity (MFI).

Survival of cell grafts

Survival of cell grafts and teratoma development were assessed *in vivo* by injecting 10^7 NT-ESCs or isoESCs in 80 μ l saline intramuscularly into the indicated recipients. Cell survival leading to teratoma formation was monitored every third day for 30 days using the digimatic caliper (Mitutoyo). Usually, teratoma formation occurred within 30 days. However, animals not developing teratomas were followed for 150 days to exclude late teratoma development. The overall fractions of animals that developed teratomas are shown in separate adjacent graphs.

Statistics

In box blot graphs, the median is shown, the edges of the box are the 25th and 75th percentiles, and the whiskers extend to the most extreme data points. In scatter blots, the central mark is the mean. Intergroup differences were appropriately assessed by either unpaired Student's t test or one-way analysis of variance (ANOVA) with Bonferroni's postHoc test. * $p < 0.05$, † $p < 0.01$.

Supplemental References

Deuse, T., Hoyt, G., Koyanagi, T., Robbins, R.C., and Schrepfer, S. (2008). Prevention and inhibition but not reversion of chronic allograft vasculopathy by FK778. *Transplantation* 85, 870-877.

Edgar, R.C. (2004). MUSCLE: a multiple sequence alignment method with reduced time and space complexity. *BMC Bioinformatics* 5, 113.

Eggan, K., Akutsu, H., Loring, J., Jackson-Grusby, L., Klemm, M., Rideout, W.M., 3rd, Yanagimachi, R., and Jaenisch, R. (2001). Hybrid vigor, fetal overgrowth, and viability of mice derived by nuclear cloning and tetraploid embryo complementation. *Proc Natl Acad Sci USA* 98, 6209-6214.

Okonechnikov, K., Golosova, O., Fursov, M., and team, U. (2012). Unipro UGENE: a unified bioinformatics toolkit. *Bioinformatics* 28, 1166-1167.

Trifunovic, A., Wredenberg, A., Falkenberg, M., Spelbrink, J.N., Rovio, A.T., Bruder, C.E., Bohlooly, Y.M., Gidlof, S., Oldfors, A., Wibom, R., *et al.* (2004). Premature ageing in mice expressing defective mitochondrial DNA polymerase. *Nature* 429, 417-423.